สกว
TRF

รายงานวิจัยฉบับสมบูรณ์

โครงการ การออกแบบระบบควบคุมโรบัสแบบดีสครีตของตัวชดเชยสเตติกซ์ซิงโครนัสแบบอนุกรมเพื่อการควบคุมเสถียรภาพของการแกว่งของความถี่ในระบบไฟฟ้ากำลังที่เชื่อมโยง

Robust Discrete Control Design of Static Synchronous Series Compensator (SSSC) for Stabilization of Frequency Oscillations in an Interconnected Power System

โดย ผศ.ดร. อิสระชัย งามหรู และ ผศ.ดร. วารี กงประเวชนนท์

มิถุนายน 2546

รายงานวิจัยฉบับสมบูรณ์

โครงการ การออกแบบระบบควบคุมโรบัสแบบดีสครีตของตัวชดเชยสเตติกซ์ซิงโครนัสแบบอนุกรมเพื่อการควบคุมเสถียรภาพของการแกว่งของความถี่ในระบบไฟฟ้ากำลังที่เชื่อมโยง

Robust Discrete Control Design of Static Synchronous Series Compensator (SSSC) for Stabilization of Frequency Oscillations in an Interconnected Power System

โดย ผศ.ดร. อิสระชัย งามหรู และ ผศ.ดร. วารี กงประเวชนนท์

มิถุนายน 2546

สัญญาเลขที่ PDF/33/2543

รายงานวิจัยฉบับสมบูรณ์

โครงการ การออกแบบระบบควบคุมโรบัสแบบดีสครีตของตัวชดเชยสเตติกซ์ซิงโครนัสแบบอนุกรมเพื่อการควบคุมเสถียรภาพของการแกว่งของความถี่ในระบบไฟฟ้ากำลังที่เชื่อมโยง

Robust Discrete Control Design of Static Synchronous Series Compensator (SSSC) for Stabilization of Frequency Oscillations in an Interconnected Power System

คณะผู้วิจัย	สังกัด
ผศ. ดร. อิสระชัย งามหรู	สถาบันเทคโนโลยีนานาชาติสิรินธร
ผศ. ดร. วารี กงประเวชนนท์	สถาบันเทคโนโลยีนานาชาติสิรินธร

สนับสนุนโดยสำนักงานกองทุนสนับสนุนการวิจัย

Project Code: PDF/71/2544

Project Title: การออกแบบระบบควบคุมโรบัสแบบดีสครีตของตัวชดเชยสเตติกซิงโครนัสแบบอนุกรม เพื่อการควบคุมเสถียรภาพของการแกว่งของความถี่ในระบบไฟฟ้ากำลังที่เชื่อมโยง
Robust Discrete Control Design of Static Synchronous Series Compensator (SSSC) for Stabilization of Frequency Oscillations in an Interconnected Power System

Investigator: ผศ. ดร. อิสระชัย งามหรู
E-mail address: ngamroo@siit.tu.ac.th

Project Period: 1 กรกฎาคม 2544 - 30 มิถุนายน 2546

Abstract

As an AC interconnected power system is subjected to a large load with rapid change, system frequency may be severely disturbed and becomes oscillatory. To stabilize the frequency oscillations, the dynamic power flow control of the Static Synchronous Series Compensator (SSSC) located in series with the tie line between interconnected power systems, is employed. By regarding the system interconnection as the control channel, the power flow control by an SSSC via the interconnection creates a sophisticated method of frequency stabilization. To implement this concept, the robust design method of the lead/lag controller equipped with the SSSC is proposed. In the design process, not only the attenuation performance of system disturbances, but also the robust stability against system uncertainties are taken into consideration. The optimal parameters of the lead/lag controller are obtained by using the tabu search algorithm (TSA), so that both performance and robustness are satisfied. The frequency stabilizer developed by the proposed design can be implemented in both continuous and discrete time domains. Simulation study exhibits the significant damping effects of designed frequency stabilizer on frequency oscillations under different load disturbances and negative damping.

บทคัดย่อ

ในปัจจุบัน ความต้องการทางด้านพลังงานไฟฟ้าและการแข่งขันกันระหว่างผู้ประกอบการไฟฟ้าอิสระมีแนวโน้มที่สูงขึ้นอย่างมากทั่วโลกในสภาพการเช่นนี้ การควบคุมในระบบไฟฟ้ากำลังเช่น การควบคุมเสถียรภาพทางความถี่และแรงดันเป็นต้น นั้นจะเปลี่ยนไปในรูปลักษณะเป็นการให้บริการที่เรียกว่า Ancillary Services โดยเฉพาะอย่างยิ่งในระบบไฟฟ้ากำลังที่มีการติดตั้งภาระ (load) ทางไฟฟ้าที่มีความต้องการกำลังไฟฟ้าอย่างมากและยังมีการเปลี่ยนแปลงภาระอย่างรวดเร็ว อย่างเช่น รถไฟฟ้าความเร็วสูง, โรงงานอุตสาหกรรมหนักขนาดใหญ่ เป็นต้น นั้นก่อให้เกิดปัญหาการแกว่งของความถี่อย่างรุนแรง ซึ่งแม้แต่ระบบควบคุมเสถียรภาพทางความถี่ที่ใช้ในปัจจุบัน คือ ระบบโกเวอร์เนอร์นั้นก็ยังไม่สามารถลดความรุนแรงของการแกว่งของความถี่ได้ การแกว่งของความถี่อย่างรุนแรงนี้จะส่งผลเสียต่อเสถียรภาพโดยรวมของระบบไฟฟ้ากำลังโดยตรงซึ่งจะทำให้ระบบนั้นไม่สามารถจ่ายกำลังไฟฟ้าได้ นอกจากนี้ แนวโน้มการเพิ่มขึ้นอย่างสูงของผู้ผลิตไฟฟ้าอิสระ ซึ่งความสามารถในการควบคุมความถี่ไม่เพียงพอก็มีผลเสียอย่างมากต่อเสถียรภาพทางความถี่ของระบบ ภายใต้สถานการณ์ดังกล่าวข้างต้นวิธีการให้บริการการควบคุมเสถียรภาพทางความถี่แบบใหม่ ซึ่งมีประสิทธิภาพสูงกว่าระบบควบคุมที่ใช้ในปัจจุบันจึงมีความต้องการเป็นอย่างสูง งานวิจัยนี้นำเสนอการนำอุปกรณ์ทางอิเลคทรอนิกส์กำลังซึ่งมีความเร็วในการควบคุมสูงที่เรียกว่า Static Synchronous Series Compensator, (SSSC) ซึ่งมีความสามารถในการควบคุมการไหลของกำลังไฟฟ้าในสายเชื่อมโยงแบบไดนามิกส์ และสามารถนำมาประยุกต์ใช้เพื่อควบคุมเสถียรภาพทางการแกว่งของความถี่ของระบบไฟฟ้ากำลังได้อย่างรวดเร็ว โดยงานวิจัยนี้มุ่งเน้นไปในด้านการออกแบบระบบควบคุมโรบัสแบบต่อเนื่องและดีสครีตของ SSSC นอกจากเพื่อให้มีประสิทธิภาพในการลดความรุนแรงของการแกว่งของการแกว่งของความถี่และยังเพิ่มคุณสมบัติ Robustness ของตัวควบคุมต่อความไม่แน่นอนต่างๆซึ่งจะเกิดขึ้นในระบบ (system uncertainties) ให้เหนือกว่าตัวควบคุมที่ไม่มีคุณสมบัตินี้ นอกจากนี้ โครงสร้างของระบบควบคุมที่ใช้ในงานวิจัยนี้มีลักษณะเป็นตัวชดเชยแบบ second-order lead/lag จึงเป็นการง่ายในการนำมาใช้งานจริง ในงานวิจัยนี้ ได้นำ Tabu Search Algorithm มาใช้สำหรับการหาค่าพารามิเตอร์ที่เหมาะสมที่สุดของตัวควบคุม ผลการจำลองศึกษาแสดงให้เห็นถึงประสิทธิภาพและคุณสมบัติ Robustness ของตัวควบคุมที่นำเสนอ

Keywords: Flexible AC Transmission Systems (FACTS), Static synchronous series compensator (SSSC), robust control, system uncertainties, tabu search algorithm, overlapping decompositions, power system stabilization, frequency oscillations, ancillary services.

หน้าสรุปโครงการ (Executive Summary)

1. ปัญหาที่ทำการวิจัย และความสำคัญของปัญหา

ในปัจจุบันความต้องการทางด้านพลังงานไฟฟ้าและการแข่งขันกันระหว่างผู้ประกอบการไฟฟ้าอิสระมีแนวโน้มที่สูงขึ้นอย่างมากทั่วโลก ในสภาพการเช่นนี้ การควบคุมในระบบไฟฟ้ากำลังเช่น การควบคุมเสถียรภาพทางความถี่และแรงดันเป็นต้นนั้นจะเปลี่ยนไปในรูปลักษณะเป็นการให้บริการที่เรียกว่า Ancillary Services โดยเฉพาะอย่างยิ่งในระบบไฟฟ้ากำลังที่มีการติดตั้งภาระ (load) ทางไฟฟ้าที่มีความต้องการกำลังไฟฟ้าอย่างมากและยังมีการเปลี่ยนแปลงภาระอย่างรวดเร็ว อย่างเช่น รถไฟฟ้าความเร็วสูง, โรงงานอุตสาหกรรมหนักขนาดใหญ่ เป็นต้น นั้นก่อให้เกิดปัญหาการแกว่งของความถี่อย่างรุนแรง ซึ่งแม้แต่ระบบควบคุมเสถียรภาพทางความถี่ที่ใช้ในปัจจุบันคือระบบโกเวอร์เนอร์นั้นก็ยังไม่สามารถลดความรุนแรงของการแกว่งของความถี่ได้ การแกว่งของความถี่อย่างรุนแรงนี้จะส่งผลเสียต่อเสถียรภาพโดยรวมของระบบไฟฟ้ากำลังโดยตรงซึ่งจะทำให้ระบบนั้นไม่สามารถจ่ายกำลังไฟฟ้าได้ นอกจากนี้ แนวโน้มการเพิ่มขึ้นอย่างสูงของผู้ผลิตไฟฟ้าอิสระ (Independent Power Producers, IPPs) ซึ่งความสามารถในการควบคุมความถี่ไม่เพียงพอก็มีผลเสียอย่างมากต่อเสถียรภาพทางความถี่ของระบบ ภายใต้สถานการณ์ดังกล่าวข้างต้นวิธีการให้บริการการควบคุมเสถียรภาพทางความถี่แบบใหม่ซึ่งมีประสิทธิภาพสูงกว่าระบบควบคุมที่ใช้ในปัจจุบันจึงมีความต้องการเป็นอย่างสูง

งานวิจัยนี้นำเสนอการนำอุปกรณ์ทางอิเลคทรอนิกส์กำลังซึ่งมีความเร็วในการควบคุมสูงที่เรียกว่า Static Synchronous Series Compensator, SSSC ซึ่งมีความสามารถในการควบคุมการไหลของกำลังไฟฟ้าในสายเชื่อมโยงแบบไดนามิกส์และสามารถนำมาประยุกต์ใช้เพื่อควบคุมเสถียรภาพทางการแกว่งของความถี่ของระบบไฟฟ้ากำลังได้อย่างรวดเร็ว โดยงานวิจัยนี้มุ่งเน้นไปในด้านการออกแบบระบบควบคุมโรบัสแบบแบบต่อเนื่องและดิสครีตของ SSSC นอกจากเพื่อให้มีประสิทธิภาพในการลดความรุนแรงของการแกว่งของการแกว่งของความถี่และยังเพิ่มคุณสมบัติ Robustness ของตัวควบคุมต่อความไม่แน่นอนต่าง ๆซึ่งจะเกิดขึ้นในระบบ (System Uncertainties) ให้ม...นือกว่าตัวควบคุมที่ไม่มีคุณสมบัติที่ไม่มีคุณสมบัตินี้

2. วัตถุประสงค์

เพื่อศึกษาถึงปัญหาในการออกแบบตัวควบคุมโรบัสแบบต่อเนื่องและดิสครีตของ SSSC พร้อมวิธีแก้ไขปัญหา เพื่อใช้ในการควบคุมเสถียรภาพของการแกว่งของความถี่ในระบบไฟฟ้ากำลังที่เชื่อมโยงกันในลักษณะต่าง ๆ เช่น Loop, Radial เป็นต้น

2.1. เพื่อศึกษาวิธีการออกแบบตัวควบคุมโรบัสแบบต่อเนื่องและดิสครีตของ SSSC เพื่อให้ได้ตัวควบคุมโรบัสที่มีประสิทธิภาพสูงและมีโครงสร้างที่ไม่ซับซ้อนเพื่อที่จะสามารถนำมาประยุกต์ในการใช้งานจริงได้

2.2. เพื่อศึกษาถึงแนวทางการทำงานร่วมกันระหว่างตัวควบคุมโรบัสของ SSSC ที่นำเสนอและระบบควบคุมเสถียรภาพทางความถี่ที่ใช้กันอยู่ในปัจจุบันคือ ระบบโกเวอร์เนอร์

2.3. เพื่อศึกษาเปรียบเทียบความแตกต่างระหว่างตัวควบคุมโรบัสที่ถูกออกแบบโดยวิธีที่นำเสนอ และตัวควบคุมที่ไม่มีคุณสมบัติ Robustness

3. ระเบียบวิธีวิจัย

3.1 ตั้งปัญหาการออกแบบตัวควบคุมโรบัสแบบต่อเนื่องของ SSSC ในระบบไฟฟ้ากำลังแบบเชื่อมโยงซึ่งเกิดการแกว่งของความถี่อย่างรุนแรงจากสาเหตุต่าง ๆ เช่น การเปลี่ยนแปลงภาระไฟขนาดใหญ่อย่างรวดเร็ว เป็นต้น

3.2 สร้างแบบจำลองคณิตศาสตร์ของตัวควบคุมโรบัสแบบต่อเนื่องของ SSSC ในระบบไฟฟ้ากำลังแบบเชื่อมโยงที่กำลังพิจารณา โดยรวมไปถึงแบบจำลองทางคณิตศาสตร์ซึ่งแทนความไม่แน่นอนในระบบที่เกิดขึ้น

3.3 ศึกษาแนวความคิดในการออกแบบตัวควบคุมของ SSSC รวมไปถึงการนำทฤษฎีระบบควบคุมโรบัสแบบต่อเนื่องมาประยุกต์ใช้ในการออกแบบตัวควบคุมของ SSSC

3.4 ออกแบบตัวควบคุมโรบัสแบบต่อเนื่องของ SSSC

3.5 เปรียบเทียบตัวควบคุมโรบัสแบบต่อเนื่องที่ถูกออกแบบมากับตัวควบคุมแบบต่อเนื่องที่ไม่มีคุณสมบัติ Robustness หลังจากนั้นทำการรวบรวมผลการทดสอบตัวควบคุมนำมาเขียนเป็นบทความวิชาการเพื่อลงในวารสาร Electric Power System Research และได้รับการยอมรับในการตีพิมพ์เรียบร้อยแล้ว

3.6 ศึกษาทฤษฎีการออกแบบตัวควบคุมแบบดีสครีต หลังจากนั้นทำการออกแบบตัวควบคุมแบบดีสครีต โดยการพัฒนา

มาจากการออกแบบตัวควบคุมแบบต่อเนื่อง

3.7 นำตัวควบคุมแบบดีสครีตที่ทำการออกแบบมาแล้วมาทดสอบประสิทธิภาพ เปรียบเทียบกับตัวควบคุมแบบดีสครีตที่ไม่มีคุณสมบัติ Robustness ในด้านต่างๆ อาทิ เช่น ความทนทานต่อความไม่แน่นอนในระบบ, ความสามารถในการลดความรุนแรงในการแกว่งของความถี่ในระบบไฟฟ้ากำลัง เป็นต้น แล้วนำผลการวิจัยที่ได้จากขั้นตอนดังกล่าวนำมาเขียนเป็นบทความวิชาการเพื่อลงในวารสาร ASEAN Journal on Science & Technology for Development ซึ่งได้ส่งบทความไปแล้ว กำลังรอผลการ Review อยู่

Robust Discrete Control Design of Static Synchronous Series Compensator (SSSC) for Stabilization of Frequency Oscillations in An Interconnected Power System

Issarachai Ngamroo

A research submitted to the Thailand Research Fund for the Post-Doctoral Research Fellow Program

30 June 2003

Acknowledgements

I would like to express my gratitude to Assistant Professor Dr. Waree Kongprawechnon, my mentor for his support, patience, guidance and encouragement during the research.

I gratefully acknowledge the generous support I have received throughout the research from the Thailand Research Fund through the postdoctoral program.

Contents

Chapter 1

Introduction

1.1 Motivation of The Research

Nowadays, electric power systems all over the world are undergoing drastic restructuring. The trend is toward deregulating an industry that has traditionally been a regulated monopoly to allow for economic competition. The restructuring of the conventional vertically integrated utilities into separated generation, transmission and distribution companies has been accomplished first in United Kingdom and almost everywhere up to now. This not only prompts a heavy competition among utilities but also increase the diversity of resource options for customers [1, 2].

The major change that has happened in the deregulated power system is the proliferation of the non-utility generation such as Independent Power Producers (IPPs) that play an important role in participating in power transactions. In the case that many IPPs which have not sufficient abilities of frequency and voltage controls, have been concentrated in any power system, it is very important to consider that how the control services of system frequency and voltage should be implemented.

Furthermore, it is reasonably expected that the power system in the future will be more and more interconnected with significant inter-area power flows along tie lines. Interconnected tie lines have the benefits of providing inter-area support for abnormal conditions as well as transmission paths for contractual energy exchanges between areas. Under this situation, there is possibility of the occurrence of unbalanced area power demands which may cause instability problems of frequency and inter-area power oscillations. To overcome this problem, a dynamic control of tie line power flow with the aim of not only alleviating the heavy tie line power flows, but also stabilizing the system frequency oscillations against the sudden changes in load demands, is significantly required.

In a deregulated power industry, any power system controls such as frequency and voltage controls will be served as ancillary services [3-6]. Especially, stabilization service of frequency oscillations in an interconnected system becomes challenging when implemented in the future competitive environment [7,8]. A new stabilization service which emphasizes not only on efficiency, reliability and economics but also on advanced and improved control for satisfying the requirement of power system operation, is highly expected.

1.2 Current Technology and Problems of Stabilization of Frequency Oscillations in Interconnected Power System

At present, the control of system frequency is operated by the Automatic Generation Controls (AGC) strategy of governor system developed nearly half a century ago [9-10]. The primary objectives of AGC in multi-area interconnected system are to regulate frequency to the specified nominal value and to maintain the interchange power between interconnected areas at the scheduled values by adjusting the output of selected generators. This function is commonly referred to as Load-Frequency Control (LFC) [11-13]. Current LFC strategies are based on three popular methods, i.e., Tie Lie Bias Control (TBC), Flat Frequency Control (FFC) and Flat Tie Line Control (FTC). For example, the purpose of TBC scheme is to alleviate not only the system frequency deviation but also the tie line power deviation due to changes in load demand by adjusting and coordinating the generation power between interconnected areas.

The AGC strategy is widely accepted and is well entrenched in practice in many countries. Nevertheless, its performance has never been viewed as fully satisfactory. There are significant reasons which explain about its deficiencies and why AGC performance might be less than ideal as follows [9]. AGC strategy is incapable of absorbing an abrupt large power mismatch between the load demand and the generation power due to its slow response characteristics. Even in the case of the operation by governor free, it is unable to play any role in suppressing the magnitude of the transient frequency which occurs within seconds after a rapid change in generation or load in the system. In addition, the capability of AGC is also deteriorated by some inevitable system nonlinearities such as the influences of deadbands in mechanical linkage and transport delays.

In addition, in the view point of dynamics between interconnected system, there is a possibility that the low frequency oscillations of inter-area power flows occur due to the heavy power transfer in tie line and the unbalance of area power demands [14-15]. This may cause a serious instability problem of frequency oscillations in interconnected systems. AGC scheme is neither able nor can be expected to play any role in damping eletromechanical dynamic including inter-area oscillations [9]. Present AGC scheme may no longer be able to solve these problems. A new stabilization strategy of frequency oscillations in interconnected power system to provide not only a dynamic control of interconnected tie line power flow but also a fast stabilization of the transient frequency deviation is significantly required.

1.3 Purpose of This Report

Recently, the concept of utilizing power electronics devices for power system control has been purposed as FACTS (Flexible AC Transmission Systems) [16]. The FACTS concept [17-19] is to increase the capability, controllability and flexibility of power transfer of existing AC transmission facilities while maintaining the reliability of the power delivery. FACTS devices play an active role in determining real and reactive power flow by dynamic control of the power transfer parameters, i.e., transmission voltage, line impedance and phase angle. In other words, the AC transmission system is changed from a passive element to an active power delivery element. Among of them, a Static Synchronous Series Compensator [20-21] (SSSC) has been highly expected as an effective apparatus with an ability of fast power flow control. By virtue of this characteristic, SSSC is utilized for dynamically adjusting the network configuration to enhance steady state performance as well as transient stability in power systems.

In the AGC scheme, the interconnections among some areas have been considered as the channels of disturbances. Therefore, it has been important to suppress the frequency fluctuations by the coordination of governor systems among interconnected areas. On the contrary, the dynamic power flow control by the SSSC located in series with the tie line between two areas interconnected system, has the possibility to stabilize the system frequency through the interconnections. In this thesis, a new control method using an SSSC to provide a dynamic control of tie-line power flow for stabilization of frequency oscillations in AC interconnected power system is proposed. The active control of tie line power by SSSC is not only effective to stabilize the dynamic oscillatory behavior of the inter-are mode, but also capable of suppressing the transient frequency deviations. According to the proposed control, the power system which has a large frequency control capability, is able to offer the stabilization service of frequency oscillations to other interconnected areas which have not sufficient capabilities. The proposed frequency stabilization by SSSC can be expected to be an advanced method of interconnection of AC power systems competing against the interconnection by High Voltage Direct Current (HVDC) transmission system or Back To Back (BTB) system. Moreover, the proposed control is expected as a new ancillary service for stabilization of frequency oscillations in any interconnected systems which have insufficient control capabilities, instead of the installation of large power generation units for frequency control.

Chapter 2

Stabilization of Frequency Oscillations by Static Synchronous Series Compensator

2.1 Introduction

Flexible AC Transmission System (FACTS) [16-19] is a sophisticated technology sponsored by Electric Power Research Institute (EPRI) to help the utility industry in order to fully utilize available AC transmission system. A major thrust of FACTS technology is based on the utilization of reliable high-speed power electronics that provide dynamic control of the power transfer actively [22]. Among of FACTS devices, a phase shifter with a solid-state voltage source inverter using gate turn-off (GTO) thyristors [20] such as Static Synchronous Series Compensator (SSSC) [21], Unified Power Flow Controller (UPFC) [23] etc., has several attractive characteristics for power system applications. Especially, it is capable of emulating an inductive or a capacitive reactance, therefore, influences the power flow in the transmission directly. Moreover, even if the tie line power flow is very small, in other words the tie line current is near zero, a phase shifter still has effect on power flow control. This exhibits the superior characteristics of phase shifter beyond the series capacitance or reactance. The sophisticated characteristics of solid-state phase shifter motivate many power system applications, e.g., enhancement of transient stability [24], improvement of system power dynamics [25], power system stabilization [26], loop power flow control [27], damping of subsynchronous resonance [28] etc. Several studies about modeling and experiment with the aim of realizing the solid-state phase shifter in practice have been also reported [29-30]. Moreover, some types of solid-state phase shifter have been already operated in real power system [31].

In this report, a new control strategy using a Static Synchronous Series Compensator (SSSC) to provide an active control facility for stabilization of frequency oscillations in an interconnected power system is proposed. An SSSC located in series with the tie line between two areas interconnected system is capable of controlling the tie line power flow dynamically. Moreover, it has the possibility to stabilize the system frequency oscillations by fast tie line power modulations through the interconnections.

This chapter focuses on the concept and practical motivation of the proposed stabilization of frequency oscillations in an interconnected power system by SSSC. In addition, the derivation of mathematical model of SSSC is curried out.

2.2 Concept and Practical Motivations of Proposed Control Strategy

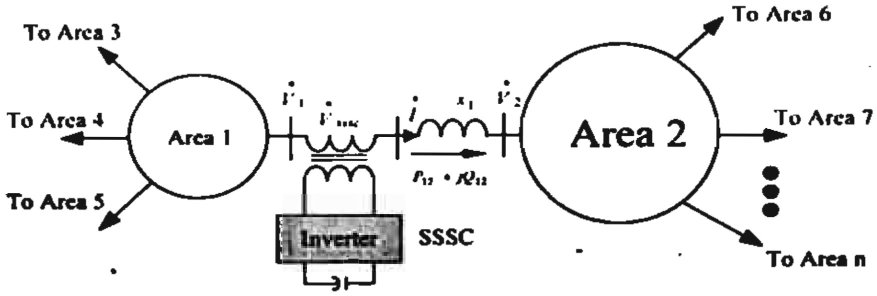

Figure.2.1: An SSSC in a multi-area interconnected power system

Figure 2.1 shows a general multi-area interconnected power system. Both areas have several interconnections other than area 1 or 2. A phase shifter is located in series with the tie line between areas 1 and 2. It is assumed that frequency control of area 1 is beyond its capability while the area 2 has the capability enough to spare for stabilization service of frequency oscillations in an area 1. Accordingly, the tie line power modulation by a phase shifter which is supported by the capability of area 2, is utilized to stabilize the frequency oscillations of area 1.

The practical motivations for application of the proposed phase shifter to stabilization of frequency oscillations are as follows,

1. In a competitive deregulated system, non-utility generations such as many Independent Power Producers (IPPs) which have not sufficient abilities of frequency control, tend to increase significantly. When they have been concentrated in an area, it is important to pay attention to how this area frequency should be controlled. Under this circumstance, the proposed phase shifter can utilize the frequency control capabilities of other interconnected areas to stabilize the frequency oscillation of this area. The proposed control strategy will be a new option of stabilization service of frequency oscillation for any power system which has not sufficient frequency control capabilities, instead of the installation of large power generation units for frequency control.
2. Nowadays, various kinds of apparatus with large capacity and consumptions increase significantly; for typical examples, a magnetic levitation transportation, large scale accelerator, testing plant for nuclear fusion and so on. In addition, even in the case that an ordinary scale factory like a steel manufacture is installed in a small power system, it may cause a serious frequency fluctuation problem. Under this situation, the conventional governor systems, even in the case of the operation of governor free, may no longer be able to absorb the frequency oscillations. In order to compensate these

sudden load perturbations and stabilize system frequency oscillations quickly, the proposed phase shifter is expected as one of the most effective countermeasure.

3. Due to the benefits of scale merit, the construction of power generation unit with large capabilities tends to increase considerably. This may cause a transient depressed frequency when the losses of generation units suddenly occur. To tackle this situation, the proposed control is very suitable option. Phase shifter is capable of borrowing the control capabilities of other interconnected areas in order to alleviate the transient frequency deviations rapidly.

2.3 Mathematical Model of SSSC

In this study, the mathematical model of the SSSC for stabilization of frequency oscillations is derived from the characteristic of power flow control by SSSC [20-21]. By adjusting the output voltage of SSSC ($\bar{V}_{SSSC}$), the tie-line power flow ($P_{12} + jQ_{12}$), can be directly controlled as shown in Fig.2.1. Since the SSSC fundamentally controls only the reactive power, then the phasor $\bar{V}_{SSSC}$ is perpendicular to the phasor of line current $\bar{I}$, which can be expressed as

$$\bar{V}_{SSSC} = jV_{SSSC} \cdot \bar{I}/I \tag{2.1}$$

where V_{SSSC} and I are the magnitudes of $\bar{V}_{SSSC}$ and $\bar{I}$, respectively. Note that, $\bar{I}/I$ is a unit vector of line current. Therefore, the current $\bar{I}$ in Fig. 2.1, can be expressed as

$$\bar{I} = \frac{\bar{V}_1 - \bar{V}_2 - jV_{sssc}\bar{I}/I}{jX_L} \tag{2.2}$$

where X_L is the reactance of a tie-line, $\bar{V}_1$ and $\bar{V}_2$ are the voltages at buses 1 and 2, respectively. The active power and reactive power flow through bus 1 are

$$P_{12} + jQ_{12} = \bar{V}_1\bar{I}^* \tag{2.3}$$

where $\bar{I}^*$ is a conjugate of $\bar{I}$. Substituting $\bar{I}$ from (2.2) into (2.3) yields

$$P_{12} + jQ_{12} = \frac{V_1V_2}{X_L}\sin(\delta_1 - \delta_2) - V_{sssc}\frac{\bar{V}_1\bar{I}^*}{X_L I} + j\left(\frac{V_1^2}{X_L} - \frac{V_1V_2}{X_L}\cos(\delta_1 - \delta_2)\right) \tag{2.4}$$

where $\bar{V}_1 = V_1e^{j\delta_1}$ and $\bar{V}_2 = V_2e^{j\delta_2}$. In the second term of the right hand side of (2.4), $\bar{V}_1\bar{I}^*$ is equal to $P_{12} + jQ_{12}$ (see (3.3)). Accordingly, the relation in the real part of (2.4) provides

$$P_{12} = \frac{V_1V_2}{X_l}\sin(\delta_1 - \delta_2) - \frac{P_{12}}{X_l I}V_{sssc} \tag{2.5}$$

In (2.5), the second term of the right hand side is the active power controlled by SSSC. Here, it is assumed that V_1 and V_2 are constant and the initial value of V_{sssc} is zero, i.e. $V_{sssc0} = 0$. By linearizing (2.5) about an initial operating point,

$$\Delta P_{12} = \frac{V_1 V_2 \cos(\delta_{10} - \delta_{20})}{X_l}(\Delta\delta_1 - \Delta\delta_2) - \frac{P_{120}}{X_l I_0}\Delta V_{sssc} \qquad (2.6)$$

where the subscript " 0 " denotes the value at the initial operating point. As the voltage deviation of SSSC (ΔV_{sssc}) is adjusted, the power output deviation injected by SSSC can be controlled as $\Delta P_{SSSC} = -(P_{120}/X_l I_0)\Delta V_{sssc}$. Equation (2.6), therefore, implies that the SSSC is capable of controlling the active power independently. Here, the SSSC is represented by the active power controller. The control effect by SSSC is expressed by the injected power deviation ΔP_{SSSC} instead of $-(P_{120}/X_l I_0)\Delta V_{sssc}$. As a result, (2.6) can be expressed as

$$\Delta P_{12} = \Delta P_{T12} + \Delta P_{sssc} \qquad (2.7)$$

where

$$\Delta P_{T12} = \frac{V_1 V_2 \cos(\delta_{10} - \delta_{20})}{X_l}(\Delta\delta_1 - \Delta\delta_2)$$

$$= T_{12}(\Delta\delta_1 - \Delta\delta_2) \qquad (2.8)$$

and T_{12} is a synchronizing power coefficient.

2.4 Structure of Frequency Stabilizer

In this study, the structure of the frequency stabilizer is based on a second-order lead/lag compensator as shown in Fig. 2.2. There are five parameters for each designed frequency stabilizer consisting of a stabilization gain K, time constants T_1, T_2, T_3, and T_4.

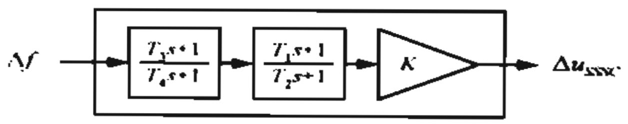

Figure 2.2: Configuration of 2nd order lead/lag based SSSC frequency stabilizer

Since the control purpose of the frequency stabilizer is to enhance the damping of the inter-area mode. The frequency deviation of each target area (Δf_i, $i = 1$ and 3) which provides information of each mode of interest, is used as the input signal for each frequency stabilizer. The control parameters of each frequency stabilizer are searched based on the proposed objective function explained in the following chapter.

Chapter 3

Design of Robust Frequency Stabilizer of SSSC in Continuous Time Domain

3.1 Purpose of this chapter

In this chapter, the robust design method based on continuous time domain of the frequency stabilizer is proposed. First, the problem statement is explained. Next, the design methodology, that is a concept of coordinated control of SSSC and governor, a linearized model of power system, a model reduction by overlapping decompositions technique, a tabu search algorithm for solving optimization problem are described. Subsequently, the effects of the designed frequency stabilizer are evaluated in the four-area interconnected power systems.

3.2 Problem Statement

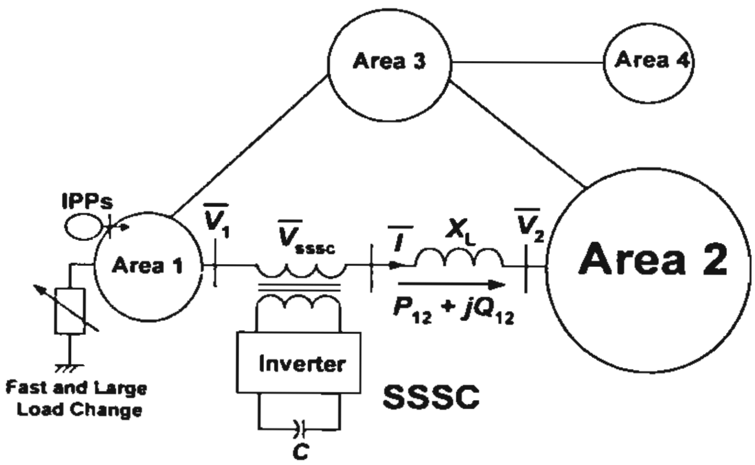

Figure 3.1: An SSSC in a four-area interconnected power system

Figure 3.1 shows the four-area interconnected power system with a loop configuration. This system is used to explain the motivation of the proposed control design. It is assumed that a large load with rapid change has been installed in an area 1. This load change causes serious frequency oscillations. Moreover, IPPs that do not possess frequency control capabilities are included in an area 1. Under this situation, the governors in an area 1 can not sufficiently provide adequate frequency control. On the contrary, the area 2 has large control capability enough to spare for other areas. Therefore, an area 2 offers a service of frequency stabilization to an area 1 by using the SSSC. Since SSSC is a series-connected device, the power flow control effect is independent of an installed location. In the proposed design method, the SSSC controller uses the frequency deviation of area 1 as a local signal input. Therefore, the SSSC is placed at the point near an area 1. Note that the SSSC is utilized as the energy transfer device from area 2 to area 1. As the frequency fluctuation in an area 1 occurs, the SSSC will provide the dynamic control of a tie line power via the system connections. By exploiting the system interconnections as the control channels, the frequency oscillations can be stabilized.

Additionally, in the interconnected system, variations of system parameters, various load changes etc. cause several system uncertainties. To achieve the high robust stability of system, the effect of uncertainties should be taken into account in the design process. In this study, the aim of the proposed frequency stabilizer design is not only to enhance the damping of interested inter-area oscillation modes, but also to improve the robust stability of system against uncertainties.

3.3 Design Methodology

3.3.1 Coordinated Control of SSSC and Governor

The response of SSSC is extremely rapid when compared to the conventional frequency control system, i.e. a governor. The difference in responses signifies that the SSSC and governor can be coordinated. When a power system is subjected to a sudden load disturbance, the SSSC quickly acts to damp frequency oscillation in the transient period. Subsequently, the governor continues to eliminate the steady-state error in frequency oscillation. As the periods of operation for the SSSC and governor do not overlap, the dynamic of governor can then be neglected in the design of frequency stabilizer for the sake of simplicity.

3.3.2 Linearized Power System Model

A study system depicted in Fig. 3.1 is used to explain the proposed control design of SSSC. The linearized four-area interconnected system including the active power model of SSSC is delineated in Fig.3.2. Based on the coordinated control of SSSC and governors, the dynamics of governors are eliminated in this figure. The active power controller of SSSC has a structure of the lead/lag compensator $K_{RB}(s)$ with an output signal ΔP_{ref}. In this study, the dynamic characteristic of SSSC is modeled as the first order controller with time constant

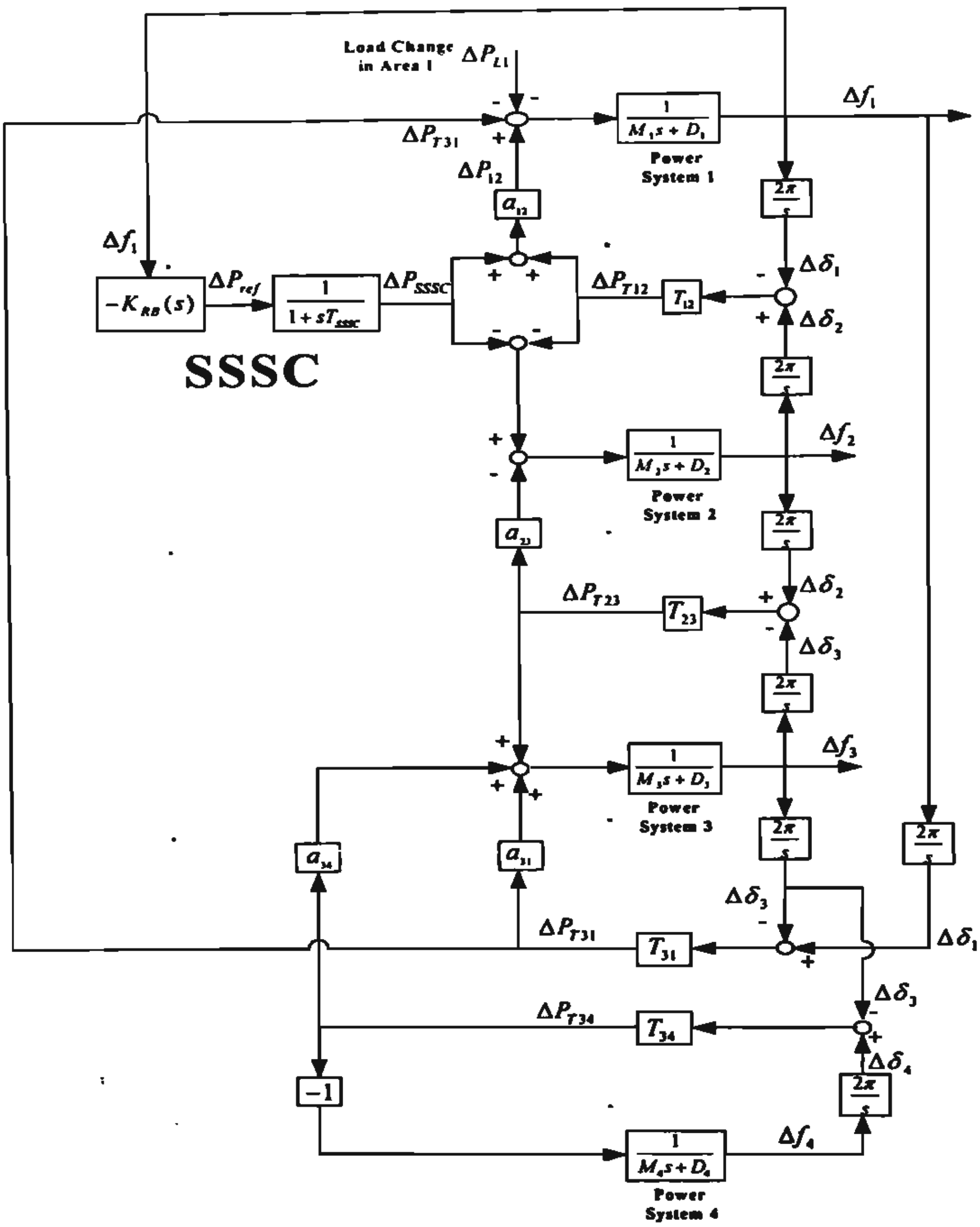

Figure 3.2: An SSSC in a linearized four-area interconnected system without governors

T_{SSSC}. Note that the injected power deviation of SSSC, ΔP_{SSSC} acting positively on the area 1 reacts negatively on the area 2. Therefore, ΔP_{SSSC} flows into both areas with different signs (+, -), simultaneously. This characteristic represents the physical meaning of (2.7). The linearized system in Fig.3.2 can be expressed as

$$S: \begin{bmatrix} \dot{\Delta f_1} \\ \dot{\Delta P_{T12}} \\ \dot{\Delta f_2} \\ \dot{\Delta P_{T23}} \\ \dot{\Delta f_3} \\ \dot{\Delta P_{T34}} \\ \dot{\Delta f_4} \end{bmatrix} = \begin{bmatrix} -\frac{D_1}{M_1} & a_{S12} & 0 & a_{S14} & 0 & 0 & 0 \\ -2\pi T_{12} & 0 & 2\pi T_{12} & 0 & 0 & 0 & 0 \\ 0 & -\frac{1}{M_2} & -\frac{D_2}{M_2} & -\frac{a_{23}}{M_2} & 0 & 0 & 0 \\ 0 & 0 & 2\pi T_{23} & 0 & -2\pi T_{23} & 0 & 0 \\ 0 & a_{S52} & 0 & a_{S54} & -\frac{D_3}{M_3} & \frac{a_{34}}{M_3} & 0 \\ 0 & 0 & 0 & 0 & -2\pi T_{34} & 0 & 2\pi T_{34} \\ 0 & 0 & 0 & 0 & 0 & -\frac{1}{M_4} & -\frac{D_4}{M_4} \end{bmatrix} \begin{bmatrix} \Delta f_1 \\ \Delta P_{T12} \\ \Delta f_2 \\ \Delta P_{T23} \\ \Delta f_3 \\ \Delta P_{T34} \\ \Delta f_4 \end{bmatrix} + \begin{bmatrix} \frac{a_{12}}{M_1} \\ 0 \\ -\frac{1}{M_2} \\ 0 \\ 0 \\ 0 \\ 0 \end{bmatrix} \Delta P_{SSSC} \quad (3.1)$$

Δf_i is the frequency deviation of area i, ΔP_{Tij} is the power deviation between areas i and j, M_i is the inertia constant of area i, D_i is the damping coefficient of area i, a_{ij} is the area capacity ratio between areas i and j, T_{ij} is the synchronizing power coefficient of the tie-line between areas i and j, where $i, j = 1,..,3$. Here $a_{S12} = (a_{12} + T_{31}/T_{12})/M_1$, $a_{S14} = -T_{31}/(M_1T_{23})$, $a_{S52} = -a_{31}T_{31}/(M_3T_{12})$, $a_{S54} = (1 + a_{31}T_{31}/T_{23})/M_3$. The variable ΔP_{T31} is represented in terms of ΔP_{T12} and ΔP_{T23} by

$$\Delta P_{T31} = -\frac{T_{31}}{T_{12}}\Delta P_{T12} + \frac{T_{31}}{T_{23}}\Delta P_{T23} \quad (3.2)$$

Thus, ΔP_{T31} has disappeared in (3.1). This system has three conjugate pairs of complex eigenvalues and a negative real eigenvalue. The former corresponds to three inter-area oscillation modes, and the latter the inertia center mode. In this paper, the design purpose of SSSC is to enhance the damping of the inter-area mode between areas 1 and 2.

3.3.3 Model Reduction by Overlapping Decompositions [32]

The concept of overlapping decompositions is applied to the system (3.1) with the aim of extracting the subsystem where the inter-area mode between areas 1 and 2 is preserved. The system (3.1) is referred to as the system S. The state variables of S are classified into three groups, i.e. $x_1 = [\Delta f_1]$, $x_2 = [\Delta P_{T12}]$, $x_3 = [\Delta f_2, \Delta P_{T23}, \Delta f_3, \Delta P_{T34}, \Delta f_4]^T$. Therefore, the system S can be expressed in compact form as

$$S \; : \; \begin{bmatrix} \dot{x}_1 \\ \dot{x}_2 \\ \dot{x}_3 \end{bmatrix} = \begin{bmatrix} A_{11} & A_{12} & A_{13} \\ A_{21} & A_{22} & A_{23} \\ A_{31} & A_{32} & A_{33} \end{bmatrix} \begin{bmatrix} x_1 \\ x_2 \\ x_3 \end{bmatrix} + \begin{bmatrix} B_{11} \\ B_{21} \\ B_{31} \end{bmatrix} \Delta P_{SSSC} \tag{3.3}$$

The sub-matrices A_{ij} and B_{i1}, $(i, j = 1,2,3)$ have appropriate dimensions identical to the corresponding state and input vectors. According to the process of overlapping decompositions, the system S can be expanded as

$$\tilde{S} \; : \; \begin{bmatrix} \dot{z}_1 \\ \dot{z}_2 \end{bmatrix} = \begin{bmatrix} A_{11} & A_{12} & 0 & A_{13} \\ A_{21} & A_{22} & 0 & A_{23} \\ A_{21} & 0 & A_{22} & A_{23} \\ A_{31} & 0 & A_{32} & A_{33} \end{bmatrix} \begin{bmatrix} z_1 \\ z_2 \end{bmatrix} + \begin{bmatrix} B_{11} \\ B_{21} \\ B_{21} \\ B_{31} \end{bmatrix} \Delta P_{SSSC} \tag{3.4}$$

where $z_1 = \left[x_1^T, x_2^T\right]^T$ and $z_2 = \left[x_2^T, x_3^T\right]^T$. The system $\tilde{S}$ in (3.4) can be decomposed into two interconnected overlapping subsystems,

$$\tilde{S}_1 \; : \; \dot{z}_1 = \left(\begin{bmatrix} A_{11} & A_{12} \\ A_{21} & A_{22} \end{bmatrix} z_1 + \begin{bmatrix} B_{11} \\ B_{21} \end{bmatrix} \Delta P_{SSSC} \right) + \begin{bmatrix} 0 & A_{13} \\ 0 & A_{23} \end{bmatrix} z_2 \tag{3.5}$$

$$\tilde{S}_2 \; : \; \dot{z}_2 = \left(\begin{bmatrix} A_{22} & A_{23} \\ A_{32} & A_{33} \end{bmatrix} z_2 \right) + \begin{bmatrix} A_{21} & 0 \\ A_{31} & 0 \end{bmatrix} z_1 + \begin{bmatrix} B_{21} \\ B_{31} \end{bmatrix} \Delta P_{SSSC} \tag{3.6}$$

The state variable x_2, i.e. the tie line power deviation between areas 1 and 2 (ΔP_{T12}), is repeatedly included in both subsystems, which implies " *Overlapping Decompositions* ".

For system stabilization, consider two interconnected subsystems $\tilde{S}_1$ and $\tilde{S}_2$. The terms in the right hand sides of (3.5) and (3.6) can be separated into the decoupled subsystems (as indicated in the parenthesis in (3.5) and (3.6)) and the interconnection subsystems. As mentioned in [32], if each decoupled subsystem can be stabilized by its own input, the asymptotic stability of the interconnected overlapping subsystems $\tilde{S}_1$ and $\tilde{S}_2$ are maintained. Moreover, the asymptotic stability of the original system S is also guaranteed. Consequently, the interactions of the decoupled subsystems with the interconnection subsystems in (3.5) and (3.6) are regarded as perturbations. They can be neglected during control design. As a result, the decoupled subsystems of $\tilde{S}_1$ and $\tilde{S}_2$ can be expressed as

$$\tilde{S}_{D1} \; : \; \dot{z}_1 = \begin{bmatrix} A_{11} & A_{12} \\ A_{21} & A_{22} \end{bmatrix} z_1 + \begin{bmatrix} B_{11} \\ B_{21} \end{bmatrix} \Delta P_{SSSC} \tag{3.7}$$

$$\tilde{S}_{D2} \; : \; \dot{z}_2 = \begin{bmatrix} A_{22} & A_{23} \\ A_{32} & A_{33} \end{bmatrix} z_2 \tag{3.8}$$

In (3.7) and (3.8), there is a control input ΔP_{SSSC} appearing only in the subsystem $\tilde{S}_{D1}$. Here, the decoupled subsystem $\tilde{S}_{D1}$ is regarded as the designed system, which can be expressed as

$$G \ : \ \begin{bmatrix} \Delta\dot{f}_1 \\ \Delta\dot{P}_{T12} \end{bmatrix} = \begin{bmatrix} -D_1/M_1 & a_{S12} \\ -2\pi T_{12} & 0 \end{bmatrix} \begin{bmatrix} \Delta f_1 \\ \Delta P_{T12} \end{bmatrix} + \begin{bmatrix} a_{12}/M_1 \\ 0 \end{bmatrix} \Delta P_{SSSC} \tag{3.9}$$

It can be verified that the eigenvalues of (3.9) are complex conjugate and are assumed to be $-\sigma \pm j\omega_d$. These complex eigenvalues correspond to the inter-area oscillation mode between areas 1 and 2 in the original system S. By virtue of overlapping decompositions, the physical characteristic of the original system S is still preserved after the process of system reduction. This explicitly shows the merit of overlapping decompositions.

By incorporating the dynamic characteristic of the SSSC, (3.9) becomes

$$G \ : \ \begin{bmatrix} \Delta\dot{f}_1 \\ \Delta\dot{P}_{T12} \\ \Delta\dot{P}_{sssc} \end{bmatrix} = \begin{bmatrix} -D_1/M_1 & a_{S12} & a_{12}/M_1 \\ -2\pi T_{12} & 0 & 0 \\ 0 & 0 & -1/T_{SSSC} \end{bmatrix} \begin{bmatrix} \Delta f_1 \\ \Delta P_{T12} \\ \Delta P_{sssc} \end{bmatrix} + \begin{bmatrix} 0 \\ 0 \\ 1/T_{SSSC} \end{bmatrix} \Delta P_{ref} \tag{3.10}$$

For the input signal of SSSC controller, two available local signals, i.e., area 1 frequency deviation (Δf_1) and the tie line 1-2 power deviation (ΔP_{T12}) are taken into consideration. By calculating the right eigenvector of the oscillation mode between areas 1 and 2, the degree of activity [12] of Δf_1 and ΔP_{T12} in this mode can be evaluated. From (3.9), the eigenvalues representing the oscillation mode are $\lambda_{1,2} = -0.015 \pm j3.5316$. The magnitudes of elements of the right-eigenvectors that correspond to Δf_1 and ΔP_{T12} are 0.6088 and 0.1953, respectively. As a result, Δf_1 provides higher degree of activity in this mode. Consequently, Δf_1 is used as the input signal of SSSC controller. The negative feedback control scheme of SSSC controller can be expressed by

$$\Delta P_{ref} = -K_{RB}(s)\Delta f_1 \tag{3.11}$$

The robust controller $K_{RB}(s)$ is in form of a lead/lag stabilizer as

$$K_{RB}(s) \ = \ K \frac{T_w s}{1+T_w s} \frac{(1+T_1 s)}{(1+T_2 s)} \frac{(1+T_3 s)}{(1+T_4 s)} \tag{3.12}$$

where K : a controller gain

T_1, T_2, T_3, T_4: lead/lag time constants [sec]

T_w : a washout time constant [sec]

Here, T_w is set to 10 [sec]. The control parameters K, T_1, T_2, T_3, and T_4 are searched based on the objective function explained in the next section.

3.3.4 Determination of Objective Function

In derivation of the objective function, both attenuation performance of system disturbances, and robust stability of controller against system uncertainties are taken into consideration. Since the main purpose of SSSC is to limit the peak frequency deviation following a sudden load perturbation, the peak frequency deviation can be used as a design specification. Assume that the eigenvalues corresponding to the mode of frequency oscillation in the uncontrolled system G are determined as $-\sigma \pm j\omega_d$. Thus, the system peak response to the unit step input [33] is given by

$$M_{P(actual)} = 1 + \exp(-\sigma\pi/\omega_d) \tag{3.13}$$

If the peak allowable frequency deviation of the controlled system is specified to be $M_{P(design)}$, then the magnitude of the difference between the design and the actual peak frequency deviations can be defined as

$$\psi = \left| M_{P(design)} - M_{P(actual)} \right| \tag{3.14}$$

This is the part of disturbance attenuation performance in the objective function that will be minimized.

Next, the robust stability against system uncertainties is taken into consideration. The possible uncertainties are ignored nonlinear characteristics of the study system, ranges and bounds for uncertain system parameters etc. Practically, it is hardly to know about the information of all uncertainties existing in the system. To consider such system uncertainties, the unstructured uncertainty can be applied. In general, an upper bound of the magnitude (or size) of unstructured uncertainty can be estimated. If the magnitude of system uncertainties is less than this upper bound, the robust stability of system is guaranteed. Here, the multiplicative uncertainty [33-25] is applied to represent the unstructured uncertainty in the system, as shown in Fig.3.3. Note that $\tilde{G}$ is a nominal system transfer function, Δ_m is a stable multiplicative perturbation, and $\tilde{K}$ is a controller designed to ensure the internal stability of the nominal closed loop.

Based on the small-gain theorem [33-35], the closed loop system will be robustly stable if

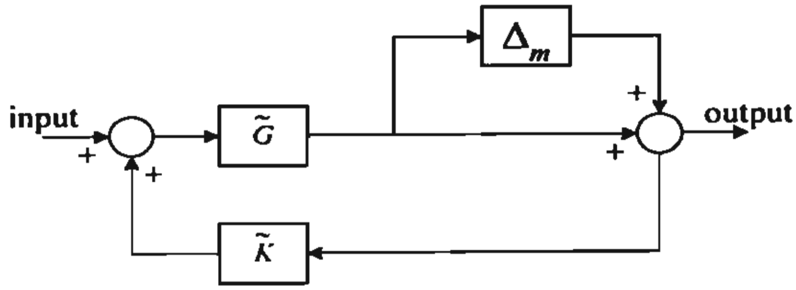

Figure 3.3: Feedback system with multiplicative uncertainty

$$|\Delta_m| \; < \; \frac{1}{\left|\tilde{G}\tilde{K}(1+\tilde{G}\tilde{K})^{-1}\right|} \tag{3.15}$$

where, the symbol $|\Delta_m|$ shows the magnitude of uncertainty. $\left|\tilde{G}\tilde{K}(1+\tilde{G}\tilde{K})^{-1}\right|$ is the magnitude of complementary sensitivity function which is referred to as $|T|$.

As mentioned in [33-35], the multiplicative stability margin (MSM) is defined as

$$MSM \; = \; 1/\|T\|_\infty \tag{3.16}$$

where $\|T\|_\infty$ is the ∞-norm of T. The MSM can be used to measure the robust stability of the system. Large value of MSM exhibits high robust stability of the system.

From (3.15) and (3.16), it is cleared that if the controller $\tilde{K}$ can be designed to minimize $\|T\|_\infty$, the MSM increases. As a result, the upper bound of $|\Delta_m|$ is enlarged, and the high robust stability will be ensured. Thus, the robustness index in the objective function can be defined in normalized form as,

$$\gamma \; = \; \|T\|_\infty / \|T\|_{\infty(initial)} \tag{3.17}$$

where $\|T\|_{\infty(initial)}$ is the ∞-norm of T at the initial solution of search process.

Combining (3.14) and (3.17), the objective function F can be formulated as,

$$\begin{aligned} &\text{Minimize} \quad F \; = \; c \cdot \psi + \gamma \\ &\text{Subject to} \quad K_{min} \; \le \; K \; \le \; K_{max} \\ &\qquad\qquad\quad T_{i,\,min} \; \le \; T_{\,i} \le \; T_{i,\,max} \end{aligned} \tag{3.18}$$

The constant coefficient "c" is used to weight ψ-term, so that $c \cdot \psi$ dominates γ during the parameters optimization. Note that, since γ is normalized to 1 at the initial solution, it is easy to find the value of "c" so that $c \bullet \psi$ is greater than 1. Eventually, the search process minimizes both terms until $c \bullet \psi$ meets the design specification and γ decreases to the possible minimum value. The minimum and maximum values of the gain K are set as 0.1 and 500, respectively. The minimum and maximum values of the time constants T_i $(i = 1,2,3,4)$ are set as 0.01 and 5, respectively. In this research, tabu searach algorithm (TSA) is employed to solve this optimization problem and search for optimal parameters of controller.

3.3.5 TSA for Parameter Determination

The TSA [36-37] is a promising tool for solving combinatorial optimization problem. The algorithm is an iterative improvement procedure that can start from any initial solution. Three basic components of TSA are used as follows: the trial solution generation, tabu list (TL) restriction, and termination criterion.

The concatenated encoding method is employed as shown in Fig. 3.4.

| aaaaaaaaaa | bbbbbbbbbb | cccccccccc |

x x x x x x x x x x

2^9 2^8 2^7 2^6 2^5 2^4 2^3 2^2 2^1 2^0

Figure 3.4: Example of a 30 bit concatenated encoding scheme

Each parameter is encoded in a binary string normalized over its range. This encoding method stacks each normalized string in series with each other to construct the string individual. The same number of n bits is used to represent each parameter string.

To obtain the actual value of each parameter, (3.19) is used to decode each normalized string to its decimal value for objective function evaluation.

$$P_i = P_{i,min} + \frac{B_i \times \left[P_{i,max} - P_{i,min}\right]}{2^n - 1} \tag{3.19}$$

where P_i is the actual value of the i-th parameter, $P_{i,min}$ is the minimum value of the i-th parameter, $P_{i,max}$ is the maximum value of the i-th parameter, B_i is the decimal integer value of binary string of the i-th parameter, and n is the number of bits representing each parameter. In the design process, 10 bits are used to represent each parameter.

To generate a trial solution of an initial feasible solution, one bit of binary string is flipped at a time. The maximum number of trial solutions per iteration is referred to a neighborhood solution space (NS). In this study, NS is set to 95% of the total number of bits $\lfloor 0.95 \times n \times N \rfloor$, where N is a number of parameter searched.

The example of generating trial solutions is shown in Fig.3.5.

Initial solution :	1001011010	1100011010	1110010011
Trial solution 1:	$\boxed{0}$001011010	1100011010	1110010011
Trial solution 2:	1$\boxed{1}$01011010	1100011010	1110010011
Trial solution 3:	10$\boxed{1}$1011010	1100011010	1110010011

Figure 3.5: Concept of Trial Solution Generation

The tabu list (TL) is referred to as an adaptive memory. The mechanism of TL is to keep attributes (bit positions) that created the best solution of the past iterations in the TL for a certain period. The attributes included in the TL cannot be used to create new solution candidates as long as they are in the TL. As the iteration proceeds, a new attribute enters into the TL as a fixed attribute. At the same time, the oldest attribute is released from the TL and becomes a free attribute, as illustrated in Fig. 3.6.

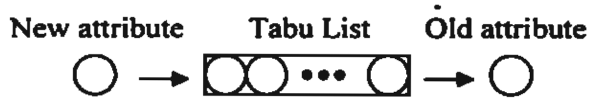

Figure 3.6: Mechanism of tabu list

In particular, a size of TL affects the quality of the solution. It controls the search process to avoid being trapped in local optima. Note that the size of TL or so-called the tabu length, is only the control parameter of TSA. Basically, the tabu length that provided good solutions usually grows with the size of the problem.

However, observing the quality of the solution can identify the appropriate tabu length. If the tabu lenght is too small, the cycling of solution occurs in the search process. On the other hand, if the size is too large, the search process is too restricted and may deteriorate the solution. Here, the tabu length is set to $\lfloor 0.7 \times n \times N \rfloor$.

Termination criterion refers to the condition that the search process will terminate. In the design, the search will terminate when the number of iterations reaches 100.

To apply the TSA for optimal parameter determination, the initial feasible solution is generated arbitrarily. A move to a neighbor solution is performed if the TL does not restrict it. The best solution is updated during the search process until the termination criterion is satisfied. The following notations are used for the TSA procedure:

TL: the tabu list.

NS: the neighborhood solution space.

$F(X)$: the objective function of solution X.

F_b^k: the best objective function at iteration k.

X_o^k: the initial feasible solution at iteration k,

X_m^k: a trial m solution at iteration k,

X_{cb}^k: the current best trial solution at iteration k,

X_b^k: the best solution reached at iteration k,

k_{max}: the maximum allowable number of iterations.

The tabu search procedure can be described as follows:

1. Read the constraints of searched parameters, the initial feasible solution X_o^k, and specification of the controller.
2. Specify the length of TL. k_{max}, and size of NS.
3. Initialize iteration counter k and empty TL.
4. Set $X_b^k = X_o^k$.
5. Execute tabu search procedure:
   - 5.1 Initialize the trial counter m to zero.
   - 5.2 Generate a trial solution X_m^k from X_o^k.
   - 5.3 If X_m^k is not feasible, go to 5.8.
   - 5.4 If X_m^k is the first feasible solution, set $X_{cb}^k = X_m^k$.
   - 5.5 Perform the tabu test. If X_m^k is tabued, then go to 5.8.
   - 5.6 If $F(X_m^k) < F(X_{cb}^k)$, set $X_{cb}^k = X_m^k$.
   - 5.7 If $F(X_m^k) < F(X_b^k)$, set $X_b^k = X_m^k$.
   - 5.8 If m is less than NS, $m = m + 1$ and go to 5.2.
   - 5.9 If there is no feasible solution, set $X_o^{k+1} = X_b^k$. Otherwise, set $X_o^{k+1} = X_{cb}^k$, and update TL.
6. If $k < k_{max}$, then $k = k + 1$, and go to 5.
7. X_b^k is the best solution found.

3.4 Simulation Results and Evaluation

To determine five control parameters by the TSA, the values of N, NS and the tabu length are set to 5, 47 and 35 respectively. Following the design procedures and appropriately setting $c = 1.4$ in the objective function, the following transfer function was obtained for the robust controller of SSSC when the peak frequency deviation was limited to $M_{p(design)} = 1.2$.

$$K_{RR}(s) = 3.5206 \frac{10s}{1+10s} \frac{(1+0.7758s)}{(1+2.5074s)} \frac{(1+1.9660s)}{(1+3.7269s)} \tag{3.20}$$

The SSSC controller in (3.20) is compared to the designed SSSC with $M_{p(design)} = 1.2$ but without robustness consideration. By neglecting γ in the objective function and setting $c = 1.0$, the designed result is given by

$$K_{NRR}(s) = 5.4753 \frac{10s}{1+10s} \frac{(1+0.1271s)}{(1+2.7026s)} \frac{(1+3.8781s)}{(1+2.4440s)} \tag{3.21}$$

Note that the designed controllers in (3.20) and (3.21) are referred to as " Robust SSSC " and " Non-robust SSSC " respectively.

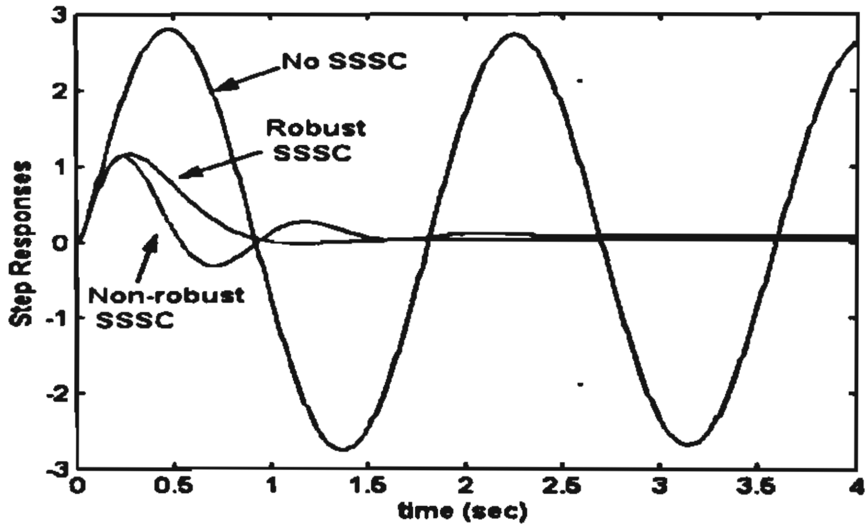

Figure 3.7: System step responses

Figure 3.7 depicts the step responses of G. Without SSSC, the oscillations are undamped with the first peak value about 2.7875. On the other hand, the first peak values are reduced to 1.2025 and 1.1225 in cases of Robust and Non-robust SSSCs, respectively. In addition, the MSM of system G with Robust SSSC is increased to 0.90 from 0.57 in case of system with Non-robust SSSC. This reveals the higher robustness of the system G with Robust SSSC.

To prove that the robust controller designed in the decoupled subsystem (3.7) can guarantee the stability of the expanded system (3.4) and also the original system (3.3), the eigenvalue analysis is employed. Table 3.1 shows the eigenvalues of decoupled subsystems

(3.7) and (3.8). The eigenvalues $\lambda_{1,2}$ of (3.7) represent the inter-area mode between areas 1 and 2. After applying the control input ΔP_{SSSC}, this oscillation mode is stabilized effectively. On the other hand, eigenvalues of (3.8) have not been changed. This is due to no control input ΔP_{SSSC} in (3.8). Table 3.2 shows the eigenvalues of expanded system (3.4). By considering the participation factor [12], it can be verified that $\lambda_{1,2}$ represents the inter-area mode between areas 1 and 2. As expected, ΔP_{SSSC} can stabilize this oscillation mode. For other modes, they are stable after the controller is included. Note that λ_8 is approximately zero which has no physical meaning. This is because of a redundant state variable ΔP_{T12} in (3.4). For the eigenvalues of the original system (3.3) demonstrated in Table 3.3, $\lambda_{1,2}$ can also be stabilized by ΔP_{SSSC}. Other modes are also stable after control. These eigenvalue analysis results confirm the concept of overlapping decompositions that the stability of the original system can be guaranteed if the decoupled subsystems can be stabilized by its own input.

Table 3.1: Eigenvalue Analysis Results of Decoupled Subsystems (3.7) and (3.8)

	Before Control	After Control
Decoupled Subsystem (3.15)	$\lambda_{1,2} = -0.015 \pm j3.5316$	$\lambda_{1,2} = -3.6077 \pm j3.7967$ $\lambda_{3,4} = -0.1027 \pm j0.0642$ $\lambda_5 = -0.5020$ $\lambda_6 = -12.8613$
Decoupled Subsystem (3.16)	$\lambda_{1,2} = -0.0152 \pm j1.6777$ $\lambda_{3,4} = -0.0168 \pm j3.6922$ $\lambda_{5,6} = -0.0247 \pm 2.1532$	Not change

Table 3.2: Eigenvalue Analysis Results of Expanded System (3.4)
(or interconnected overlapping subsystems (3.5) and (3.6))

	Before Control	After Control
Expanded System (3.12)	$\lambda_{1,2} = -0.0171 \pm j4.4134$ $\lambda_{3,4} = -0.0184 \pm j3.5602$ $\lambda_{5,6} = -0.0157 \pm j1.7520$ $\lambda_7 = -0.0409$ $\lambda_8 = -4.18 \times 10^{-14}$	$\lambda_{1,2} = -3.8240 \pm j5.0223$ $\lambda_{3,4} = -0.0461 \pm j3.6994$ $\lambda_{5,6} = -0.0061 \pm j1.7364$ $\lambda_7 = -0.0414$ $\lambda_8 = -2.84 \times 10^{-14}$ $\lambda_{9,10} = -0.1232 \pm j0.0483$ $\lambda_{11} = -0.4485$ $\lambda_{12} = -12.4$

Table 3.3: Eigenvalue Analysis Results of Original System (3.1)

	Before Control	After Control
Original System (3.11)	$\lambda_{1,2} = -0.0171 \pm j4.4134$ $\lambda_{3,4} = -0.0184 \pm j3.5602$ $\lambda_{5,6} = -0.0157 \pm j1.7520$ $\lambda_7 = -0.0409$	$\lambda_{1,2} = -3.8240 \pm j5.0223$ $\lambda_{3,4} = -0.0461 \pm j3.6994$ $\lambda_{5,6} = -0.0061 \pm j1.7364$ $\lambda_7 = -0.0414$ $\lambda_{8,9} = -0.1232 \pm j0.0483$ $\lambda_{10} = -0.4485$ $\lambda_{11} = -12.4217$

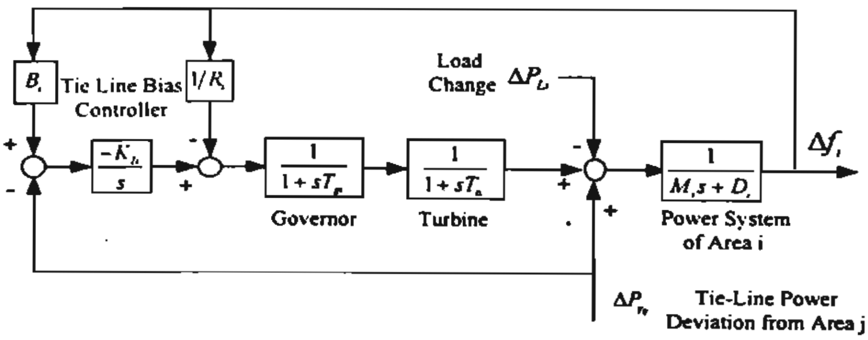

Figure 3.8: Linearized system model of area *i* including governor

Table 3.4: Data of Four-area Interconnected Power System
(Area Capacity Ratio 5 : 10 : 2 : 0.8)

System Parameters	Area 1	Area 2	Area 3	Area 4
Inertia Constant (MW.s/Hz)	$M_1 = 0.2$	$M_2 = 0.0167$	$M_3 = 0.15$	$M_4 = 0.2$
Damping Coefficient (MW/Hz)	$D_1 = 0.006$	$D_2 = 0.00833$	$D_3 = 0.005$	$D_4 = 0.006$
Turbine Time Constant (s)	$T_{t1} = 0.25$	$T_{t2} = 0.3$	$T_{t3} = 0.25$	$T_{t4} = 0.25$
Governor Time Constant (s)	$T_{g1} = 0.1$	$T_{g2} = 0.08$	$T_{g3} = 0.1$	$T_{g4} = 0.1$
Regulation Ratio (Hz/MW)	$R_1 = 2.4$	$R_2 = 2.4$	$R_3 = 2.4$	$R_4 = 2.4$
Bias Coefficient (MW/Hz)	$B_1 = 0.5$	$B_2 = 0.5$	$B_3 = 0.5$	$B_4 = 0.5$
Integral Controller Gain (1/s)	$K_{I1} = 0.5$	$K_{I2} = 0.5$	$K_{I3} = 0.5$	$K_{I4} = 0.5$
Synchronizing Power Coefficient (MW/rad)	$T_{12} = 0.159$, $T_{23} = 0.064$, $T_{31} = 0.079$, $T_{31} = 0.079$			
Area Capacity Ratio	$a_{12} = 2.0$, $a_{23} = 0.2$, $a_{31} = 2.5$, $a_{31} = 0.4$			

Next, the disturbance attenuation performance and robustness of both designed controllers are investigated in the linearized model of the four-area interconnected system. The dynamic of governor [11] is also incorporated into each area, as delineated in Fig. 3.8. System parameters are given in Table 3.4.

In order to evaluate the disturbance attenuation performance of both controllers, a sudden step load of 0.01 [p.u. MW] is applied to area 1 at t = 1.0 [sec]. The frequency deviation of each area is depicted in Figs. 3.9 – 3.12. Without control of the SSSC, the fluctuations of frequency deviations in all areas are large with poor damping. After the inclusion of both controllers, frequency oscillations in all areas are effectively stabilized. Especially, the peak value of frequency deviation in the controlled area 1 is significantly suppressed. In addition, the oscillating shapes are also stabilized completely. Meanwhile, steady-state errors of frequency deviations are eliminated slowly due to the effects of the governors. Furthermore, the tie line 1-2 power deviation illustrated in Fig. 3.13 is also effectively stabilized by Robust SSSC. As shown in Fig. 3.14, the maximum injected power deviation of Non-robust SSSC is 0.0094 [p.u. MW], which is almost equal to the size of load change. In contrast, due to consideration of both performance and robustness in design process, the injected power deviation of Robust SSSC is 0.0058 [p.u. MW].

Here, the robustness of each designed controller is evaluated. A random load disturbance composed of several oscillation frequencies, $\Delta P_{L1} = 0.002\sin(3t) + 0.005\sin(6t) - 0.007\sin(9t)$ [p.u. MW] is applied to area 1. At the same time, the damping coefficient in area 1 (D_1) is changed from 0.006 [p.u. MW / Hz] (positive damping) to –0.75 [p.u. MW / Hz] (negative damping). Note that the negative damping signifies an unstable system operation. As clearly illustrated by the area 1 frequency oscillations in Fig. 3.15, the system completely loses stability in cases of a Non-robust SSSC and no SSSC. Moreover, frequency oscillations in other areas (not shown here) severely fluctuate and finally diverge. On the other hand, the Robust SSSC explicitly maintains its performance against large uncertainties and severe perturbations. Frequency oscillations in area 1 and other areas are perfectly stabilized. The efficiency of the proposed SSSC is also evident in Figs. 3.16 and 3.17, where the power deviation in the tie line 1-2 and the injected power deviation of SSSC are shown.

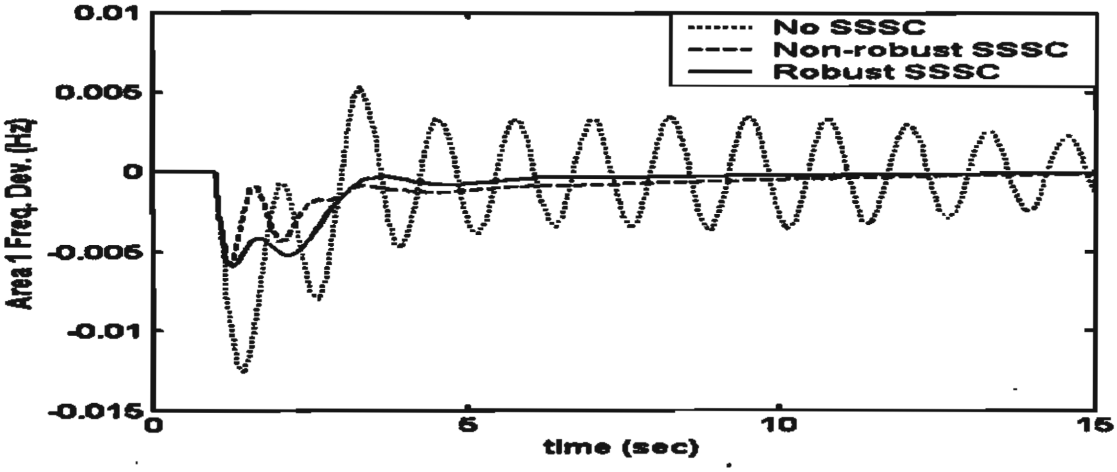

Figure 3.9: Frequency deviation of area 1

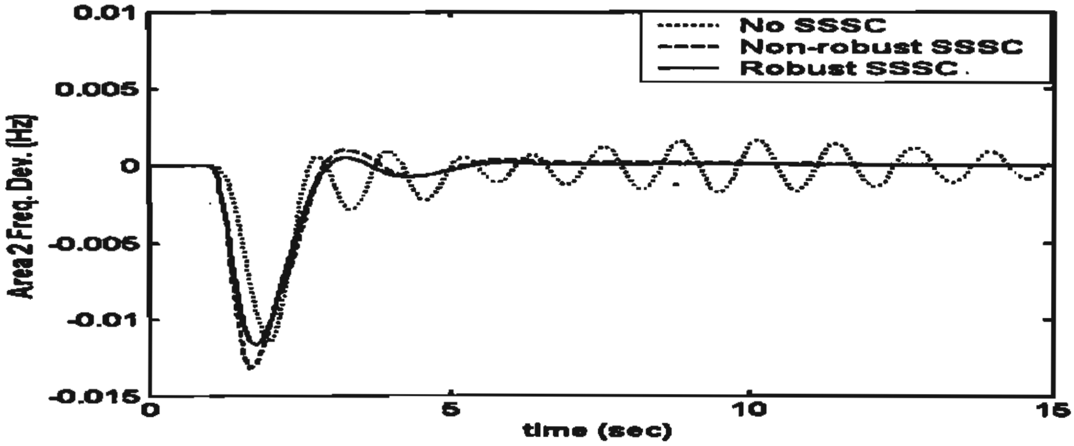

Figure 10: Frequency deviation of area 2

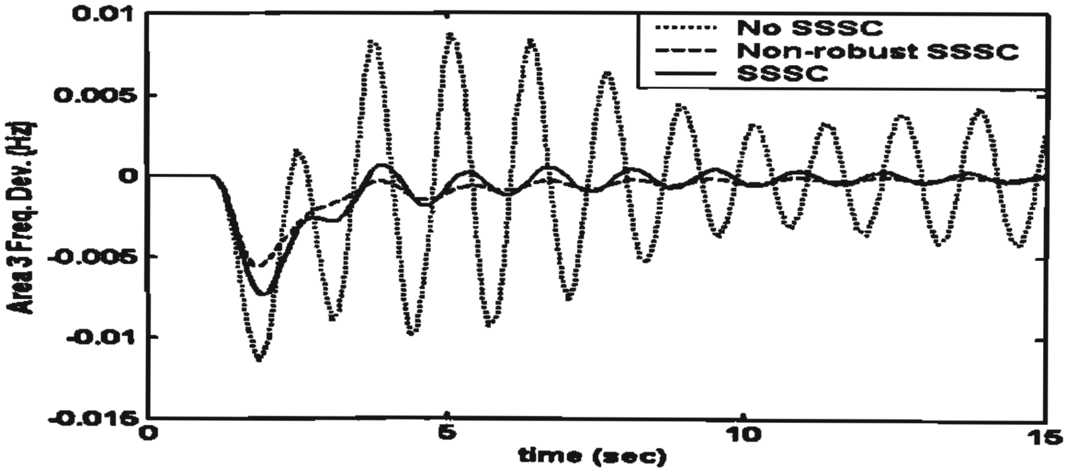

Figure 3.11: Frequency deviation of area 3

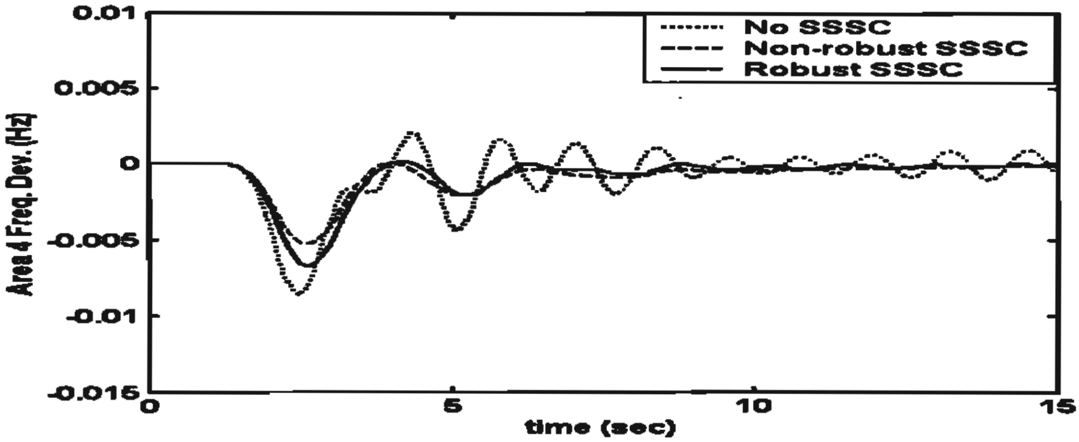

Figure 3.12: Frequency deviation of area 4

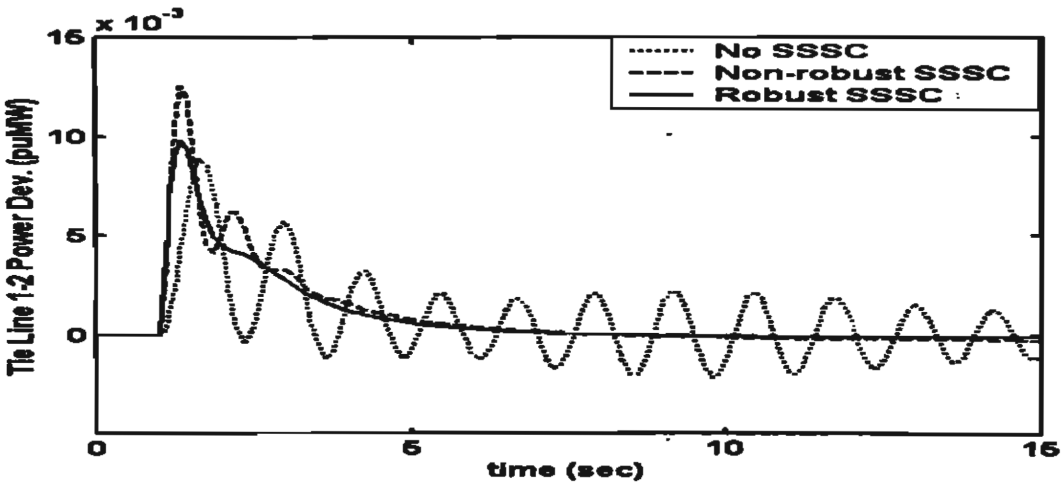

Figure 3.13: Tie line 1-2 power deviation

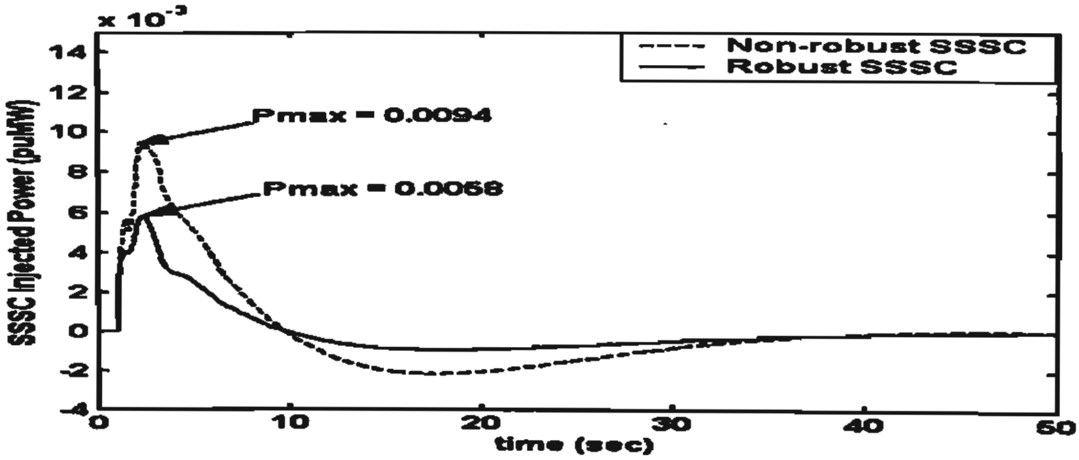

Figure 3.14: Injected power deviation of SSSC

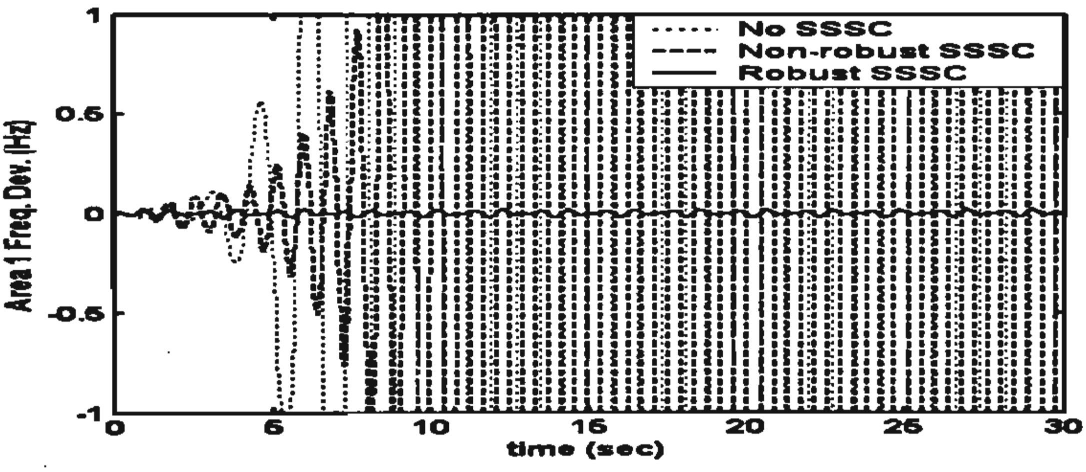

Figure 3.15: Frequency deviation of area 1

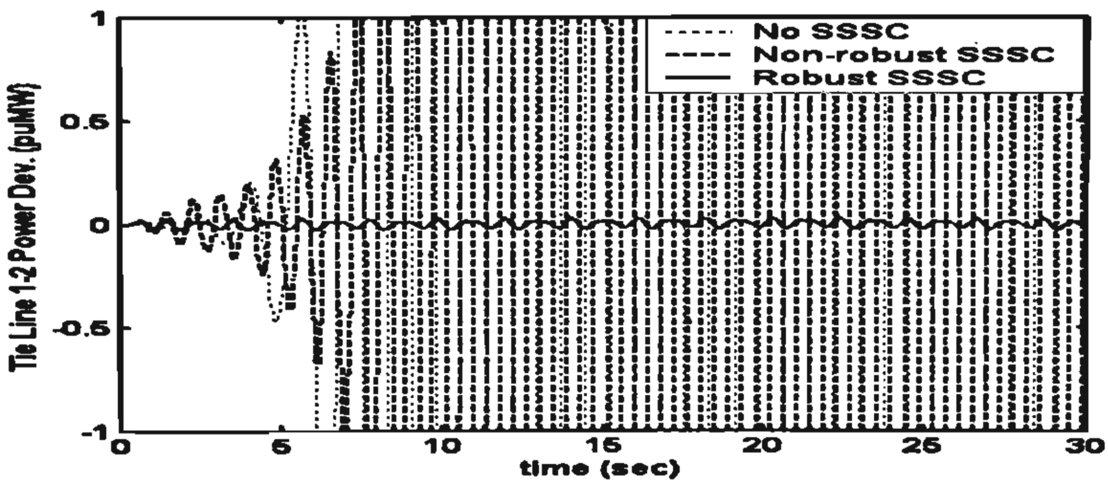

Figure 3.16: Tie line 1-2 power deviation

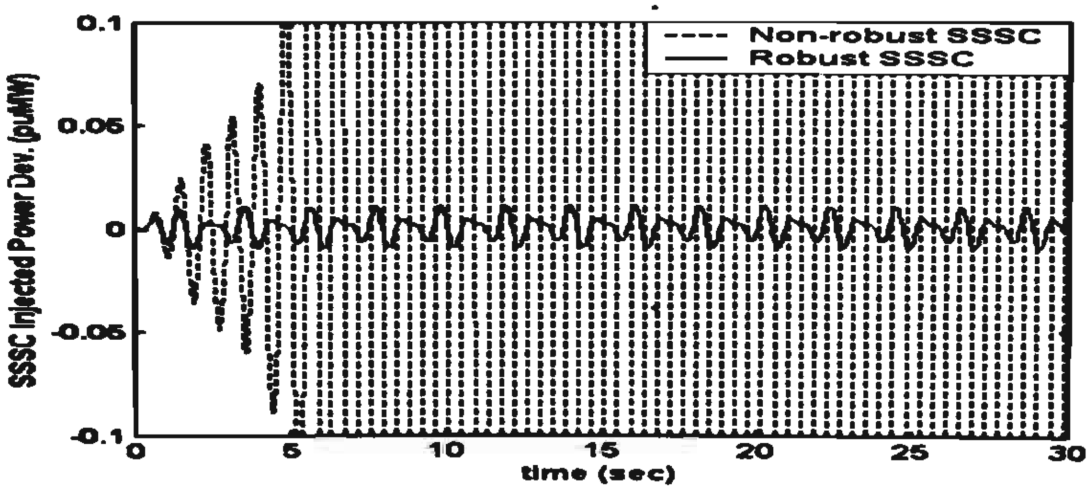

Figure 3.17: Injected power deviation of SSSC

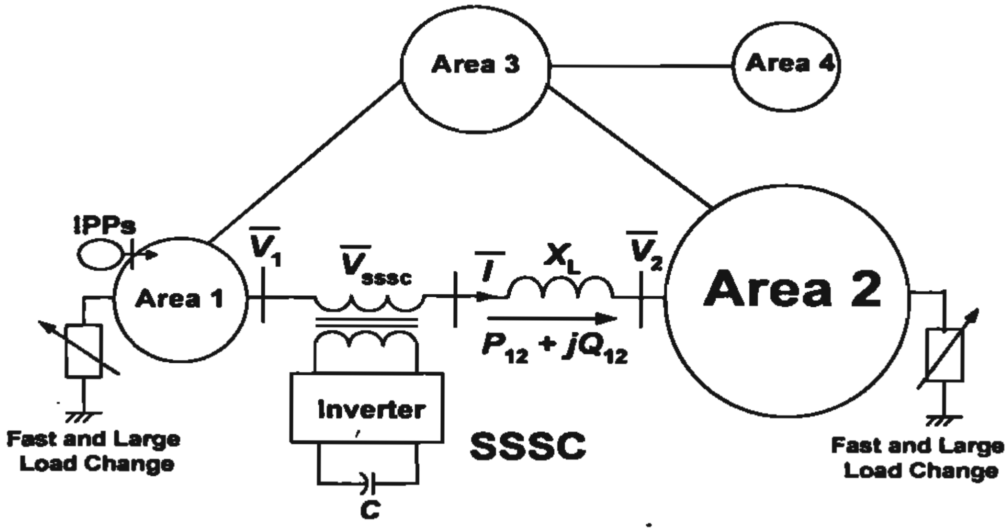

Figure 3.18: An additional load change in area 2

Finally, the performances of both SSSC controllers are evaluated when the load change occurs in area 2. Figure 3.18 shows an additional load change in area 2. It is assumed that a sudden step load of 0.01 [MW] occurs in area 2 at t = 1.0 [sec]. As depicted in Fig. 3.19, both Non-robust SSSC and Robust SSSC are capable of stabilizing frequency oscillations of area 1, even though a load disturbance occurs in area 2. For frequency deviations in other areas (Figs. 3.20-3.22) and tie line 1-2 power deviation (Fig. 3.23), the performance of Robust SSSC is comparatively better than that of Non-robust SSSC. As illustrated in Fig. 3.24, the peak values of injected power deviations of Robust SSSC and Non-robust SSSC are 0.01 [p.u. MW] and 0.027 [p.u. MW], respectively. This implies that the required MW capacity of robust SSSC is lower than that of Non-robust SSSC.

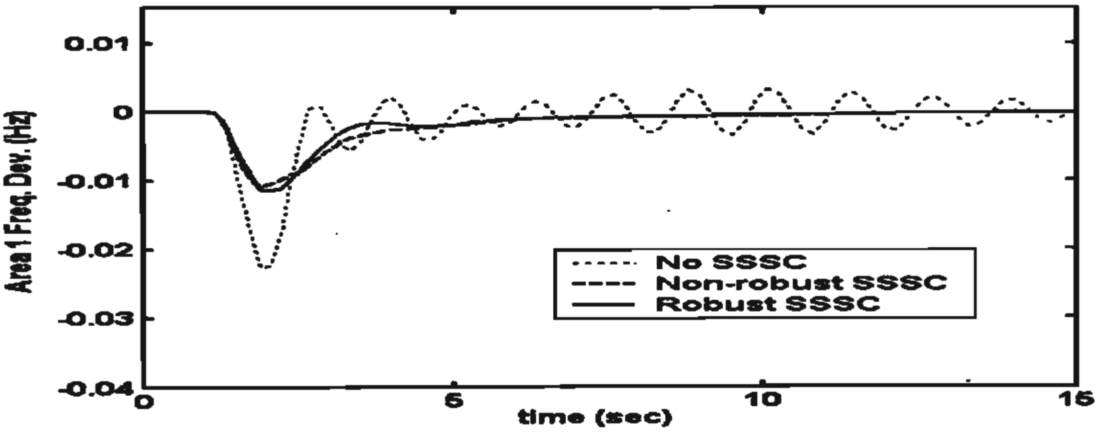

Figure 3.19: Area 1 frequency deviation

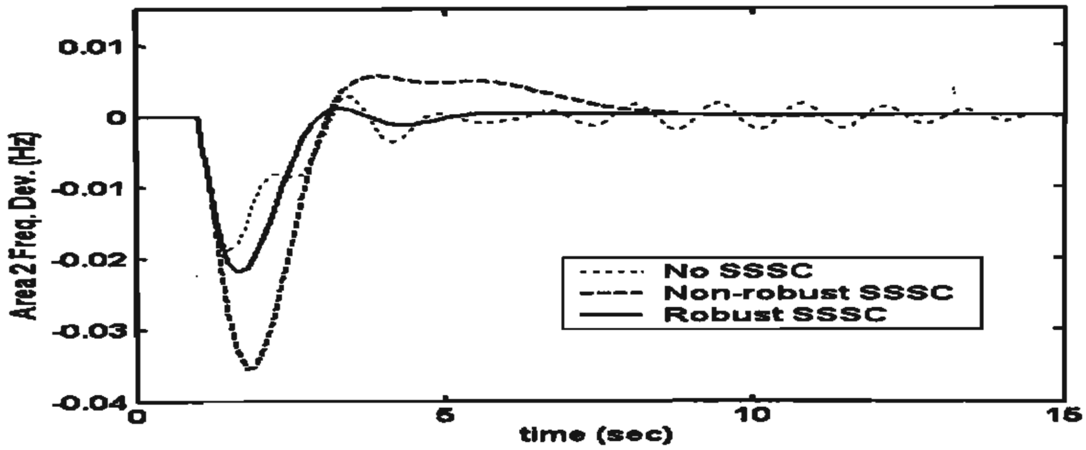

Figure 3.20: Area 2 frequency deviation

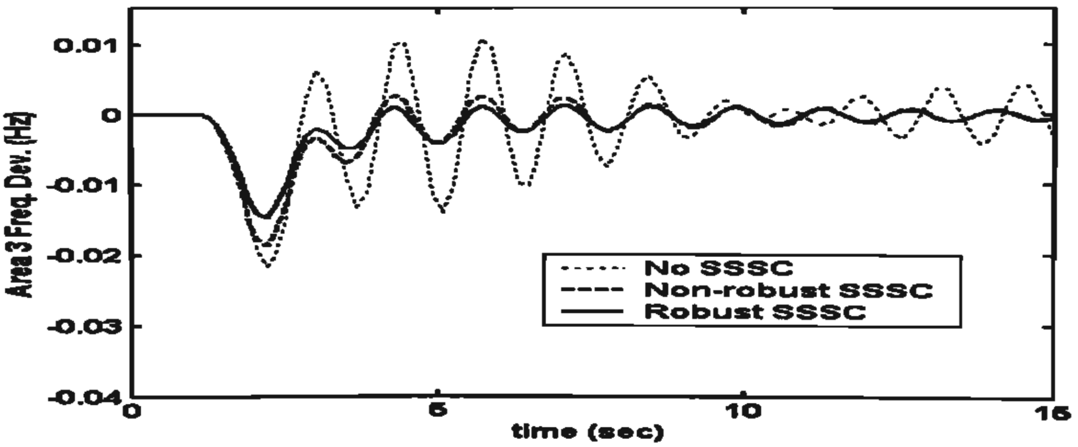

Figure 3.21: Area 3 frequency deviation

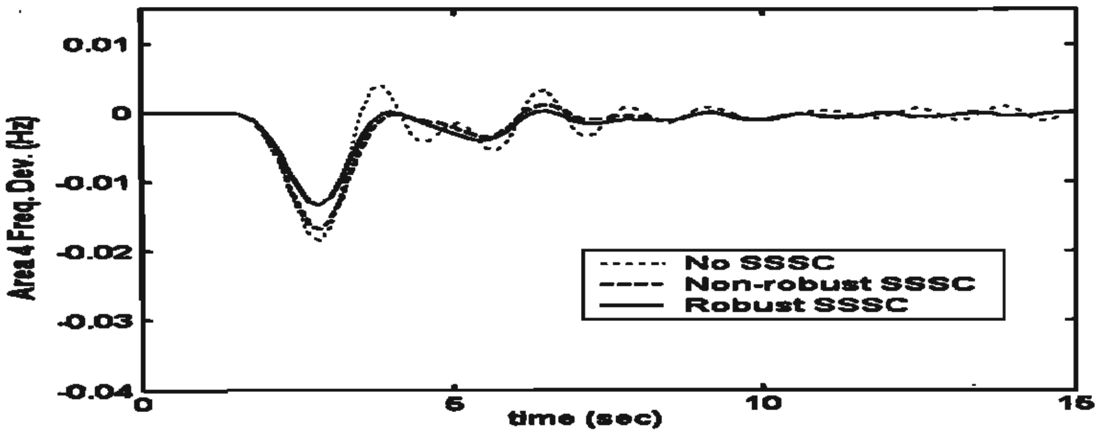

Figure 3.22: Area 4 frequency deviation

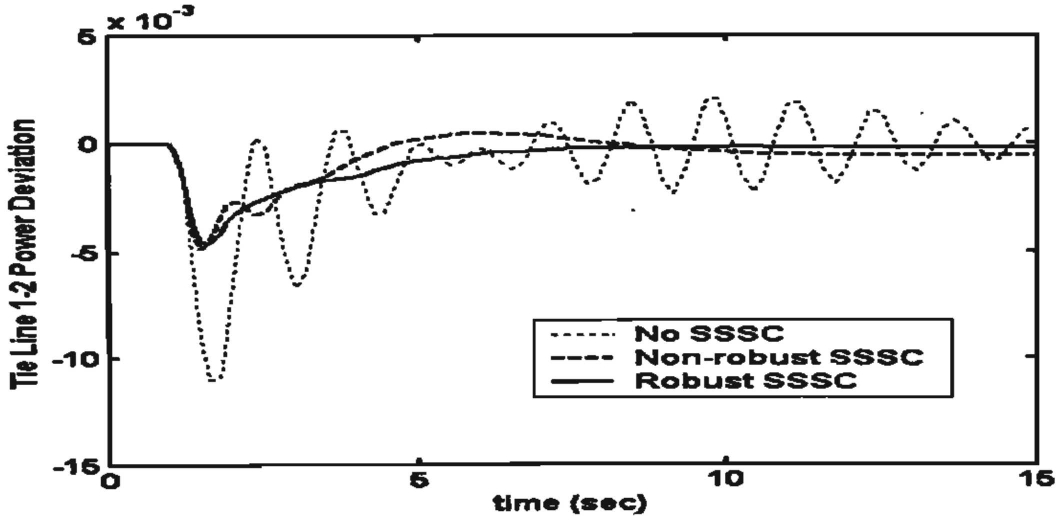

Figure 3.23: Tie line 1-2 power deviation

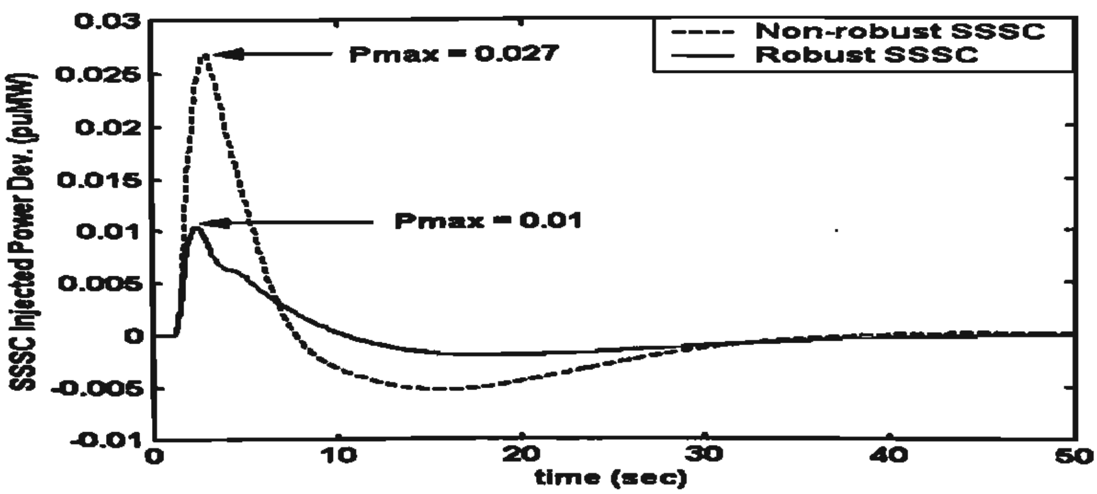

Figure 3.24: SSSC injected power deviation

3.5 Conclusions

This chapter presents the robust design of the lead/lag frequency stabilizer in the continuous time domain. The tabu search algorithm was employed to achieve the optimal parameters. By virtue of the objective function that limits the peak frequency deviation and maximizes the robust stability margin, the proposed design guarantees both performance and robustness of the resulted frequency stabilizer. More specifically, the designed robust frequency stabilizer uses only the frequency deviation of the controlled area as the feedback input signal. This allows practical realization and implementation in a power system. Simulation results clearly demonstrate the superior robustness and performance of the frequency stabilizer designed by the proposed method.

Chapter 4

Design of Robust Frequency Stabilizer of SSSC in Discrete Time Domain

4.1 Purpose of this chapter

Many of today's control systems use digital computers to provide the compensation. In this chapter, to implement the frequency stabilizer in real system, the proposed robust design is applied to establish a discrete-based frequency stabilizer of SSSC. First, the continuous-based frequency stabilizer is designed by the proposed method in Chapter 3. Subsequently, the resulted continuous-based frequency stabilizer is transformed to the discrete-based frequency stabilizer via a digital control technique. In addition, the proposed method is applied to a design problem in case of many frequency stabilizers of SSSCs are installed in an interconnected power system. Simulation study in a three-area loop system shows the significant effects of the designed frequency stabilizers against load changes and negative damping.

4.2 Problem Statement

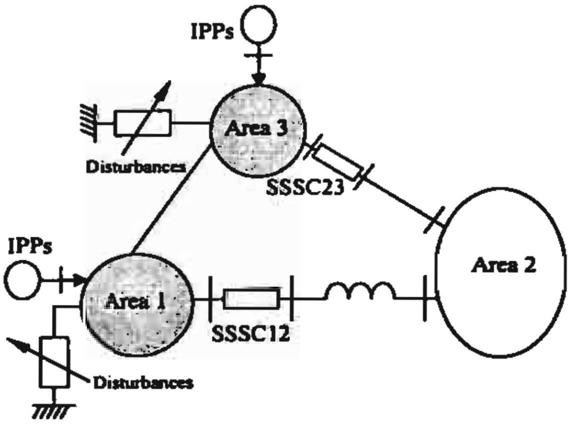

Figure 4.1: Three-area loop interconnected power system with SSSC

A three-area loop interconnected power system depicted in Fig.4.1 is used to explain the motivation of the proposed frequency stabilizer design. SSSC12 and SSSC23 are connected in series with tie-lines between areas 1 and 2, and areas 2 and 3, respectively. It is assumed that large loads with changing frequency in the vicinity of the inter-area oscillation cause frequency and tie-line power oscillations. In addition, Independent Power Producers (IPPs) that do not possess frequency control capabilities are also included in areas 1 and 3. Thus, it becomes beyond the abilities of governors in areas 1 and 3 to provide adequate frequency controls. Therefore, both SSSCs are applied to utilize the control capabilities of area 2 to compensate for fast load changes in areas 1 and 3. Moreover, by utilizing the area interconnections as the control channels of dynamic power flow control of SSSCs, the frequency oscillations in areas 1 and 3, as well as tie-line power oscillations due to inter-area modes can be effectively stabilized.

Additionally, in the interconnected system, variations of system parameters, various load changes etc. cause several system uncertainties. To achieve the high robust stability of system, the effect of uncertainties should be taken into account in the design process. In this study, the aim of the proposed frequency stabilizer design is not only to enhance the damping of interested inter-area oscillation modes, but also to improve the robust stability of system against uncertainties.

4.3 Design Methodology

4.3.1 Coordinated Control of SSSC and Governor

The response of SSSC is extremely rapid when compared to the conventional frequency control system, i.e. a governor. The difference in responses signifies that the SSSC and governor can be coordinated. When a power system is subjected to a sudden load disturbance, the SSSC quickly acts to damp frequency oscillation in the transient period. Subsequently, the governor continues to eliminate the steady-state error in frequency oscillation. As the periods of operation for the SSSC and governor do not overlap, the dynamic of governor can then be neglected in the design of frequency stabilizer for the sake of simplicity.

4.3.2 Linearized Power System Model

The power system shown in Fig. 4.1 can be represented by a linearized power system model, as shown in Fig. 4.2. Note that the governors are eliminated in this system. The SSSC model is represented by the active power flow controller. The dynamic characteristic of SSSC is modeled as the first order controller with a time constant $T_{SSSC} = 0.05$ sec. The designed discrete frequency stabilizers of SSSC12 and SSSC23 are represented by $K_{12}(z)$ and $K_{23}(z)$, respectively. The discrete frequency stabilizer consists of three main components, i.e., an analog-to-digital converter (ADC), a discrete controller ($K(z)$) and a digital-to-analog converter (DAC).

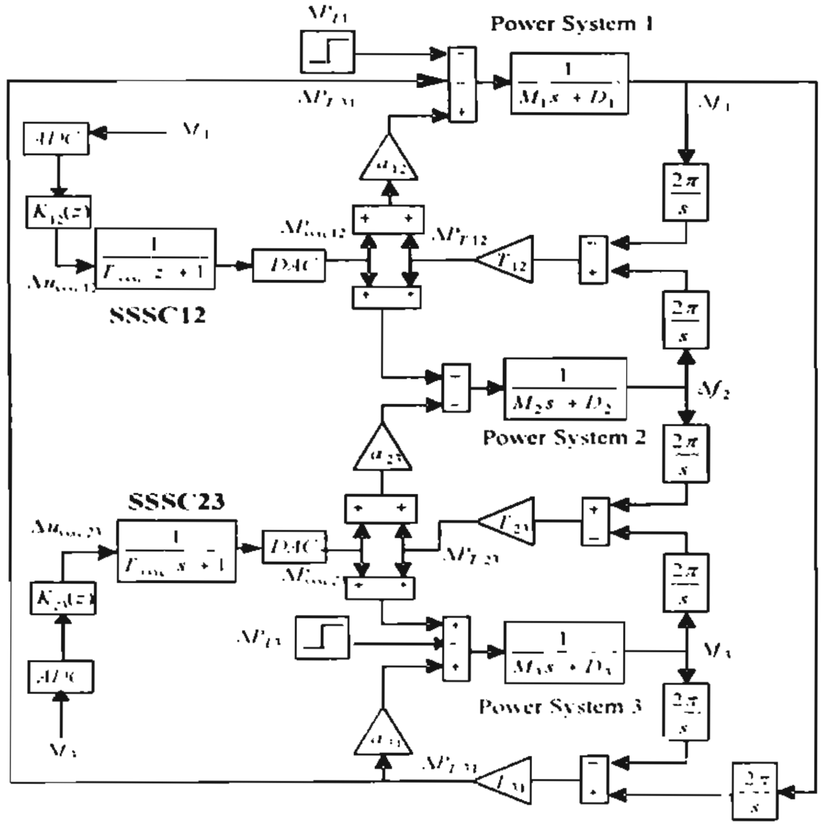

Figure 4.2: Discrete-based frequency stabilizers of SSSCs in a linearized power system model without governors

Usually, a continuous error signal, i.e. a frequency deviation (Δf) is digitized by an ADC. The on-board computer processes this signal to provide a control signal to the plant. Because most plants are continuous, the computer's output is passed through a DAC. The injected power deviation of each SSSC (ΔP_{SSSC12} and ΔP_{SSSC23}) acting positively on an area reacts negatively on another area. Thus, each injected power flows into both areas with different signs (+,-), simultaneously. By neglecting T_{SSSC}, the linearized state equation of Fig. 4.2 can be expressed as

$$\Delta \dot{x} = A\Delta x + B\Delta u \tag{4.1}$$

where

$$A = \begin{bmatrix} -D_1/M_1 & a_{S12} & 0 & a_{S14} & 0 \\ -2\pi T_{12} & 0 & 2\pi T_{12} & 0 & 0 \\ 0 & -1/M_2 & -D_2/M_2 & -a_{23}/M_2 & 0 \\ 0 & 0 & 2\pi T_{23} & 0 & -2\pi T_{23} \\ 0 & a_{S32} & 0 & a_{S34} & -D_3/M_3 \end{bmatrix},$$

$$B = \begin{bmatrix} a_{12}/M_1 & 0 \\ 0 & 0 \\ -1/M_2 & -a_{23}/M_2 \\ 0 & 1/M_3 \\ 0 & 0 \end{bmatrix},$$

$$\Delta x = [\Delta f_1 \quad \Delta P_{T12} \quad \Delta f_2 \quad \Delta P_{T23} \quad \Delta f_3]^T,$$

$$\Delta u = [\Delta P_{SSSC12} \quad \Delta P_{SSSC23}]^T.$$

Δf_i is the frequency deviation of area i, ΔP_{Tij} is the power deviation between areas i and j, M_i is the inertia constant of area i, D_i is the damping coefficient of area i, a_{ij} is the area capacity ratio between areas i and j, T_{ij} is the synchronizing power coefficient of the tie-line between areas i and j, where $i,j = 1,..,3$. Here $a_{S12} = (a_{12} + T_{31}/T_{12})/M_1$, $a_{S14} = -T_{31}/(M_1T_{23})$, $a_{S52} = -a_{31}T_{31}/(M_3T_{12})$, $a_{S54} = (1 + a_{31}T_{31}/T_{23})/M_3$. The variable ΔP_{T31} is represented in terms of ΔP_{T12} and ΔP_{T23} by

$$\Delta P_{T31} = -\frac{T_{31}}{T_{12}}\Delta P_{T12} + \frac{T_{31}}{T_{23}}\Delta P_{T23} \tag{4.2}$$

Thus, ΔP_{T31} has disappeared in (4.1). This system has two conjugate pairs of complex eigenvalues and a negative real eigenvalue. The former corresponds to two inter-area oscillation modes, and the latter the inertia center mode. Based on the mode controllability matrix [12], the inter-area modes between areas 1 and 2, and areas 2 and 3 are controllable for the control inputs Δu_{SSSC12} and Δu_{SSSC23}, respectively. Accordingly, the design purpose of frequency stabilizer is to enhance the damping of the mentioned inter-area modes.

4.3.3 Model Reduction by Overlapping Decompositions

The technique of overlapping decompositions is applied to reduce the system (4.1) to a subsystem embedded with only the inter-area mode of interest. The original system (4.1) is referred to as the system S.

$$S: \begin{bmatrix} \dot{x}_1 \\ \dot{x}_2 \\ \dot{x}_3 \end{bmatrix} = \begin{bmatrix} A_{11} & A_{12} & A_{13} \\ A_{21} & A_{22} & A_{23} \\ A_{31} & A_{32} & A_{33} \end{bmatrix} \begin{bmatrix} x_1 \\ x_2 \\ x_3 \end{bmatrix} + \begin{bmatrix} B_{11} & B_{12} \\ B_{21} & B_{22} \\ B_{31} & B_{32} \end{bmatrix} \begin{bmatrix} u_1 \\ u_2 \end{bmatrix} \tag{4.3}$$

The sub-matrices A_{ij} and B_{ij}, $(i,j = 1,2,3)$ have appropriate dimensions identical to the corresponding states and input vectors. According to the process of overlapping decompositions, the system S can be expressed as

$$\tilde{S} \; : \; \begin{bmatrix} \dot{z}_1 \\ \dot{z}_2 \end{bmatrix} = \begin{bmatrix} A_{11} & A_{12} & 0 & A_{13} \\ A_{21} & A_{22} & 0 & A_{23} \\ A_{21} & 0 & A_{22} & A_{23} \\ A_{31} & 0 & A_{32} & A_{33} \end{bmatrix} \begin{bmatrix} z_1 \\ z_2 \end{bmatrix} + \begin{bmatrix} B_{11} \\ B_{21} \\ B_{21} \\ B_{31} \end{bmatrix} \begin{bmatrix} u_1 \\ u_2 \end{bmatrix} \tag{4.4}$$

where $z_1 = \left[x_1^T, x_2^T\right]^T$ and $z_2 = \left[x_2^T, x_3^T\right]^T$. Subsequently, the system $\tilde{S}$ can be decomposed into two interconnected overlapping subsystems, i.e.

$$\tilde{S}_1 \; : \; \dot{z}_1 = \left(\begin{bmatrix} A_{11} & A_{12} \\ A_{21} & A_{22} \end{bmatrix} z_1 + \begin{bmatrix} B_{11} \\ B_{21} \end{bmatrix} u_1 \right) + \begin{bmatrix} 0 & A_{13} \\ 0 & A_{23} \end{bmatrix} z_2 + \begin{bmatrix} B_{12} \\ B_{22} \end{bmatrix} u_2 \tag{4.5}$$

and

$$\tilde{S}_2 \; : \; \dot{z}_2 = \left(\begin{bmatrix} A_{22} & A_{23} \\ A_{32} & A_{33} \end{bmatrix} z_2 + \begin{bmatrix} B_{21} \\ B_{31} \end{bmatrix} u_2 \right) + \begin{bmatrix} A_{21} & 0 \\ A_{31} & 0 \end{bmatrix} z_1 + \begin{bmatrix} B_{21} \\ B_{31} \end{bmatrix} u_1 \tag{4.6}$$

The state variable x_2 is repeatedly included in both subsystems, which implies "Overlapping Decompositions".

For system stabilization, two interconnected subsystems $\tilde{S}_1$ and $\tilde{S}_2$ are considered. The terms in the right hand sides of (4.5) and (4.6) can be separated into the decoupled subsystems (as indicated in the parenthesis in (4.5) and (4.6)) and the interconnected subsystems. As mentioned in [32], if each decoupled subsystem can be stabilized by its own input, the asymptotic stability of the interconnected overlapping subsystem $\tilde{S}_1$ and $\tilde{S}_2$ are maintained. Moreover, the asymptotic stability of the original system S is also guaranteed. Consequently, the interactions of the decoupled subsystems with the interconnection subsystems in (4.5) and (4.6) are regarded as perturbations. They can be neglected during control design. As a result, the decoupled subsystems of (4.5) and (4.6) can be expressed as

$$\tilde{S}_{D1} \; : \; \dot{z}_1 = \begin{bmatrix} A_{11} & A_{12} \\ A_{21} & A_{22} \end{bmatrix} z_1 + \begin{bmatrix} B_{11} \\ B_{21} \end{bmatrix} u_1 \tag{4.7}$$

and

$$\tilde{S}_{D2} \; : \; \dot{z}_2 = \begin{bmatrix} A_{22} & A_{23} \\ A_{32} & A_{33} \end{bmatrix} z_2 + \begin{bmatrix} B_{22} \\ B_{32} \end{bmatrix} u_2 \tag{4.8}$$

By regarding the power deviation between areas 1 and 2 (ΔP_{T12}) as the overlapped variable for design of frequency stabilizer of SSSC12, the subsystem embedded with the inter-area mode between areas 1 and 2 can be expressed as

$$\tilde{G}_{s1} \; : \; \begin{bmatrix} \Delta \dot{f}_1 \\ \Delta \dot{P}_{T12} \end{bmatrix} = \begin{bmatrix} -D_1/M_1 & a_{S12} \\ -2\pi T_{12} & 0 \end{bmatrix} \begin{bmatrix} \Delta f_1 \\ \Delta P_{T12} \end{bmatrix} + \begin{bmatrix} a_{12}/M_1 \\ 0 \end{bmatrix} \Delta P_{SSSC12} \tag{4.9}$$

Next, by considering the power deviation between areas 2 and 3 (ΔP_{T23}) as the overlapped variable for design of frequency stabilizer of SSSC23, the subsystem embedded with the inter-area mode between areas 2 and 3 can be expressed as

$$\tilde{G}_{s2} \;:\; \begin{bmatrix} \Delta\dot{P}_{T23} \\ \Delta\dot{f}_3 \end{bmatrix} = \begin{bmatrix} 0 & -2\pi T_{23} \\ a_{s54} & -D_3/M_3 \end{bmatrix} \begin{bmatrix} \Delta P_{T23} \\ \Delta f_3 \end{bmatrix} + \begin{bmatrix} 0 \\ 1/M_3 \end{bmatrix} \Delta P_{SSSC23} \tag{4.10}$$

By incorporating the dynamic characteristic of each SSSC as shown in Fig. 4.2, (4.9) and (4.10) become

$$G_{S1} \;:\; \begin{bmatrix} \Delta\dot{f}_1 \\ \Delta\dot{P}_{T12} \\ \Delta\dot{P}_{SSSC12} \end{bmatrix} = \begin{bmatrix} -D_1/M_1 & a_{S12} & a_{12}/M_1 \\ -2\pi T_{12} & 0 & 0 \\ 0 & 0 & -1/T_{SSSC12} \end{bmatrix} \begin{bmatrix} \Delta f_1 \\ \Delta P_{T12} \\ \Delta P_{SSSC12} \end{bmatrix} + \begin{bmatrix} 0 \\ 0 \\ 1/T_{SSSC12} \end{bmatrix} \Delta u_{SSSC12} \tag{4.11}$$

and

$$G_{S2} \;:\; \begin{bmatrix} \Delta\dot{P}_{T23} \\ \Delta\dot{f}_3 \\ \Delta\dot{P}_{SSSC23} \end{bmatrix} = \begin{bmatrix} -D_1/M_1 & a_{S12} & a_{12}/M_1 \\ -2\pi T_{12} & 0 & 0 \\ 0 & 0 & -1/T_{SSSC23} \end{bmatrix} \begin{bmatrix} \Delta P_{T23} \\ \Delta f_3 \\ \Delta P_{SSSC23} \end{bmatrix} + \begin{bmatrix} 0 \\ 0 \\ 1/T_{SSSC23} \end{bmatrix} \Delta u_{SSSC23} \tag{4.12}$$

where Δu_{SSSC12} and Δu_{SSSC23} are output signals of frequency stabilizers for SSSC12 and SSSC23, respectively. Equations (4.11) and (4.12) are used to design SSSC12 and SSSC23, respectively.

4.3.4 Structure of Discrete-based Frequency Stabilizer

In this study, the structure of the frequency stabilizer is based on a second-order lead/lag discrete compensator as shown in Fig. 4.3. There are five parameters for each designed frequency stabilizer consisting of a stabilization gain K, time constants T_1, T_2, T_3, and T_4.

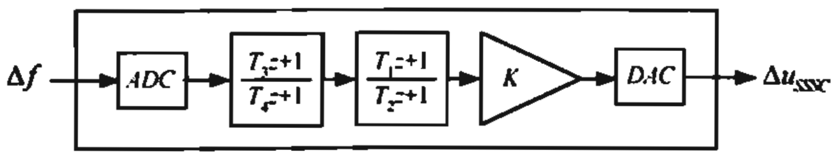

Figure 4.3: Configuration of 2nd order discrete-based frequency stabilizer

For the brief design procedure, first, the control parameters of the continuous-based frequency stabilizer are optimized by a tabu search algorithm. Next, the continuous-based frequency stabilizer is converted to the discrete-based frequency stabilizer by using z-transformation [33]. In this study, the sampling time is set to 0.01 sec.

4.3.5 Formulation of Objective Function

In deriving the objective function, not only the enhancement of system damping, but also the robust stability against system uncertainties are taken into account. Since the main purpose of the designed frequency stabilizer is to improve the system damping following any load disturbances, therefore, the damping ratio (ζ) of the inter-area mode is used as a design specification. Assuming that the eigenvalues corresponding to the mode of oscillation can be determined as $-\sigma \pm j\omega_d$, the damping ratio is given by

$$\zeta_{actual} = \frac{-\sigma}{\sqrt{\sigma^2 + \omega_d^2}} \tag{4.13}$$

The desired damping ratio of the eigenvalues corresponding to the mode of oscillation is specified as $\zeta_{desired}$. Accordingly, the difference between the desired and the actual damping ratios can be defined as

$$\alpha = \left|\zeta_{desired} - \zeta_{actual}\right| \tag{4.14}$$

For robust stability, the system uncertainties are modeled as a multiplicative form demonstrated in Fig. 4.4. $\tilde{G}$ is a system and $\tilde{K}$ is a designed controller. Δ_m is a stable multiplicative uncertainty.

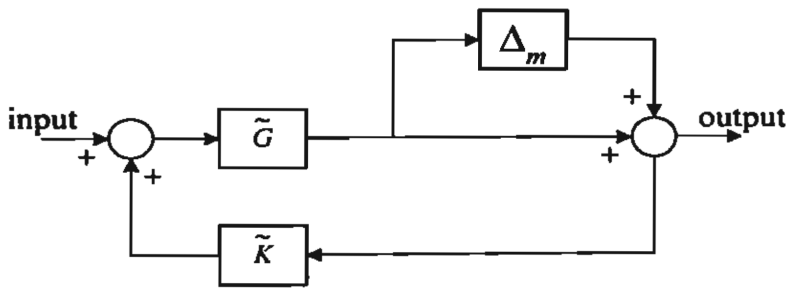

Figure 4.4: Control system with multiplicative uncertainty model

Based on the small-gain theorem, the closed loop system will be robustly stable if

$$\left|\Delta_m\right| < \frac{1}{\left|\tilde{G}\tilde{K}\left(1-\tilde{G}\tilde{K}\right)^{-1}\right|} \tag{4.15}$$

where $\tilde{G}\tilde{K}\left(1-\tilde{G}\tilde{K}\right)^{-1}$ is the complementary sensitivity function (T). Note that $|\bullet|$ is the magnitude of the transfer function "$\bullet$".

Based on the multiplicative uncertainty model, the robust stability margin can be guaranteed in terms of multiplicative stability margin (MSM) as

$$MSM = 1/\|T\|_\infty \tag{4.16}$$

where $\|T\|_\infty$ is the ∞-norm of T. From (4.15) and (4.16), it is clear that by minimizing $\|T\|_\infty$, the MSM increases and the robust stability is ensured. Thus, the normalized robustness index of the objective function is defined as

$$\gamma = \|T\|_\infty / \|T\|_{\infty(initial)} \tag{4.17}$$

where $\|T\|_{\infty(initial)}$ is the ∞-norm of T at the initial of a search process.

Combining (4.14) and (4.17), the control problem can be formulated as the following optimization problem:

$$\begin{aligned} &\text{Minimize} \quad F(K,\ T_i) = c \bullet \alpha + \gamma \\ &\text{Subject to} \quad K_{\min} \le K \le K_{\max} \\ &\qquad T_{i,\ \min} \le T_i \le T_{i,\ \max}, \quad i = 1,\ldots,4 \end{aligned} \tag{4.18}$$

where $F(K,\ T_i)$ is the objective function. The minimum and maximum values of the gain K are set to 0.1 and 5, respectively. The minimum and maximum values of the time constants T_i are set to 0.01 and 2, respectively. The constant coefficient "c" is used to weight α-term, so that $c \bullet \alpha$ dominates γ during the parameters optimization. Note that, since γ is normalized to 1 at the initial solution, it is easy to find the value of c so that $c \bullet \alpha$ is greater than 1. Eventually, the search process minimizes both terms until $c \bullet \alpha$ meets the design specification and γ decreases to the possible minimum value. All searched parameters are optimized by a tabu search algorithm.

4.3.6 TSA for Parameter Determination

Tabu Search (TS) is an iterative improvement procedure that can start from any initial feasible solution (searched parameters) and attempted to determine a better solution. As a meta-heuristic, TS is based on a local search technique with the ability to escape from being trapped in local optima. Hereafter, components of TS and TS procedure are discussed.

Encoding and Decoding: The concatenated encoding method is used to encode each parameter into a binary string normalized over its range and also stack each normalized string in series with each other to construct the string individual. The same number of ***nb*** bits is used for each searched parameter. Figure 4.5 illustrates the example of concatenated encoding scheme.

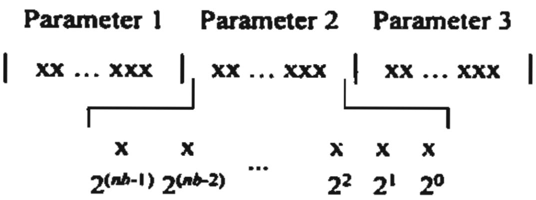

Figure 4.5: Example of Concatenated Encoding Scheme

On the other hand, a decoding scheme is carried out by converting encoded parameters to their actual values by (4.19) prior to evaluation of objective function.

$$P_i = P_{i,\min} + \frac{B_i \times \left[P_{i,\max} - P_{i,\min}\right]}{2^n - 1} \tag{4.19}$$

where P_i is the actual value of the i-th parameter, $P_{i,\max}$ and $P_{i,\min}$ are the maximum and minimum value of the i-th parameter. B_i is the decimal integer value of binary string of the i-th parameter. In this study, 16 bits are used to represent each parameter. The more the number of bits per searched parameter is, the higher the resolution will be.

Trial Solution Generation: To generate a trial solution, one bit of a binary string of an initial solution is flipped at a time. Figure 4.6 conceptually illustrates the process. The maximum number of trial solutions in each iteration is referred to a neighborhood solution space (NS). In this paper, NS is set to 90 % of a total number of bits in a string individual ($\lfloor 0.9 \times nb \times NP \rfloor$ where NP is a number of searched parameters.

Initial solution :	1001011010	1100011010	1110010011
Trial solution 1:	0001011010	1100011010	1110010011
Trial solution 2:	1101011010	1100011010	1110010011
Trial solution 3:	1011011010	1100011010	1110010011

Figure 4.6: Concept of Trial Solution Generation

Tabu List Restriction: Tabu List (TL) is utilized to keep attributes (bit positions) that created the best solution in the past iterations for iterations so that they can not be used to create new solution candidates. As the iteration proceeds, TL stores a new attribute and releases the oldest one, as shown in Fig. 4.7. Particularly, the size of TL is the only control parameter of TS. The size of TL that provided good solutions usually grows with the size of the problem. In this paper, $\lfloor \sqrt{nb \times NP} \rfloor$ is used to determine the best size of TL.

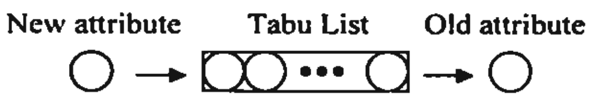

Figure 4.7: Mechanism of tabu list

Aspiration Level Criterion: The aspiration level (AL) criterion allows an attribute included in TL to override its tabu status if it leads to a more attractive solution. In particular, the AL is satisfied if the tabued attribute yields a solution that is better than the best solution reached at that iteration. After the AL is satisfied, updating TL is carried out by moving the tabued attribute back to the first position of the TL.

Termination Criteria: This criterion is set to allow the search process to stop and return the best solution found. The search process will terminate if the maximum allowable number of iterations is reached.

TS Procedure: firstly, the initial feasible solution is generated arbitrarily. A trial solution is searched if either it is not tabued or, in case of being tabued it passes the AL test. The best solution is always updated during the search process until the termination criterion is satisfied. The following notations are used for the TS procedure.

TL : the tabu list,

NS : the neighborhood solution space,

F(X) : the objective function of solution *X*,

X_o^k : the initial feasible solution at iteration *k*,

X_m^k : a trial solution *m* at iteration *k*,

X_{cb}^k : the current best trial solution at iteration *k*,

X_b^k : the best solution reached at iteration *k*,

k_{max} : the maximum allowable number of iterations.

The TS procedure can be described as follows.

1. Read constraints of searched parameters, the initial feasible solution X_o^k , and the design specification.
2. Specify the size of TL, k_{max}, and size of NS.
3. Initialize iteration counter *k* and termination criteria *tc* to zero, and empty TL.
4. Initialized AL by setting $X_b^k = X_o^k$.
5. Execute TS procedure:

5.1 Initialize the trial counter m to zero.

5.2 Generate a trial solution X_m^k from X_o^k.

5.3 If X_m^k is not feasible, go to 5.9.

5.4 If X_m^k is the first feasible solution, set $X_{cb}^k = X_m^k$.

5.5 Perform Tabu test. If X_m^k is tabued, then go to 5.8.

5.6 If $F(X_m^k) < F(X_{cb}^k)$, set $X_{cb}^k = X_m^k$. Otherwise, go to 5.9.

5.7 If $F(X_m^k) < F(X_b^k)$, then update AL by setting $X_b^k = X_m^k$. Go to 5.9.

5.8 Perform AL test. If $F(X_m^k) < F(X_b^k)$, set $X_{cb}^k = X_m^k$, and update AL by setting $X_b^k = X_m^k$.

5.9 If m is less than NS, $m = m+1$ and go to 5.2.

5.10 If there is no feasible solution, set $X_o^{k-1} = X_b^k$. Otherwise, set $X_o^{k+1} = X_{cb}^k$, and update TL.

6. If $k = 0$, go to 9.
7. Perform the convergence checking.
   If $X_b^k = X_b^{k-1}$, $tc = tc+1$. Otherwise, $tc = 0$.
8. If tc = size of TL, set $tc = 0$ and go to 10.
9. If $k < k_{\max}$, then $k = k+1$, and go to 5.
10. TS is terminated and X_b^k is the best solution found.

4.4 Experimental Results

In the design specification, the desired damping ratio $(\zeta_{desired})$ is set to 0.25. Also, the coefficient c is appropriately set to 5. For TS, the size of TL is set to 8 for the best solution. The area capacity ratio between areas 1, 2 and 3 is 5:10:2. System parameters are given in Table 4.1.

Table 4.1: Data of Three-area Loop Interconnected Power System
(Area Capacity Ratio 5 : 10 : 2)

System Parameters	Area 1	Area 2	Area 3
Inertia Constant (MW.s/Hz)	$M_1 = 0.2$	$M_2 = 0.0167$	$M_3 = 0.15$
Damping Coefficient (MW/Hz)	$D_1 = 0.006$	$D_2 = 0.00833$	$D_3 = 0.005$
Turbine Time Constant (s)	$T_{t1} = 0.25$	$T_{t2} = 0.3$	$T_{t3} = 0.25$
Governor Time Constant (s)	$T_{g1} = 0.1$	$T_{g2} = 0.08$	$T_{g3} = 0.1$
Regulation Ratio (Hz/MW)	$R_1 = 2.4$	$R_2 = 2.4$	$R_3 = 2.4$
Bias Coefficient (MW/Hz)	$B_1 = 0.5$	$B_2 = 0.5$	$B_3 = 0.5$
Integral Controller Gain (1/s)	$K_{i1} = 0.5$	$K_{i2} = 0.5$	$K_{i3} = 0.5$
Synchronizing Power Coefficient (MW/rad)	$T_{12} = 0.159$, $T_{23} = 0.064$, $T_{31} = 0.079$		
Area Capacity Ratio	$a_{12} = 2.0$, $a_{23} = 0.2$, $a_{31} = 2.5$		

To exhibit the results of system reduction by overlapping decompositions, Table 4.2 shows eigenvalues of the original systems (4.1) in comparison to design subsystems (4.11) and (4.12). The damping ratio and oscillation frequency of the corresponding oscillation mode in the design subsystems are nearly equal to those of the original system. This reveals that the design subsystems (4.11) and (4.12) retain the physical characteristic of the original system (4.1).

Table 4.2: Eigenvalues of Original System and Design Subsystems Before and After the Overlapping Decompositons

Original System (4.1)	Subsystem (4.11)	Subsystem (4.12)
$\lambda_1 = -0.0415$	-	-
$\lambda_{2,3} = -0.0173 \pm j4.365$ $(\zeta = 0.0035,\ f = 0.695\ \ Hz)$	$\lambda_{2,3} = -0.015 \pm j3.53$ $(\zeta = 0.0043,\ f = 0.562\ \ Hz)$	-
$\lambda_{4,5} = -0.0185 \pm j3.291$ $(\zeta = 0.0056,\ f = 0.524\ \ Hz)$	-	$\lambda_{4,5} = -0.0167 \pm j3.31$ $(\zeta = 0.005,\ f = 0.527\ \ Hz)$

As experimental results, the optimally tuned parameters of designed frequency stabilizers in (4.11) and (4.12) are obtained as given in Table 4.3. Note that the optimized frequency stabilizer based on (4.18) is referred to as "Robust frequency stabilizer".

Table 4.3: Parameters of Robust Frequency Stabilizers

Designed Robust Frequency Stabilizer	K	T_1	T_2	T_3	T_4
SSSC12	0.2188	0.2587	0.0158	0.0575	0.2316
SSSC23	0.2378	1.5025	0.5386	1.6268	0.5075

For comparison purposes, the second-order lead/lag frequency stabilizer in (4.11) and (4.12) are also designed with the same design specification, which requires the same damping ratio $\zeta_{desired} = 0.25$. The control parameters $K, T_1, T_2, T_3,$ and T_4 are searched by TS via the optimization problem (4.20). Note that the robust stability index term (γ) is excluded.

$$
\begin{aligned}
&\text{Minimize} \quad && F(K, T_i) = \alpha \\
&\text{Subject to} \quad && K_{\min} \le K \le K_{\max} \\
& && T_{i,\min} \le T_i \le T_{i,\max}, \qquad i = 1,\ldots,4
\end{aligned}
\tag{4.20}
$$

Here, the optimized frequency stabilizer based on (4.20) is referred to as "Non-robust frequency stabilizer". Table 4.4 shows the control parameters of the non-robust frequency stabilizer.

Table 4.4: Parameters of Non-Robust Frequency Stabilizers

Designed Non-robust Frequency Stabilizer	K	T_1	T_2	T_3	T_4
SSSC12	4.2863	0.1344	1.0011	1.0978	1.3807
SSSC23	4.3683	0.1344	0.9933	1.3467	1.3802

Table 4.5 shows eigenvalues of subsystems (4.11) and (4.12) in case of SSSCs with robust frequency stabilizers installed in comparison with a case of SSSCs with no frequency stabilizer and a case of SSSCs with non-robust frequency stabilizers installed. The results describe that the damping ratios of the eigenvalues corresponding to the desired inter-area modes are improved to 0.25, as design specification.

Table 4.5: Comparison of Eigenvalues of Design Subsystems

Design Subsystem	SSSC with No Frequency Stabilizer	SSSC With Non-Robust Frequency Stabilizer	SSSC With Robust Frequency Stabilizer
G_{s1}	$-0.015 \pm j3.53$ $\zeta = 0.0043$	$-1.8369 \pm j7.1143$ $\zeta = 0.25$	$-0.6093 \pm j2.3595$ $\zeta = 0.25$
G_{s2}	$-0.0167 \pm j3.31$ $\zeta = 0.005$	$-1.667 \pm j6.4559$ $\zeta = 0.25$	$-0.3534 \pm j1.3685$ $\zeta = 0.25$

Next, the MSM is used to evaluate the robust stability margin of system (4.11) and (4.12) included with each frequency stabilizer. As shown in Table 4.6, the value of MSM in case of the system with robust frequency stabilizer is greater than that in case of the system with non-robust stabilizer. This clearly signifies that the better robust stability margin of the power system incorporated with robust frequency stabilizer can be achieved by the optimization problem (4.18).

Table 4.6: Comparison of MSM

System	With Non-Robust Frequency Stabilizer	With Robust Frequency Stabilizer
G_{S1}	0.5151	0.71430
G_{S2}	0.5332	0.61240

Table 4.7 shows the eigenvalues of the original system (4.1) before and after control. After each frequency stabilizer is included in the system, the damping ratios of the corresponding inter-area modes are enhanced as expected. This confirms the merit of overlapping decompositions that if the subsystems are stabilized by their own control inputs, the stability of the original system can be guaranteed.

Table 4.7: Comparison of Eigenvalues of Original System

Inter-Area Oscillation Mode	No Frequency Stabilizer	With Non-Robust Frequency Stabilizer	With Robust Frequency Stabilizer
Between Areas 1 and 2	$-0.0173 \pm j4.365$ $\zeta = 0.0035$	$-1.7631 \pm j7.6011$ $\zeta = 0.226$	$-0.6619 \pm j2.898$ $\zeta = 0.223$
Between Areas 2 and 3	$-0.0185 \pm j3.291$ $\zeta = 0.0056$	$-1.6716 \pm j6.4702$ $\zeta = 0.25$	$-0.3596 \pm j1.376$ $\zeta = 0.253$

Here, the performance and robustness of the designed frequency stabilizers are evaluated in a linearized model of the three-area interconnected system. Here, changing load disturbances which are simultaneously applied to areas 1 and 3, are composed of three different components in the frequency domain, one of which (underlined component) has a frequency corresponding to the inter-area mode of interest (see Table 4.6), as follows.

$$Area\ 1\ :\ \Delta P_{L1} = \underline{0.003\sin(4.36t)} + 0.005\sin(5.3t) - 0.007\sin(6t) \qquad (4.21)$$

$$Area\ 3\ :\ \Delta P_{L3} = \underline{0.003\sin(3.29t)} + 0.007\sin(4t) - 0.005\sin(4.5t) \qquad (4.22)$$

Note that the dynamic of governor as illustrated in Fig. 4.9, is also included into each area in this simulation study. Table 4.8 shows operating conditions and applied disturbances.

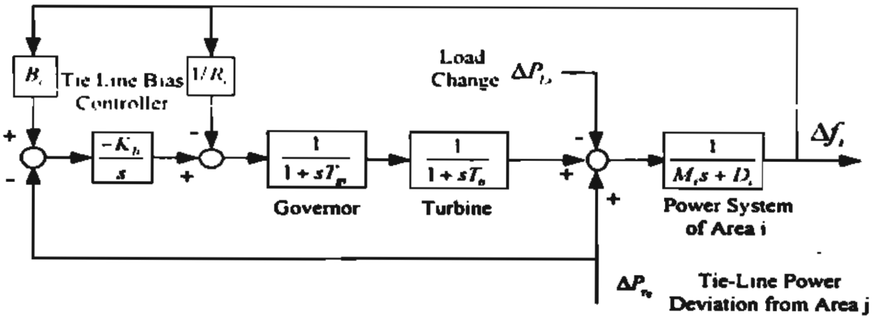

Figure 4.9: Linearized system model of area *i* including governor

Table 4.8: System Conditions and Applied Disturbances

Case	Disturbances
1	At normal (design) condition, ΔP_{L1} is applied to area 1 and ΔP_{L3} is applied to area 3. (No parameter variations)
2	At unstable condition, ΔP_{L1} is applied to area 1 and ΔP_{L3} is applied at area 3 while damping coefficients D_1 and D_3 are set -0.45.

For case 1, the damping effect of each designed stabilizer is investigated. As demonstrated in Figs. 4.10 – 4.12, both robust and non-robust frequency stabilizers are able to damp the frequency oscillation in each area, effectively. In addition, Figs. 4.13 – 4.14 depict that both tie-lines 1-2 and 2-3 power oscillations are also stabilized by both frequency stabilizers. Nevertheless, the damping effect of the robust frequency stabilizer is better than that of the non-robust case. As declared in Figs. 4.15 and 4.16, the power output deviation of the robust frequency stabilizer for each SSSC is less or equal to that of non-robust frequency stabilizer.

In case 2, not only damping effect but also robust stability of the system incorporated with each frequency stabilizer are evaluated. It is assumed that both power systems 1 and 3 are in unstable conditions, so that D_1 and D_3 are set to -0.45 (MW/Hz). As the load disturbances applied to both areas, frequency deviations of areas 1, 2 and 3 in case of the non-robust frequency stabilizer severely fluctuate and finally diverge as depicted in Figs. 4.17 – 4.19. Note that frequency deviation of each area in case of SSSCs without frequency stabilizers (not shown here) also heavily oscillates and finally diverges. On the other hand, frequency oscillations in all areas are completely stabilized by the robust frequency stabilizer. The interconnected power system can maintain the system stability. Figures 20 and 21 also exhibit the significant damping effects of robust frequency stabilizers on the tie-lines 1-2 and 2-3 power oscillations. The power output deviations of robust frequency stabilizers are illustrated in Figs. 4.22 and 4.23. These simulation results confirm that under severe load disturbances and negative damping, the robustness of robust frequency stabilizer against such system uncertainties is considerably superior to that of non-robust frequency stabilizer.

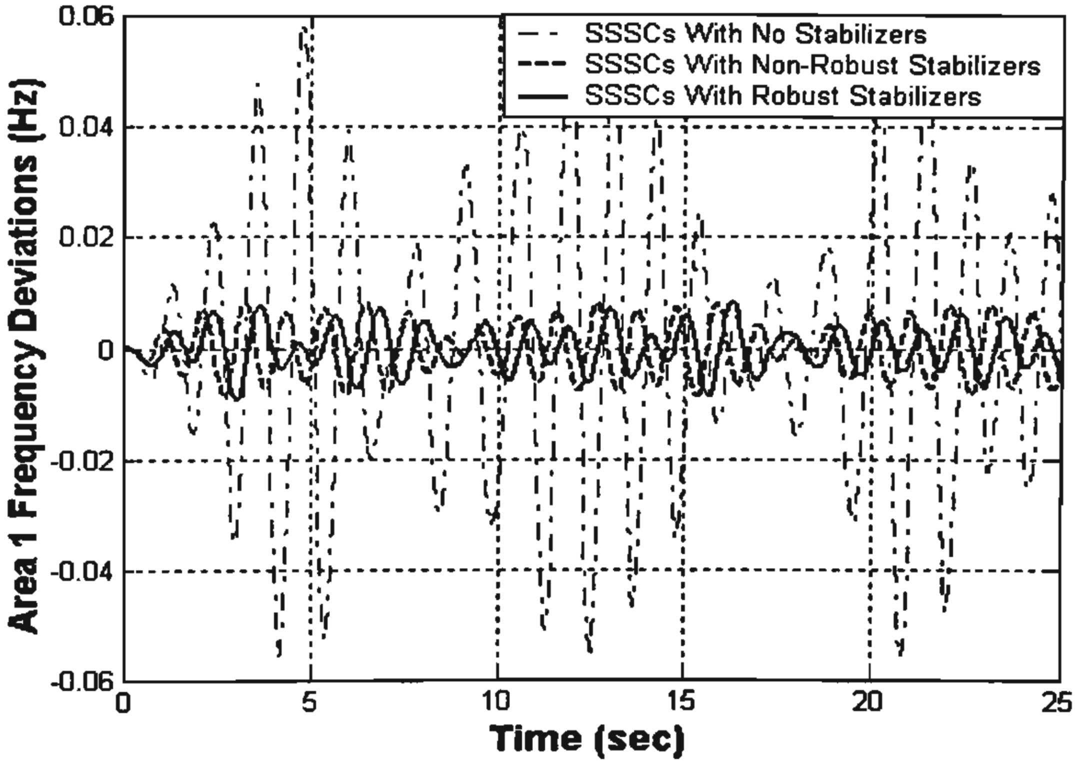

Figure 4.10: Frequency deviation of area 1 for case 1

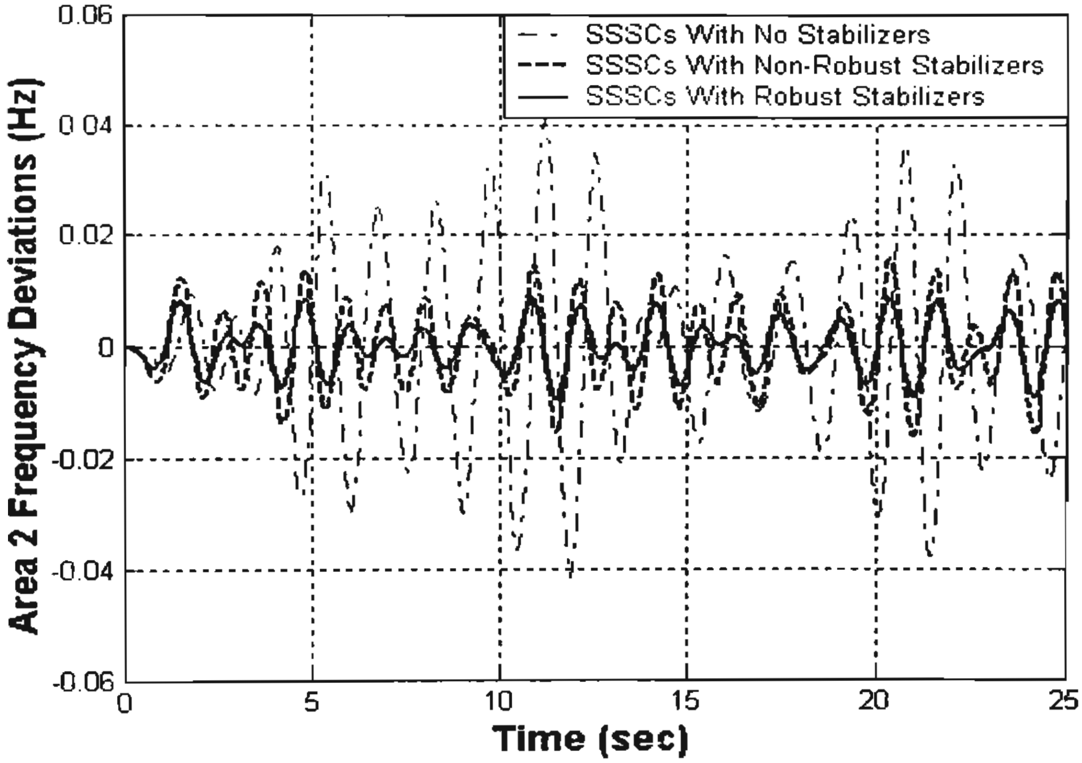

Figure 4.11: Frequency deviation of area 2 for case 1

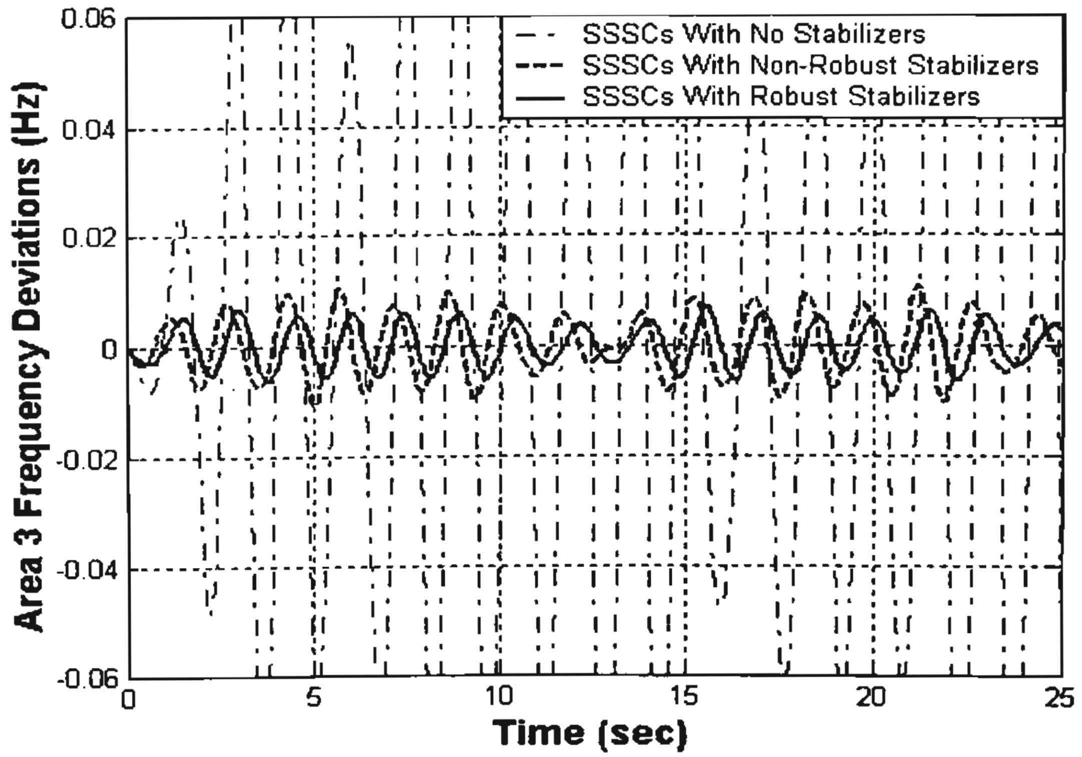

Figure 4.12: Frequency deviation of area 3 for case 1

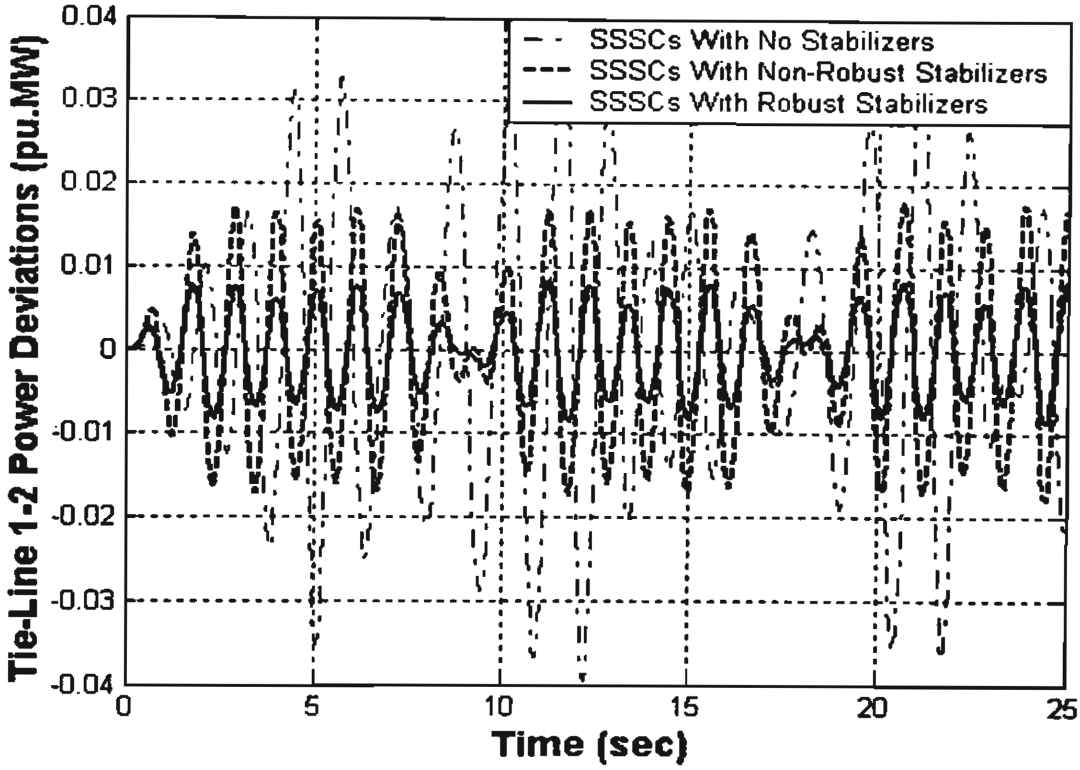

Figure 4.13: Tie-line power deviation between areas 1 and 2 for case 1

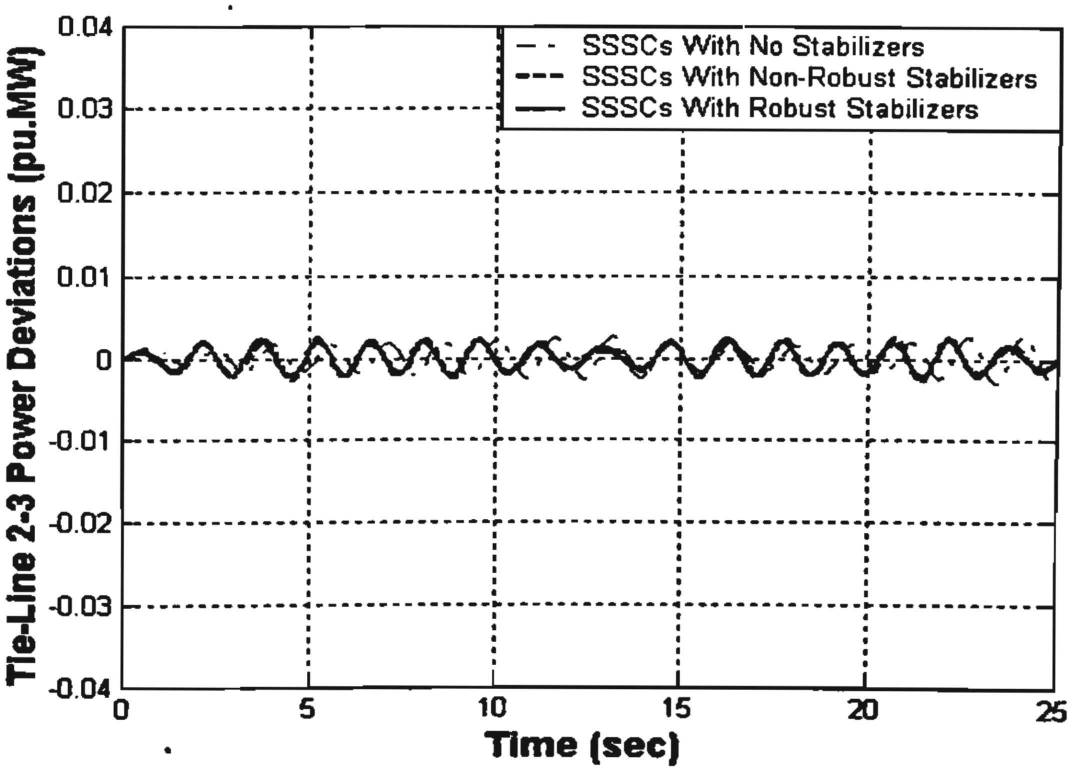

Figure 4.14: Tie-line power deviation between areas 2 and 3 for case 1

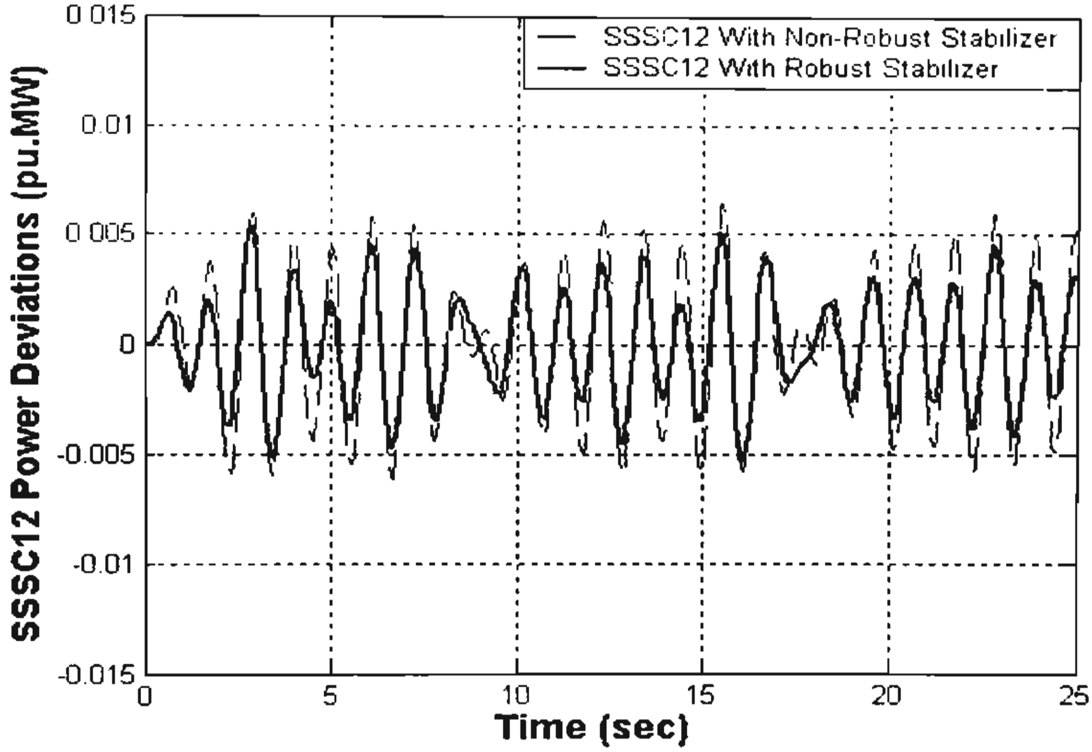

Figure 4.15: Power output deviation of SSSC12 for case 1

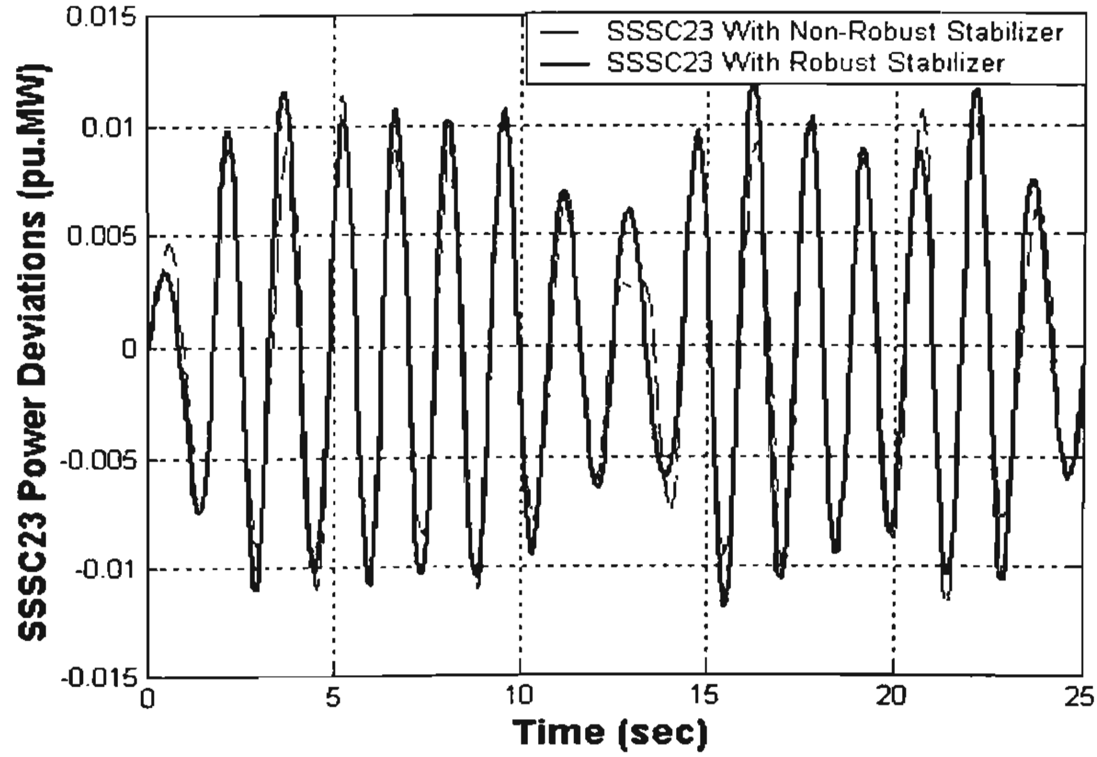

Figure 4.16: Power output deviation of SSSC23 for case 1

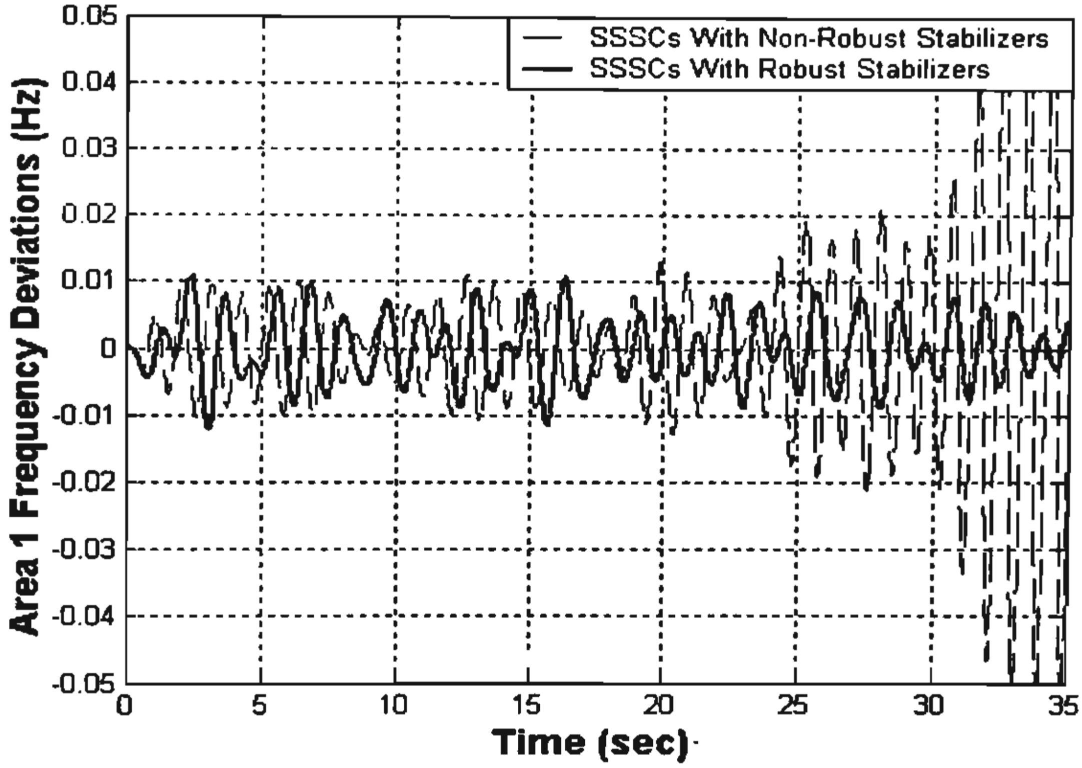

Figure 4.17: Frequency deviation of area 1 for case 2

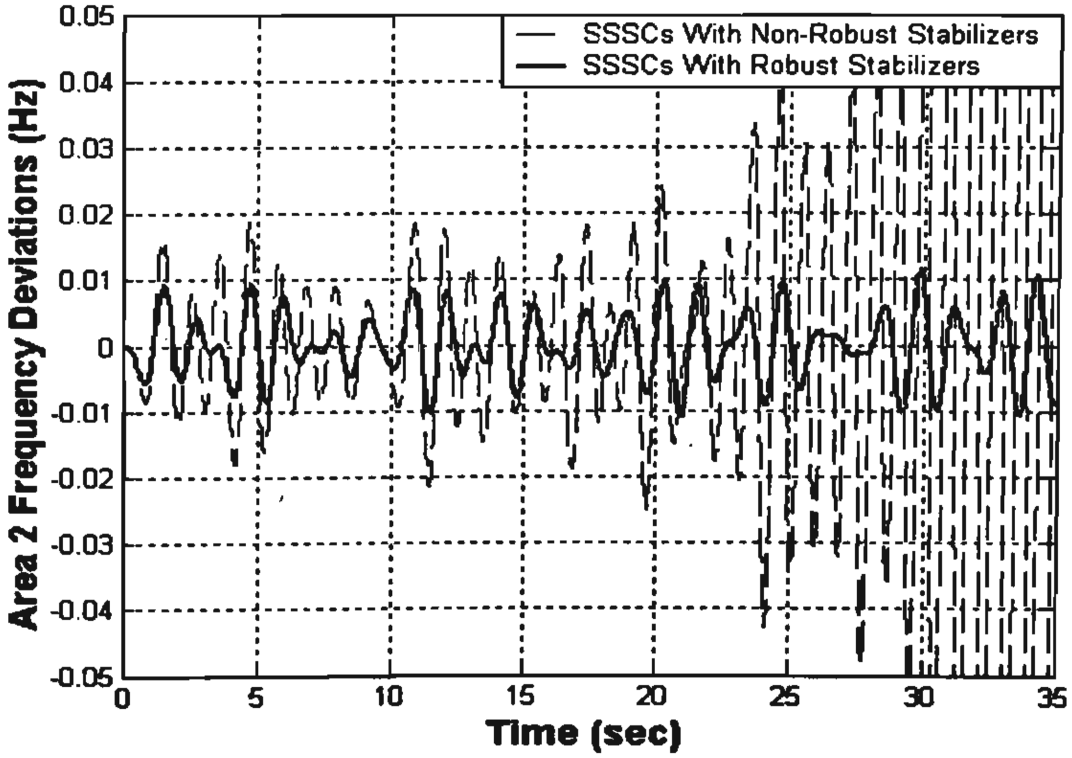

Figure 4.18: Frequency deviation of area 2 for case 2

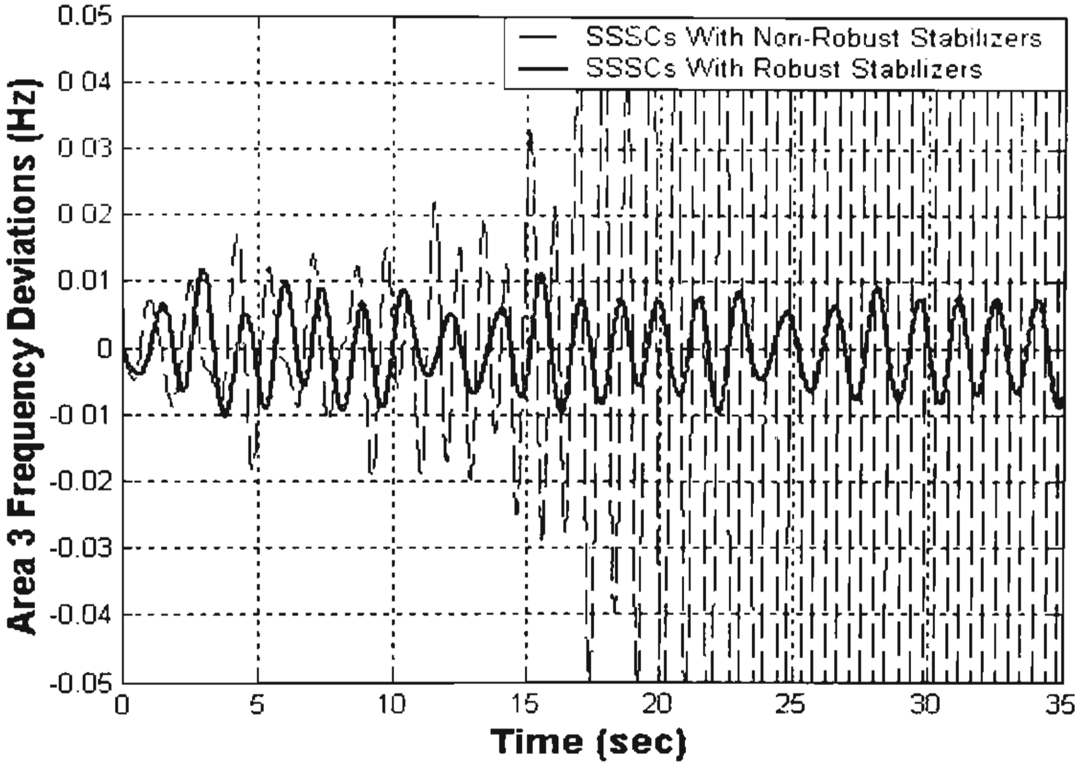

Figure 4.19: Frequency deviation of area 3 for case 2

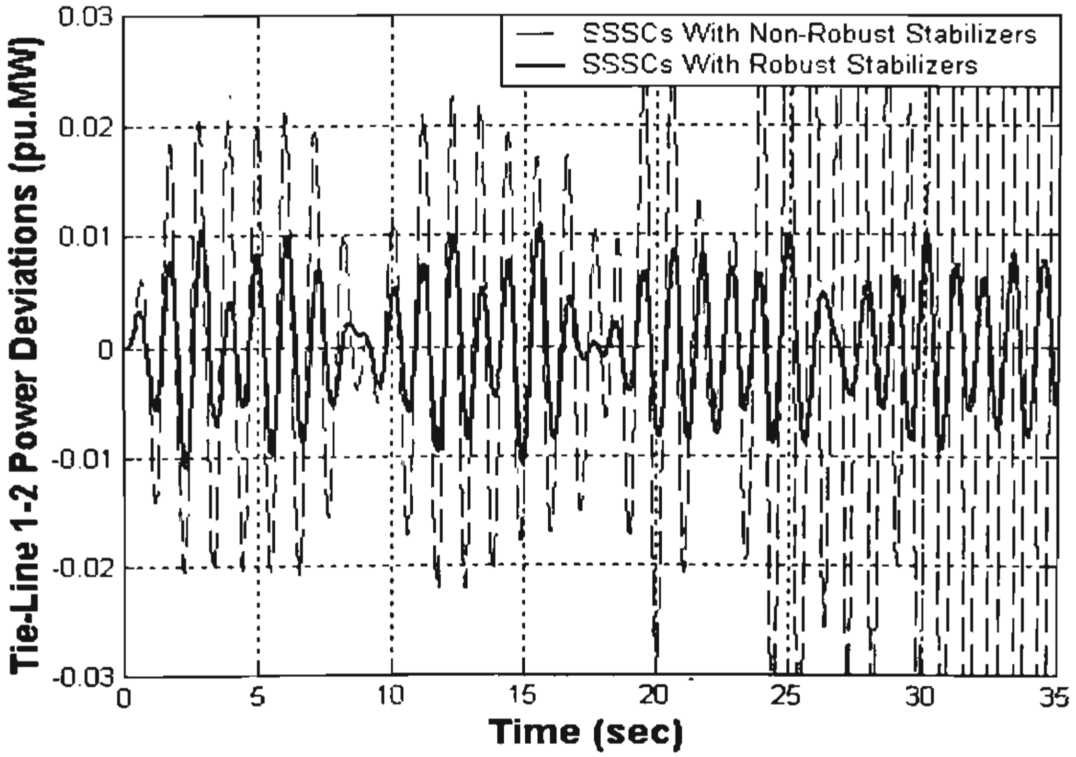

Figure 4.20: Tie-line power deviation between areas 1 and 2 for case 2

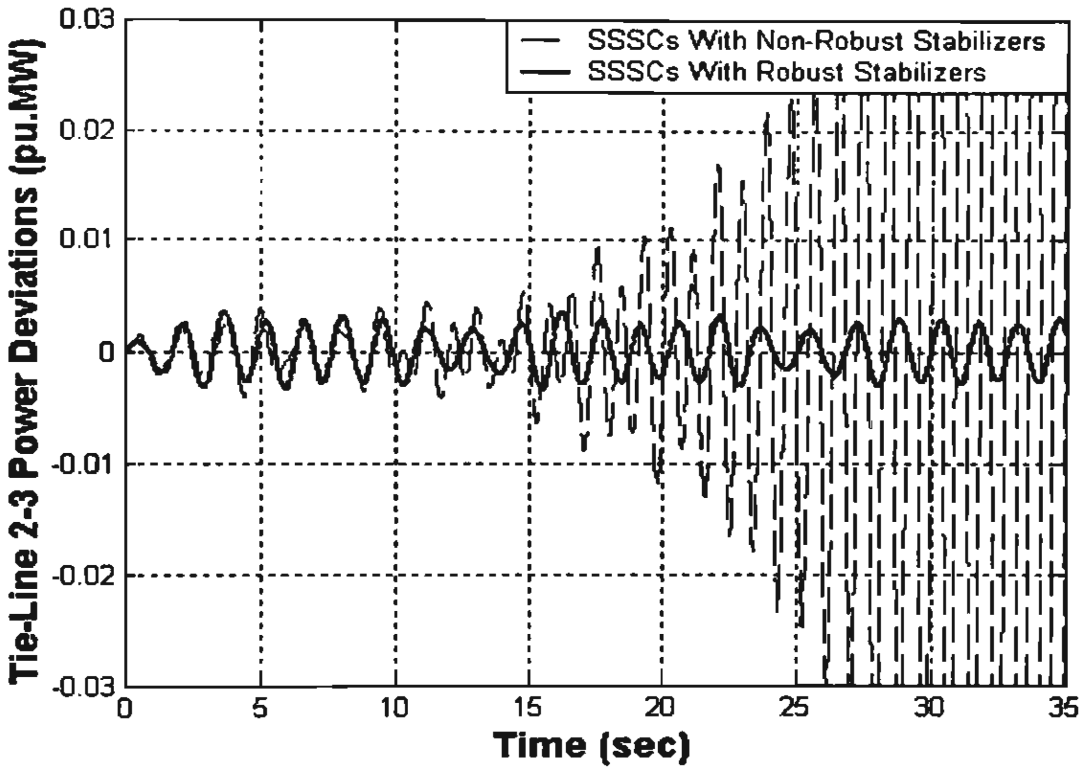

Figure 4.21: Tie-line power deviation between areas 2 and 3 for case 2

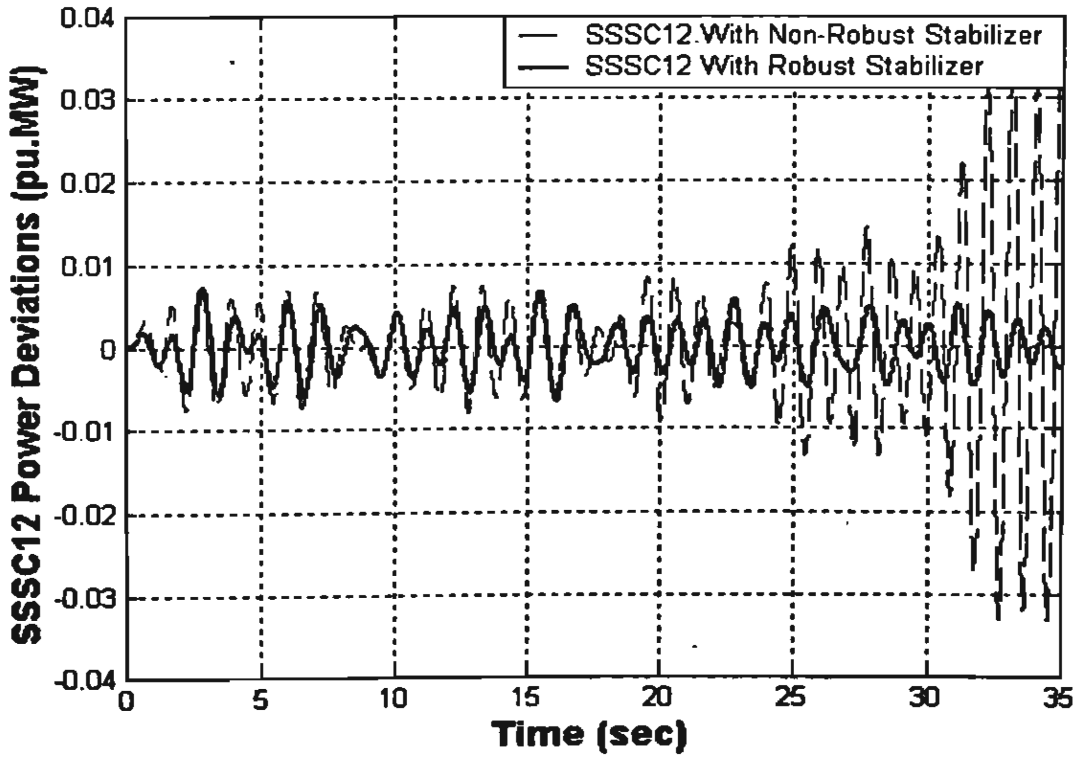

Figure 4.22: Power output deviation of SSSC12 for case 2

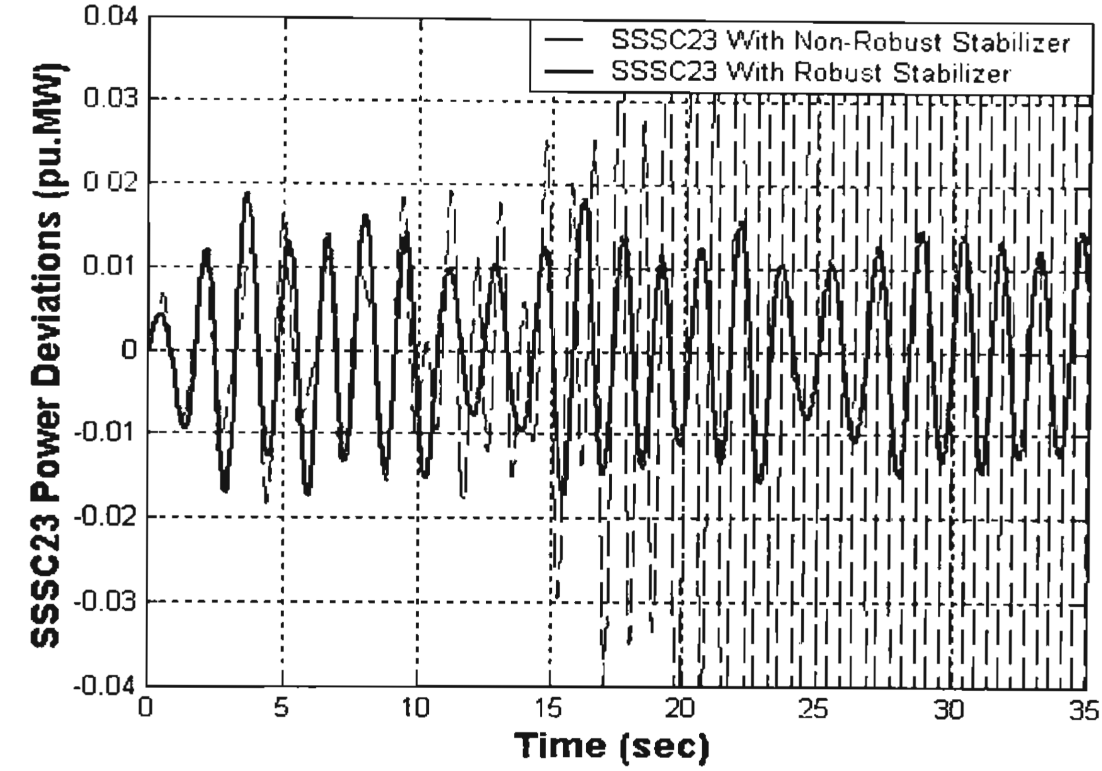

Figure 4.23: Power output deviation of SSSC23 for case 2

4.5. Conclusions

This chapter focuses on the new robust design of discrete frequency stabilizer of SSSC by taking system uncertainties into account. The design method utilizes the merit of overlapping decompositions technique to extract the subsystem embedded with the inter-area oscillation mode of interest. By including the multiplicative uncertainty model in the extracted subsystem, the robust stability index based on multiplicative stability margin can be applied in the formulation of objective function. As a result, the robust stability margin of system with designed frequency stabilizer can be improved. Without trial and error, the tabu search algorithm is automatically applied to search for the optimal control parameters of the continuous-based second-order lead/lag stabilizer. As a result, the discrete-based frequency stabilizer can be easily achieved by using z-transformation of the resulted continuous-based stabilizer. The high robustness of the discrete frequency stabilizer against various load disturbances with changing frequency in the vicinity of inter-area mode and negative damping, has been confirmed by simulation study.

Chapter 5

Summary

In this report, a new robust design method of frequency stabilizer of SSSC has been proposed. The concept and the practical motivations for application of the proposed control have been clarified. The systematic design of SSSC frequency stabilizer in a general multi-area interconnected power system has been presented. Evaluation study has confirmed the significant effects of the frequency stabilizer designed by the proposed method.

The main outcomes from this research can be summarized as follows.

- This research proposes a new application of static synchronous series compensator (SSSC) as an apparatus to stabilization of frequency oscillations in an interconnected power system. The dynamic control of tie line power flow of SSSC located in series with tie line between interconnected areas can be applied to stabilize frequency oscillations via the system interconnections.
- The coordinated control of SSSC and governor system has been implemented. The SSSC plays a role in suppressing the magnitude of the transient frequency oscillation, while the governor is responsible for eliminating the steady state error of frequency oscillation.
- The SSSC is a very effective stabilization strategy of frequency oscillations for a system which has insufficient frequency control capability. By transferring the large control capability of an interconnected system via an SSSC, the problem of frequency oscillation in the target area can be alleviated.
- The design method utilizes the merit of overlapping decompositions technique to extract the subsystem embedded with the inter-area oscillation mode of interest. By virtue of overlapping decompositions, the physical characteristic of the power system can be preserved in the reduced system.
- The multiplicative uncertainty model is applied to represent all possible unstructured uncertainties in interconnected power systems. As a result, the robust stability margin against uncertainties can be easily guaranteed in terms of the multiplicative stability margin (MSM). Based on this uncertainty model, the MSM can be also incorporated in the objective function which the index of disturbance attenuation performance is already taken into consideration.
- The configuration of frequency stabilizer presented here is practically based on a second-order lead lag compensator with a single input signal. Without trial and error, the control parameters of the frequency stabilizer are automatically

optimized by a tabu search algorithm, so that the desired damping ratio of the target inter-area mode and the best MSM are achieved.

- The robust frequency stabilizer can be designed based on the proposed method in continuous time domain. In addition, to implement in real power system, the continuous based frequency stabilizer can be easily transformed to the discrete based frequency stabilizer by digital control technique.
- Several simulation studies clearly show the high robustness of the frequency stabilizer under large load with changing frequency in the vicinity of the inter-area oscillation mode and negative damping.

References

1. F. D. Galliana and M. Illic, *Power System Restructuring*, Kluwer Academic Publishers, 1998.
2. L. Philipson and H. L. Willis, *Understanding Electric Utilities and De-Regulation*, Marcel Dekker, 1999.
3. K. N. Zadeh, R. C. Meyer and G. Cauley, Practices and new concepts in power system control, *IEEE Transactions on Power Systems*, Vol. 11, No. 1, pp. 3-9, 1996.
4. L. H. Fink and P. J. M. Van Son, On system control within a restructured Industry, *IEEE Transactions on Power Systems*, Vol.13, No. 2, pp. 611-616, 1998.
5. Interconnected Operations Service Working Group, *Defining Interconnected Operation Service Under Open Access*, 1997, available at www.nerc.com
6. M. Ilic and S. Liu, Hierarchical *Power System Control, Its Value in a Changing Industry*, Springer-Verlag, 1996.
7. R. Christie and A. Bose, Load Frequency Control Issues in Power System Operations after Deregulation, *IEEE Transactions on Power Systems*, Vol. 11, No. 3, pp. 1191-1200, 1996.
8. B. H. Bakken and O. S. Grande, Automatic Generation Control in Deregulated Power System, *IEEE Transactions on Power Systems*, Vol. 13, No. 4, pp. 1401-1406, 1998.
9. N. Jaleeli, L.S. Vanslyck, D.N. Ewart, L.H. Fink and A.G. Hoffmann, Understanding automatic generation control, *IEEE Transactions on Power Systems*, Vol. 7, No. 3, pp. 1106-1122, 1999.
10. C. Concordia and L. K. Kirchmayer, Tie Line Power and Frequency Control of Electric Power Systems, Part I, II, III: *AIEE Trans*. Vol. 72, 1954.
11. O.L. Elgerd, *Electric Energy System Theory*, An Introduction 2nd. McGraw-Hill, 1985.
12. P. Kundur, *Power System Stability and Control*, McGraw Hill, 1994.
13. A. J. Wood and B.F. Wollenberg, Power *Generation, Operation and Control*, 2nd Edition, John Wiley & Sons, 1996.
14. Yao Nan Yu, *Electric Power System Dynamics*, Academic Press, 1983.
15. J. Machowski, J. W. Bialek and J. R. Bumby, *Power System Dynamics and Stability*, John Wiley & Sons, 1997.
16. N. G. Hingorani, High Power Electronics and Flexible AC Transmission Systems, *IEEE Power Engineering Review*, pp. 3-4, 1988.
17. IEEE FACTS Working Group and GIGRE FACTS Working Group, *FACTS Overview*, IEEE 95 TP 108, 1995.
18. IEEE Power Engineering Society, *FACTS Applications*, IEEE 96 TP 116-0, 1996.

19. N. G. Hingorani and L. Gyugyi, *Understanding FACTS: Concepts and Technology of Flexible AC Transmission Systems*, IEEE PRESS, 2000.

20. L. Gyugyi, Dynamic compensator of AC transmission lines by solid-state synchronous voltage source, *IEEE Transactions on Power Delivery*, Vol. 9, No. 2, pp. 904-911, 1994.

21. L. Gyugyi, C. D. Schauder and K.K. Sen, Static Synchronous Series Compensator: A Solid-State Approach to The Series Compensation of Transmission Lines, *IEEE Transactions on Power Delivery*, Vol. 12, No. 1, pp. 406-417, 1997.

22. N. G. Hingorani, Power Electronics in Electric Utilities: Role of Power Electronics in Future Power Systems, *Proceedings of IEEE*, Vol. 76, No. 4, pp. 481-482, 1988.

23. L. Gyugyi, Unified Power Flow Control Concept for Flexible AC Transmission Systems, *IEE Proceedings, Part C*, Vol. 139, No. 4, pp. 323-331, 1992.

24. A. A. Edris, Enhancement of First Swing Stability Using A High Speed Phase Shifter, *IEEE Transactions on Power Systems*, Vol. 6, No. 3, pp. 1113-1118, 1991.

25. M. Noroozian, L. Anguist, M. Chandhari and G. Anderesson, Improving Power System Dynamics by Series-Connected FACTS Devices, *IEEE Transactions on Power Delivery*, Vol. 12, No. 4, pp. 1635-1641, 1997.

26. G. El-Saady, A Variable Structure Static Phase Shifting Transformer for Power System Stabilization, *Electric Power System Research*, Vol. 50, pp. 71-78, 1999.

27. H. Fujita, H. Kurebayashi, H. Nohara, M. Goto and Y. Kito, Loop Power System Control by High Speed Phase Shifter, *Transactions of IEE of Japan*, Vol. 114-B, No. 5, pp. 475-482, 1994.

28. K. Xing and G. L. Kusic, Damping Subsynchronous Resonance by Phase Shifters, *IEEE Transactions on Energy Conversions*, Vol. 4, No. 3, pp. 344-350, 1989.

29. K. K. Sen, SSSC – Static Synchronous Series Compensator, Theory, Modeling and Applications, *IEEE Transactions on Power Delivery*, Vol. 13, No. 1, pp. 241-246, 1998.

30. Y. Morioka, M. Kato, Y. Mishima, Y. Nakachi, M. Asada and K. Tokuhara, Implementation of Unified Power Flow Controller and Verification for Transmission Capability Improvement, *IEEE Transactions on Power Systems*, Vol. 14, No. 2, pp. 575-581, 1999.

31. B. A. Renz, A. J. F. Keri, A. S. Mehraban, J. P. Kessinger, C. D. Schauder, L. Gyugyi, L. J. Kovalskym, A. Edris, World's First Unified Power Flow Controller on the AEP System, *CIGRE*, Session 1998, Paper 14-107.

32. M. Ikeda, D.D. Siljak and D. E. White, Decentralized control with overlapping information sets. *Journal of Optimization Theory and Applications*, Vol. 34, No. 2, pp.279-310, 1981.

33. B. Shahian and M. Hassul, *Control System Design using MATLAB*, Prentice Hall, 1993.

34. S. Skogestad and I. Postlethwaite, *Multivariable Feedback Control, Analysis and Design*, John Wiley & Sons, 1998.
35. G. C. Goodwin, S. F. Graebe and M. E. Salgado, *Control System Design*, Prentice Hall, 2001.
36. F. Glover and M. Laguna, *Tabu Search*. Kluwer Academic Publishers. 2000.
37. V. J. Rayward-Smith, I. H. Osman, C.R. Reeves, and G.D. Smith, *Modern Heuristic Search Methods*, John Wiley & Sons, UK, 1996.

List of Publications

1. Issarachai Ngamroo and Waree Kongprawechnon: A robust controller design of SSSC for stabilization of frequency oscillations in interconnected power systems, *Electric Power System Research*, 2003. (Article in press)

2. Issarachai Ngamroo and Waree Kongprawechnon: Robust frequency stabilizer design of SSSC taking into consideration system uncertainties, ***Submitted to*** *ASEAN Journal on Science & Technology for Development*

M:/Elsevier Science/Shannon/EPSR/articles/EPSR1887/EPSR1887.3d[x] 20 June 2003 8:18:33

ARTICLE IN PRESS

Available online at www.sciencedirect.com

SCIENCE DIRECT

ELSEVIER

Electric Power Systems Research xxx (2003) xxx–xxx

ELECTRIC POWER SYSTEMS RESEARCH

www.elsevier.com/locate/epsr

A robust controller design of SSSC for stabilization of frequency oscillations in interconnected power systems

I. Ngamroo *, W. Kongprawechnon

Electrical Power Engineering Program, Sirindhorn International Institute of Technology, Thammasat University, Pathumthani 12121, Thailand

Received 22 July 2002; received in revised form 19 March 2003; accepted 23 March 2003

Abstract

As an AC interconnected power system is subjected to a large load with rapid change, system frequency may be severely disturbed and becomes oscillatory. To stabilize the frequency oscillations, the dynamic power flow control of the Static Synchronous Series Compensator (SSSC) located in series with the tie line between interconnected power systems, is employed. By regarding the system interconnection as the control channel, the power flow control by an SSSC via the interconnection creates a sophisticated method of frequency stabilization. To implement this concept, the robust design method of the lead/lag controller equipped with the SSSC is proposed. In the design process, not only the attenuation performance of system disturbances, but also the robust stability against system uncertainties are taken into consideration. The optimal parameters of the lead/lag controller are obtained by using the tabu search algorithm (TSA), so that both performance and robustness are satisfied. In addition, the technique of overlapping decompositions is applied to reduce the order of the study power system, meanwhile the physical characteristic is still preserved. Simulation study exhibits the significant effect of designed controller on the study four-area interconnected power system under different load disturbances and variation of system parameters.

Keywords: FACTS; SSSC; Robust control; Tabu search algorithm; Overlapping decompositions; Power system stabilization; Frequency oscillations; Ancillary services

1. Introduction

Nowadays, the electric power system is in transition to a fully competitive deregulated scenario. Under this circumstance, any power system controls such as frequency and voltage controls will be served as ancillary services [1,2]. Especially, in the case that the proliferation of non-utility generations, i.e. Independent Power Producers (IPPs) that do not possess sufficient frequency control capabilities, tends to increase considerably. Furthermore, various kinds of apparatus with large capacity and fast power consumption such as a magnetic levitation transportation, a testing plant for nuclear fusion, or even an ordinary scale factory like a steel manufacturer etc. increase significantly. When these loads are concentrated in a power system, they may cause a serious problem of frequency oscillations. Under this situation, the conventional frequency control, i.e. governor, may no longer be able to absorb the large frequency oscillations due to its slow response [3]. A new service of stabilization of frequency oscillations becomes challenging and is highly expected in the future competitive environment.

To tackle this problem, the authors have proposed a new stabilization of frequency oscillations by the Static Synchronous Series Compensator (SSSC) [4]. The SSSC is a Flexible AC Transmission Systems (FACTS) device, that has been highly expected as an effective apparatus with an ability of dynamic power flow control [5]. In [4], the SSSC is located in series with the tie line between two-area interconnected power system. By regarding the system interconnection as the channel of power flow control by SSSC, the system frequency oscillations under a sudden load disturbance can be stabilized effectively. However, the proposed control scheme of SSSC in [4] is designed based on a state feedback scheme

* Corresponding author. Tel.: +66-2986-9009, fax: +66-2986-9112.
E-mail address: ngamroo@siit.tu.ac.th (Issarachai Ngamroo)

0378-7796/03/$ - see front matter © 2003 Published by Elsevier B.V.
doi:10.1016/S0378-7796(03)00110-X

of variables. Therefore, it is not easy to implement in a multi-area interconnected power system.

In this paper, the new control design of SSSC is presented. The lead/lag controller with a single feedback signal input is equipped with an SSSC. To determine the optimal parameters of the lead/lag controller, the tabu search algorithm (TSA) [6] is employed. TSA is a meta-heuristic method that is based on a local search approach with the ability to escape from being trapped in local optima. It has been applied to solve many problems of power system optimization [7–11]. In the formulation of the objective function, not only the attenuation of system disturbances, but also the robust stability of controller against system uncertainties are taken into consideration. In addition, the technique of overlapping decompositions is applied to reduce the order of the study power system for simplicity of control design.

The organization of this paper is as follows. First, the motivation of the proposed control of SSSC is provided. Next part deals with the design methodology including the coordinated control of SSSC and governors, the mathematical model of SSSC, the system reduction by overlapping decompositions, the objective function formulation, and the TSA. Subsequently, the evaluation of the proposed controller in a four-area interconnected power system is outlined by simulation study. Lastly, a conclusion is given.

2. Motivation of proposed frequency stabilization

Fig. 1 shows the four-area interconnected power system with a loop configuration. This system is used to explain the motivation of the proposed control design. It is assumed that a large load with rapid change has been installed in an area 1. This load change causes serious frequency oscillations. Moreover, IPPs that do not possess frequency control capabilities are included in an area 1. Under this situation, the governors in an area 1 can not sufficiently provide adequate frequency control. On the contrary, the area 2 has large control capability enough to spare for other areas. Therefore, an area 2 offers a service of frequency stabilization to an area 1 by using the SSSC. Since SSSC is a series-connected device, the power flow control effect is independent of an installed location. In the proposed design method, the SSSC controller uses the frequency deviation of area 1 as a local signal input. Therefore, the SSSC is placed at the point near an area 1. Note that the SSSC is utilized as the energy transfer device from area 2 to area 1. As the frequency fluctuation in an area 1 occurs, the SSSC will provide the dynamic control of a tie line power via the system connections. By exploiting the system interconnections as the control channels, the frequency oscillations can be stabilized.

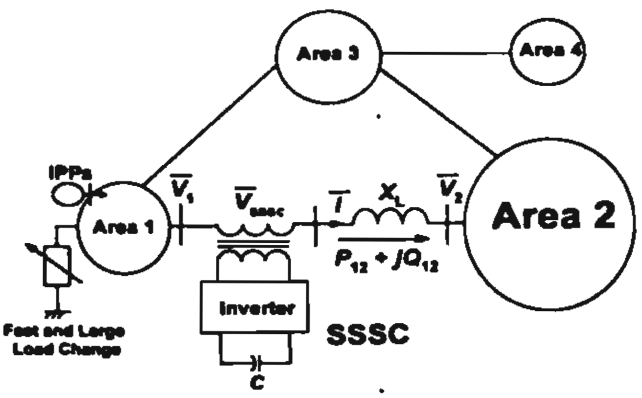

Fig. 1. An SSSC in a four-area interconnected power system.

3. Design of SSSC controller

3.1. Coordinated control of SSSC and governors

The performance of SSSC is extremely rapid when compared with the conventional frequency control system, i.e. governor. The difference in the performance signifies that SSSC and governors may be coordinated as follows. When an area is subjected to a sudden load disturbance, the SSSC quickly acts to minimize the peak value of the frequency deviation. Subsequently, the governors are responsible for eliminating the steady-state errors of frequency deviations. Based on this concept, the periods of operation for two devices do not overlap. Consequently, the dynamics of the governors can then be neglected in the control design of the SSSC for the sake of simplicity.

3.2. Mathematical model of the SSSC

In this study, the mathematical model of the SSSC for stabilization of frequency oscillations is derived from the characteristic of power flow control by SSSC [5]. By adjusting the output voltage of SSSC ($\bar{V}_{sssc}$), the tie line power flow ($P_{12}+jQ_{12}$), can be directly controlled as shown in Fig. 1. Since the SSSC fundamentally controls only the reactive power, then the phasor $\bar{V}_{sssc}$ is perpendicular to the phasor of line current $\bar{I}$, which can be expressed as

$$\bar{V}_{sssc} = jV_{sssc}\bar{I}/I \quad (1)$$

where V_{sssc} and I are the magnitudes of $\bar{V}_{sssc}$ and $\bar{I}$, respectively. Note that, $\bar{I}/I$ is a unit vector of line current. Therefore, the current $\bar{I}$ in Fig. 1, can be expressed as

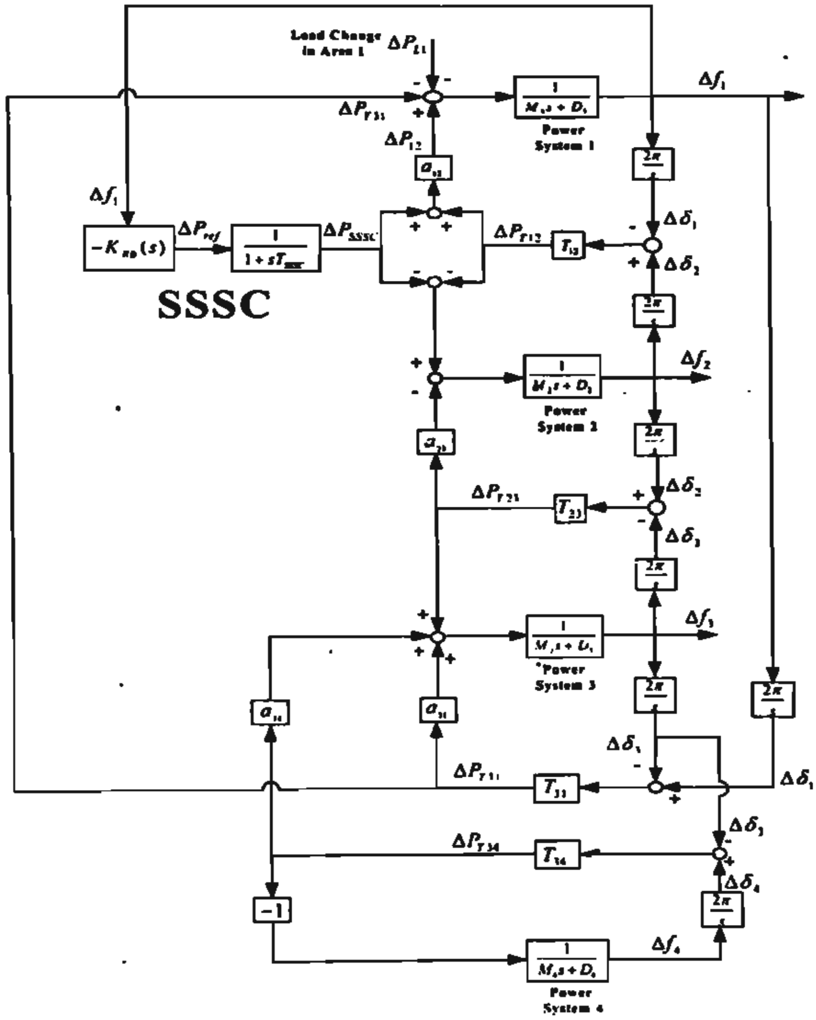

Fig. 2. An SSSC in a linearized four-area interconnected power system without governors.

$$\bar{I} = \frac{\bar{V}_1 - \bar{V}_2 - jV_{SSSC}\bar{I}/I}{jX_L} \quad (2)$$

where X_L is the reactance of a tie line, $\bar{V}_1$ and $\bar{V}_2$ are the voltages at buses 1 and 2, respectively. The active power and reactive power flow through bus 1 are

$$P_{12} + jQ_{12} = \bar{V}_1\bar{I}^* \quad (3)$$

where $\bar{I}^*$ is a conjugate of $\bar{I}$. Substituting $\bar{I}$ from (2) into (3) yields

$$P_{12} + jQ_{12} = \frac{V_1V_2}{X_L}\sin(\delta_1 - \delta_2) - V_{SSSC}\frac{\bar{V}_1\bar{I}^*}{X_L I} + j\left(\frac{V_1^2}{X_L} - \frac{V_1V_2}{X_L}\cos(\delta_1 - \delta_2)\right). \quad (4)$$

where $\bar{V}_1 = V_1e^{j\delta_1}$ and $\bar{V}_2 = V_2e^{j\delta_2}$. In the second term of the right hand side of (4), $\bar{V}_1\bar{I}^*$ is equal to $P_{12} + jQ_{12}$ (see (3)). Accordingly, the relation in the real part of (4) provides

$$P_{12} = \frac{V_1V_2}{X_l}\sin(\delta_1 - \delta_2) - \frac{P_{12}}{X_l I}V_{SSSC} \quad (5)$$

In (5), the second term of the right hand side is the active power controlled by SSSC. Here, it is assumed that V_1 and V_2 are constant and the initial value of V_{SSSC} is zero, i.e. $V_{SSSC0} = 0$. By linearizing (5) about an initial operating point,

$$\Delta P_{12} = \frac{V_1V_2\cos(\delta_{10} - \delta_{20})}{X_l}(\Delta\delta_1 - \Delta\delta_2) - \frac{P_{120}}{X_l I_0}\Delta V_{SSSC} \quad (6)$$

where the subscript "0" denotes the value at the initial operating point. As the voltage deviation of SSSC

(ΔV_{SSSC}) is adjusted, the power output deviation injected by SSSC can be controlled as $\Delta P_{SSSC} = -(P_{120}/X_l I_0)\Delta V_{SSSC}$. Equation (6), therefore, implies that the SSSC is capable of controlling the active power independently. Here, the SSSC is represented by the active power controller. The control effect by SSSC is expressed by the injected power deviation ΔP_{SSSC} instead of $-(P_{120}/X_l I_0)\Delta V_{SSSC}$. As a result, (6) can be expressed as

$$\Delta P_{12} = \Delta P_{T12} + \Delta P_{SSSC} \tag{7}$$

where

$$\Delta P_{T12} = \frac{V_1 V_2 \cos(\delta_{10} - \delta_{20})}{X_l}(\Delta\delta_1 - \Delta\delta_2) = T_{12}(\Delta\delta_1 - \Delta\delta_2) \tag{8}$$

and T_{12} is a synchronizing power coefficient.

3.3. Design methodology

A study system depicted in Fig. 1 is used to explain the proposed control design of SSSC. The linearized four-area interconnected system [12] including the active power model of SSSC is delineated in Fig. 2.

Based on the coordinated control of SSSC and governors, the dynamics of governors are eliminated in this figure. The active power controller of SSSC has a structure of the lead/lag compensator $K_{RB}(s)$ with output signal ΔP_{ref}. In this study, the dynamic characteristic of SSSC is modeled as the first order controller with time constant T_{SSSC}. Note that the injected power deviation of SSSC, ΔP_{SSSC} acting positively on the area 1 reacts negatively on the area 2. Therefore, ΔP_{SSSC} flows into both areas with different signs (+, −), simultaneously. This characteristic represents the physical meaning of (7). The linearized system in Fig. 2 can be expressed as

$$S: \begin{bmatrix} \Delta\dot{f}_1 \\ \Delta\dot{P}_{T12} \\ \Delta\dot{f}_2 \\ \Delta\dot{P}_{T23} \\ \Delta\dot{f}_3 \\ \Delta\dot{P}_{T34} \\ \Delta\dot{f}_4 \end{bmatrix} = \begin{bmatrix} -\frac{D_1}{M_1} & a_{s12} & 0 & a_{s14} & 0 & 0 & 0 \\ -2\pi T_{12} & 0 & 2\pi T_{12} & 0 & 0 & 0 & 0 \\ 0 & -\frac{1}{M_2} & -\frac{D_2}{M_2} & -\frac{a_{21}}{M_2} & 0 & 0 & 0 \\ 0 & 0 & 2\pi T_{23} & 0 & -2\pi T_{23} & 0 & 0 \\ 0 & a_{s52} & 0 & a_{s54} & -\frac{D_3}{M_3} & \frac{a_{34}}{M_3} & 0 \\ 0 & 0 & 0 & 0 & -2\pi T_{34} & 0 & 2\pi T_{34} \\ 0 & 0 & 0 & 0 & 0 & -\frac{1}{M_4} & -\frac{D_4}{M_4} \end{bmatrix} \begin{bmatrix} \Delta f_1 \\ \Delta P_{T12} \\ \Delta f_2 \\ \Delta P_{T23} \\ \Delta f_3 \\ \Delta P_{T34} \\ \Delta f_4 \end{bmatrix} + \begin{bmatrix} \frac{a_{12}}{M_1} \\ 0 \\ -\frac{1}{M_2} \\ 0 \\ 0 \\ 0 \\ 0 \end{bmatrix} \Delta P_{SSSC} \tag{9}$$

where, Δf_i is the frequency deviation of area i, ΔP_{Tij} is the tie line power deviation between areas i and j, M_i is the inertia constant of area i, D_i is the damping coefficient of area i, a_{ij} is the area capacity ratio between areas i and j, T_{ij} is the synchronizing power coefficient of the tie line between areas i and j, where $i, j = 1, \ldots, 4$. Here $a_{S12} = (a_{12} + T_{31}/T_{12})/M_1$, $a_{S14} = -T_{31}/(M_1 T_{23})$, $a_{S52} = -a_{31}T_{31}/(M_3 T_{12})$, $a_{S54} = (1 + a_{31}T_{31}/T_{23})/M_3$. The variable ΔP_{T31} is represented in terms of ΔP_{T12} and ΔP_{T23} by

$$\Delta P_{T31} = -\frac{T_{31}}{T_{12}}\Delta P_{T12} + \frac{T_{31}}{T_{23}}\Delta P_{T23} \tag{10}$$

Thus, ΔP_{T31} has disappeared in (9). This system has three conjugate pairs of complex eigenvalues and a negative real eigenvalue. The former corresponds to three inter-area oscillation modes, and the latter the inertia center mode. In this paper, the design purpose of SSSC is to enhance the damping of the inter-area mode between areas 1 and 2. The proposed design can be divided into three steps as follows.

3.3.1. Reduction of power system model by overlapping decompositions [13]

The concept of overlapping decompositions is applied to the system (9) with the aim of extracting the subsystem where the inter-area mode between areas 1 and 2 is preserved. The system (9) is referred to as the system S. The state variables of S are classified into three groups, i.e. $x_1 = [\Delta f_1]$, $x_2 = [\Delta P_{T12}]$, $x_3 = [\Delta f_2, \Delta P_{T23}, \Delta f_3, \Delta P_{T34}, \Delta f_4]^T$. Therefore, the system S can be expressed in compact form as

$$S: \begin{bmatrix} \dot{x}_1 \\ \dot{x}_2 \\ \dot{x}_3 \end{bmatrix} = \begin{bmatrix} A_{11} & A_{12} & A_{13} \\ A_{21} & A_{22} & A_{23} \\ A_{31} & A_{32} & A_{33} \end{bmatrix} \begin{bmatrix} x_1 \\ x_2 \\ x_3 \end{bmatrix} + \begin{bmatrix} B_{11} \\ B_{21} \\ B_{31} \end{bmatrix} \Delta P_{SSSC} \tag{11}$$

The sub-matrices A_{ij} and B_{i1}, ($i, j = 1, 2, 3$) have appropriate dimensions identical to the corresponding state and input vectors. According to the process of overlapping decompositions, the system S can be expanded as

$$\tilde{S}:\begin{bmatrix}\dot{z}_1\\ \dot{z}_2\end{bmatrix}=\begin{bmatrix}A_{11} & A_{12} & 0 & A_{13}\\ A_{21} & A_{22} & 0 & A_{23}\\ A_{21} & 0 & A_{22} & A_{23}\\ A_{31} & 0 & A_{32} & A_{33}\end{bmatrix}\begin{bmatrix}z_1\\ z_2\end{bmatrix}+\begin{bmatrix}B_{11}\\ B_{21}\\ B_{21}\\ B_{31}\end{bmatrix}\Delta P_{\mathrm{SSSC}} \tag{12}$$

$z_1=[x_1^T, x_2^T]$and $z_2=[x_2^T, x_3^T]^T$. The system $\tilde{S}$ in (12) can be decomposed into two interconnected overlapping subsystems.

$$\tilde{S}_1:\dot{z}_1=\left(\begin{bmatrix}A_{11} & A_{12}\\ A_{21} & A_{22}\end{bmatrix}z_1+\begin{bmatrix}B_{11}\\ B_{21}\end{bmatrix}\Delta P_{\mathrm{SSSC}}\right)+\begin{bmatrix}0 & A_{13}\\ 0 & A_{23}\end{bmatrix}z_2 \tag{13}$$

$$\tilde{S}_2:\dot{z}_2=\left(\begin{bmatrix}A_{22} & A_{23}\\ A_{32} & A_{33}\end{bmatrix}z_2\right)+\begin{bmatrix}A_{21} & 0\\ A_{31} & 0\end{bmatrix}z_1+\begin{bmatrix}B_{21}\\ B_{31}\end{bmatrix}\Delta P_{\mathrm{SSSC}} \tag{14}$$

The state variable x_2, i.e. the tie line power deviation between areas 1 and 2 (ΔP_{T12}), is repeatedly included in both subsystems, which implies "*Overlapping Decompositions*".

For system stabilization, consider two interconnected subsystems $\tilde{S}_1$ and $\tilde{S}_2$. The terms in the right hand sides of (13) and (14) can be separated into the decoupled subsystems (as indicated in the parenthesis in (13) and (14)) and the interconnection subsystems. As mentioned in [13], if each decoupled subsystem can be stabilized by its own input, the asymptotic stability of the interconnected overlapping subsystems $\tilde{S}_1$ and $\tilde{S}_2$ are maintained. Moreover, the asymptotic stability of the original system S is also guaranteed. Consequently, the interactions of the decoupled subsystems with the interconnection subsystems in (13) and (14) are regarded as perturbations. They can be neglected during control design. As a result, the decoupled subsystems of $\tilde{S}_1$ and $\tilde{S}_2$ can be expressed as

$$\tilde{S}_{D1}:\dot{z}_1=\begin{bmatrix}A_{11} & A_{12}\\ A_{21} & A_{22}\end{bmatrix}z_1+\begin{bmatrix}B_{11}\\ B_{21}\end{bmatrix}\Delta P_{\mathrm{SSSC}} \tag{15}$$

$$\tilde{S}_{D2}:\dot{z}_2=\begin{bmatrix}A_{22} & A_{23}\\ A_{32} & A_{33}\end{bmatrix}z_2+\begin{bmatrix}B_{11}\\ B_{21}\end{bmatrix}\Delta P_{\mathrm{SSSC}} \tag{16}$$

In (15) and (16), there is a control input ΔP_{SSSC} appearing only in the subsystem $\tilde{S}_{D1}$. Here, the decoupled subsystem $\tilde{S}_{D1}$ is regarded as the designed system, which can be expressed as

$$\tilde{G}:\begin{bmatrix}\Delta \dot{f}_1\\ \Delta \dot{P}_{T12}\end{bmatrix}=\begin{bmatrix}-D_1/M_1 & a_{S12}\\ -2\pi T_{12} & 0\end{bmatrix}\begin{bmatrix}\Delta f_1\\ \Delta P_{T12}\end{bmatrix}+\begin{bmatrix}a_{12}/M_1\\ 0\end{bmatrix}\Delta P_{\mathrm{SSSC}} \tag{17}$$

It can be verified that the eigenvalues of (17) are complex conjugate and are assumed to be $-\sigma\pm j\omega_d$. These complex eigenvalues correspond to the inter-area oscillation mode between areas 1 and 2 in the original system S. By virtue of overlapping decompositions, the physical characteristic of the original system S is still preserved after the process of system reduction. This explicitly shows the merit of overlapping decompositions.

By incorporating the dynamic characteristic of the SSSC, (17) becomes

$$G:\begin{bmatrix}\Delta \dot{f}_1\\ \Delta \dot{P}_{T12}\\ \Delta \dot{P}_{\mathrm{SSSC}}\end{bmatrix}=\begin{bmatrix}-D_1/M_1 & a_{S12} & a_{S12}/M_1\\ -2\pi T_{12} & 0 & 0\\ 0 & 0 & -1/T_{\mathrm{SSSC}}\end{bmatrix}\begin{bmatrix}\Delta f_1\\ \Delta P_{T12}\\ \Delta P_{\mathrm{SSSC}}\end{bmatrix}+\begin{bmatrix}0\\ 0\\ 1/T_{\mathrm{SSSC}}\end{bmatrix}\Delta P_{ref} \tag{18}$$

For the input signal of SSSC controller, two available local signals, i.e. area 1 frequency deviation (Δf_1) and the tie line 1–2 power deviation (ΔP_{T12}) are taken into consideration. By calculating the right eigenvector of the oscillation mode between areas 1 and 2, the degree of activity [14] of Δf_1 and ΔP_{T12} in this mode can be evaluated. From (18), the eigenvalues representing the oscillation mode are $\lambda_{1,2}=-0.015\pm j3.5316$. The magnitudes of elements of the right-eigenvectors that correspond to Δf_1 and ΔP_{T12} are 0.6088 and 0.1953, respectively. As a result, Δf_1 provides higher degree of activity in this mode. Consequently, Δf_1 is used as the input signal of SSSC controller. The negative feedback control scheme of SSSC controller can be expressed by

$$\Delta P_{ref}=-K_{RB}(s)\Delta f_1 \tag{19}$$

The robust controller $K_{RB}(s)$ is in form of a lead/lag stabilizer as

$$K_{RB}(s)=k\frac{T_w s}{1+T_w s}\frac{(1+T_1 s)(1+T_3 s)}{(1+T_2 s)(1+T_4 s)} \tag{20}$$

where k: a controller gain, T_1, T_2, T_3, T_4: lead/lag time constants (s), T_w: a washout time constant (s).

Here, T_w is set to 10 (s). The control parameters k, T_1, T_2, T_3, T_4 and T_4 are searched based on the objective function explained in the next section.

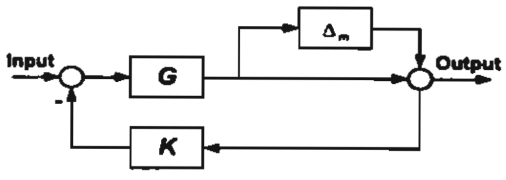

Fig. 3. Feedback system with multiplicative uncertainty.

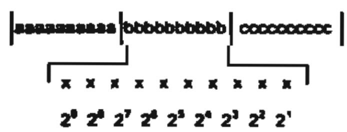

Fig. 4. Example of a 30 bit concatenated encoding scheme.

3.3.2. Determination of objective function

In derivation of the objective function, both attenuation performance of system disturbances, and robust stability of controller against system uncertainties are taken into consideration. Since the main purpose of SSSC is to limit the peak frequency deviation following a sudden load perturbation, the peak frequency deviation can be used as a design specification. Assume that the eigenvalues corresponding to the mode of frequency oscillation in the uncontrolled system G are determined as $-\sigma \pm j\omega_d$. Thus, the system peak response to the unit step input is given by

$$M_{P(actual)} = 1 + \exp(-\sigma\pi/\omega_d) \quad (21)$$

[15]. If the peak allowable frequency deviation of the controlled system is specified to be $M_{P(design)}$, then the magnitude of the difference between the design and the actual peak frequency deviations can be defined as

$$\psi = |M_{P(design)} - M_{P(actual)}| \quad (22)$$

This is the part of disturbance attenuation performance in the objective function that will be minimized.

Next, the robust stability against system uncertainties is taken into consideration. The possible uncertainties are ignored nonlinear characteristics of the study system, ranges and bounds for uncertain system parameters etc. Practically, it is hardly to know about the information of all uncertainties existing in the system. To consider such system uncertainties, the unstructured uncertainty can be applied. In general, an upper bound of the magnitude (or size) of unstructured uncertainty can be estimated. If the magnitude of system uncertainties is less than this upper bound, the robust stability of system is guaranteed. Here, the multiplicative uncertainty [15] is applied to represent the unstructured uncertainty in the system, as shown in Fig. 3. Note that G is a nominal system transfer function, Δ_m is a stable multiplicative perturbation, and K is a controller designed to ensure the internal stability of the nominal closed loop. Based on the small-gain theorem [15], the closed loop system will be robustly stable if

$$|\Delta_m| < \frac{1}{|GK(1+GK)^{-1}|} \quad (23)$$

where, the symbol $|\Delta_m|$ shows the magnitude of uncertainty. $|GK(1+GK)^{-1}|$ is the magnitude of complementary sensitivity function which is referred to as $|T|$.

As mentioned in [15], the multiplicative stability margin (MSM) is defined as

$$\text{MSM} = 1/\|T\|_\infty \quad (24)$$

where $\|T\|_\infty$ is the ∞-norm of T. The MSM can be used to measure the robust stability of the system. Large value of MSM exhibits high robust stability of the system.

From (23) and (24), it is cleared that if the controller K can be designed to minimize $\|T\|_\infty$, the MSM increases. As a result, the upper bound of $|\Delta_m|$ is enlarged, and the high robust stability will be ensured. Thus, the robustness index in the objective function can be defined in normalized form as,

$$\gamma = \|T\|_\infty / \|T\|_{\infty(\text{initial})} \quad (25)$$

where $\|T\|_{\infty(\text{initial})}$ is the ∞-norm of T at the initial solution of search process.

Combining (22) and (25), the objective function F can be formulated as,

$$\begin{aligned} &\textit{Minimize} && F = c\cdot\psi + \gamma \\ &\textit{subject to} && k_{\min} \le k \le k_{\max} \\ & && T_{i,\min} \le T_i \le T_{i,\max} \end{aligned} \quad (26)$$

The constant coefficient "c" is used to weight ψ-term, so that $c\cdot\psi$ dominates γ during the parameters optimization. Note that, since γ is normalized to 1 at the initial solution, it is easy to find the value of "c" so that $c\cdot\psi$ is greater than 1. Eventually, the search process minimizes both terms until $c\cdot\psi$ meets the design specification and γ decreases to the possible minimum value. The minimum and maximum values of the gain k are set as 0.1 and 500, respectively. The minimum and maximum values of the time constants T_i ($i = 1, 2, 3, 4$) are set as 0.01 and 5, respectively. In this research, TSA is employed to solve this optimization problem and search for optimal parameters of controller.

3.3.3. TSA for parameter determination [6]

The TSA is a promising tool for solving combinatorial optimization problem. The algorithm is an iterative improvement procedure that can start from any initial solution. Three basic components of TSA are used as follows: the trial solution generation, tabu list (TL) restriction, and termination criterion.

The concatenated encoding method is employed as shown in Fig. 4.

Initial Solution: 100101101011000110101110010011

Trial Solution 1: 000101101011000110101110010011

Trial Solution 2: 110101101011000110101110010011

Trial Solution 3: 101101101011000110101110010011

Fig. 5. Example of generating trial solutions.

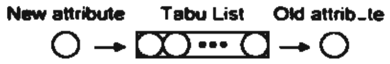

Fig. 6. Mechanism of TL.

Each parameter is encoded in a binary string normalized over its range. This encoding method stacks each normalized string in series with each other to construct the string individual. The same number of n bits is used to represent each parameter string.

To obtain the actual value of each parameter (27) is used to decode each normalized string to its decimal value for objective function evaluation.

$$P_i = P_{i,\min} + \frac{B_i \times [P_{i,\max} - P_{i,\min}]}{2^n - 1} \quad (27)$$

where P_i is the actual value of the i-th parameter, $P_{i,\min}$ is the minimum value of the i-th parameter, $P_{i,\max}$ is the maximum value of the i-th parameter, B_i is the decimal integer value of binary string of the i-th parameter, and n is the number of bits representing each parameter. In the design process, 10 bits are used to represent each parameter.

To generate a trial solution of an initial feasible solution, one bit of binary string is flipped at a time. The maximum number of trial solutions per iteration is referred to a neighborhood solution space (NS). In this study, NS is set to 95% of the total number of bits $\lfloor 0.95 \times n \times N \rfloor$ where N is a number of parameter searched.

The example of generating trial solutions is shown in Fig. 5.

The TL is referred to as an adaptive memory. The mechanism of TL is to keep attributes (bit positions) that created the best solution of the past iterations in the TL for a certain period. The attributes included in the TL cannot be used to create new solution candidates as long as they are in the TL. As the iteration proceeds, a new attribute enters into the TL as a fixed attribute. At the same time, the oldest attribute is released from the TL and becomes a free attribute, as illustrated in Fig. 6.

In particular, a size of TL affects the quality of the solution. It controls the search process to avoid being trapped in local optima. Note that the size of TL or so-called the tabu length, is only the control parameter of TSA. Basically, the tabu length that provided good solutions usually grows with the size of the problem. However, observing the quality of the solution can identify the appropriate tabu length. If the tabu length is too small, the cycling of solution occurs in the search process. On the other hand, if the size is too large, the search process is too restricted and may deteriorate the solution. Here, the tabu length is set to $\lfloor 0.7 \times n \times N \rfloor$.

Termination criterion refers to the condition that the search process will terminate. In the design, the search will terminate when the number of iterations reaches 100.

To apply the TSA for optimal parameter determination, the initial feasible solution is generated arbitrarily. A move to a neighbor solution is performed if the TL does not restrict it. The best solution is updated during the search process until the termination criterion is satisfied. The following notations is used for the TSA procedure:

TL: the tabu list,
NS: the neighborhood solution space,
$F(X)$: the objective function of solution X,
F_b^k: the best objective function at iteration k,
X_o^k: the initial feasible solution at iteration k,
X_m^k: a trial m solution at iteration k,
X_{cb}^k: the current best trial solution at iteration k,
X_b^k: the best solution reached at iteration k,
$k_{\max}$: the maximum allowable number of iterations.

The tabu search procedure can be described as follows:

1) Read the constraints of searched parameters, the initial feasible solution X_o^k, and specification of the controller.
2) Specify the length of TL, k_{max}, and size of NS.
3) Initialize iteration counter k and empty TL.
4) Set $X_b^k = X_o^k$.
5) Execute tabu search procedure:
   5.1 Initialize the trial counter m to zero.
   5.2 Generate a trial solution X_m^k from X_o^k.
   5.3 If X_m^k is not feasible, go to 5.8.
   5.4 If X_m^k is the first feasible solution, set $X_{cb}^k = X_m^k$.
   5.5 Perform the tabu test. If X_m^k is tabued, then go to 5.8.
   5.6 If $F(X_m^k) < F(X_{cb}^k)$, set $X_{cb}^k = X_m^k$.
   5.7 If $F(X_m^k) < F(X_b^k)$, set $X_b^k = X_m^k$.
   5.8 If m is less than NS, $m = m + 1$ and go to 5.2.
   5.9 If there is no feasible solution, set $X_o^{k+1} = X_b^k$. Otherwise, set $X_o^{k+1} = X_{cb}^k$, and update TL.
6) If $k < k_{max}$, then $k = k + 1$, and go to 5.
7) X_b^k is the best solution found.

4. Simulation results and evaluation

To determine five control parameters by the TSA, the values of N, NS and the tabu length are set to 5, 47 and

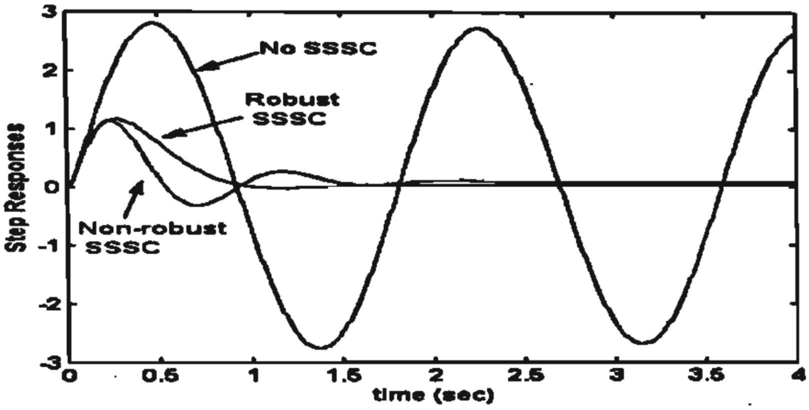

Fig. 7. System step responses.

Table 1
Eigenvalue analysis results of decoupled subsystems (15) and (16)

	Before control	After control
Decoupled subsystem (15)	$\lambda_{1,2} = -0.015 \pm j3.5316$	$\lambda_{1,2} = -3.6077 \pm j3.7967$
		$\lambda_{3,4} = -0.1027 \pm j0.0642$
		$\lambda_5 = -0.5020$
		$\lambda_6 = -12.8613$
Decoupled subsystem (16)	$\lambda_{1,2} = -0.0152 \pm j1.6777$	Not change
	$\lambda_{3,4} = -0.0168 \pm j3.6922$	
	$\lambda_{5,6} = -0.0247 \pm j2.1532$	

Table 2
Eigenvalue analysis results of expanded system (12) (or interconnected overlapping subsystems (13) and (14))

	Before control	After Control
Expanded system (12)	$\lambda_{1,2} = -0.0171 \pm j4.4134$	$\lambda_{1,2} = -3.8240 \pm j5.0223$
	$\lambda_{3,4} = -0.0154 \pm j3.5602$	$\lambda_{3,4} = -0.0461 \pm j3.6994$
	$\lambda_{5,6} = -0.0157 \pm j1.7520$	$\lambda_{5,6} = -0.0061 \pm j1.7364$
	$\lambda_7 = -0.0409$	$\lambda_7 = -0.0414$
	$\lambda_8 = -4.18 \times 10^{-14}$	$\lambda_8 = -2.84 \times 10^{-14}$
		$\lambda_{9,10} = -0.1232 \pm j0.0483$
		$\lambda_{11} = -0.4485$
		$\lambda_{12} = -12.4$

35, respectively. Following the design procedures and appropriately setting $c = 1.4$ in the objective function, the following transfer function was obtained for the robust controller of SSSC when the peak frequency deviation was limited to $M_{p(design)} = 1.2$.

$$K_{RB}(s) = 3.5206 \frac{10s}{1 + 10s} \frac{(1 + 0.7758s)}{(1 + 2.5074s)} \frac{(1 + 1.9660s)}{(1 + 3.7269s)} \tag{28}$$

The SSSC controller in Eq. (28) is compared with the designed SSSC with $M_{p(design)} = 1.2$ but without robustness consideration. By neglecting γ in the objective function and setting $c = 1.0$, the designed result is given by

$$K_{NRB}(s) = 5.4753 \frac{10s}{1 + 10s} \frac{(1 + 0.1271s)}{(1 + 2.7026s)} \frac{(1 + 3.8781s)}{(1 + 2.4440s)} \tag{29}$$

Note that the designed controllers in Eqs. (28) and (29) are referred to as "Robust SSSC" and "Non-robust SSSC", respectively.

Fig. 7 depicts the step responses of G. Without SSSC, the oscillations are undamped with the first peak value about 2.7875. On the other hand, the first peak values are reduced to 1.2025 and 1.1225 in cases of Robust and Non-robust SSSCs, respectively. In addition, the MSM of system G with Robust SSSC is increased to 0.90 from 0.57 in case of system with Non-robust SSSC. This reveals the higher robustness of the system G with Robust SSSC.

To prove that the Robust SSSC designed in the decoupled subsystem (15) can guarantee the stability of the expanded system (12) and also the original system (10), the eigenvalue analysis is employed. Table 1 shows the eigenvalues of decoupled subsystems (15) and (16). The eigenvalues $\lambda_{1,2}$ of (15) represent the inter-area mode between areas 1 and 2. After applying the control input ΔP_{SSSC}, this oscillation mode is stabilized effectively. On the other hand, eigenvalues of (16) have not been changed. This is due to no control input ΔP_{SSSC} in (16). Table 2 shows the eigenvalues of expanded system (12). By considering the participation factor [14], it can be verified that $\lambda_{1,2}$ represents the inter-area mode between areas 1 and 2. As expected, ΔP_{SSSC} can stabilize this oscillation mode. For other modes, they are stable

Table 3
Eigenvalue analysis results of original system (11)

	Before control	After control
Original system (11)	$\lambda_{1,2} = -0.0171 \pm j4.4134$	$\lambda_{1,2} = -3.8240 \pm j5.0223$
	$\lambda_{3,4} = -0.0184 \pm j3.5602$	$\lambda_{3,4} = -0.0461 \pm j3.6994$
	$\lambda_{5,6} = -0.0157 \pm j1.7520$	$\lambda_{5,6} = -0.0061 \pm j1.7364$
	$\lambda_7 = -0.0409$	$\lambda_7 = -0.0414$
		$\lambda_{8,9} = -0.1232 \pm j0.0483$
		$\lambda_{10} = -0.4485$
		$\lambda_{11} = -12.4217$

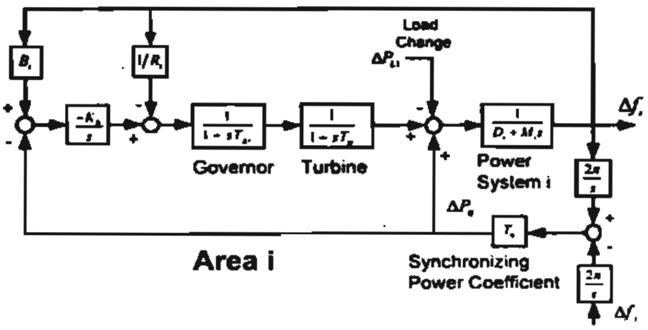

Fig. 8. Linearized model of area i ($i = 1, \ldots, 4$) with governor

after the controller is included. Note that λ_8 is approximately zero which has no physical meaning. This is because of a redundant state variable ΔP_{T12} in (12). For the eigenvalues of the original system (11) demonstrated in Table 3, $\lambda_{1,2}$ can also be stabilized by ΔP_{SSSC}. Other modes are also stable after control. These eigenvalue analysis results confirm the concept of overlapping decompositions that the stability of the original system can be guaranteed if the decoupled subsystems can be stabilized by its own input.

Next, the disturbance attenuation performance and robustness of both designed controllers are investigated in the linearized model of the four-area interconnected system. The dynamic of governor [12] is also incorporated into each area, as delineated in Fig. 8. System parameters are given in the Appendix A.

In order to evaluate the disturbance attenuation performance of both controllers, a sudden step load of 0.01 (p.u. MW) is applied to area 1 at $t = 1.0$ (s). The frequency deviation of each area is depicted in Figs. 9–12. Without control of the SSSC, the fluctuations of frequency deviations in all areas are large with poor damping. After the inclusion of both controllers, frequency oscillations in all areas are effectively stabilized. Especially, the peak value of frequency deviation in the controlled area 1 is significantly suppressed. In addition, the oscillating shapes are also stabilized completely. Meanwhile, steady-state errors of frequency deviations are eliminated slowly due to the effects of the governors. Furthermore, the tie line 1–2 power deviation illustrated in Fig. 13 is also effectively stabilized by Robust SSSC. As shown in Fig. 14, the maximum injected power deviation of Non-robust SSSC is 0.0094 (p.u. MW), which is almost equal to the size of load change. In contrast, due to consideration of both performance and robustness in design process, the injected power deviation of Robust SSSC is 0.0058 (p.u. MW).

Here, the robustness of each designed controller is evaluated. A random load disturbance composed of several oscillation frequencies, $\Delta P_{L1} = 0.002\sin(3t) + 0.005\sin(6t) - 0.007\sin(9t)$ (p.u. MW) is applied to area 1. At the same time, the damping coefficient in area 1 (D_1) is changed from 0.006 (p.u. MW/Hz) (positive damping) to -0.75 (p.u. MW/Hz) (negative damping). Note that the negative damping signifies an unstable system operation. As clearly illustrated by the area 1 frequency oscillations in Fig. 15, the system completely loses stability in cases of a Non-robust SSSC and no SSSC. Moreover, frequency oscillations in other areas (not shown here) severely fluctuate and finally diverge. On the other hand, the Robust SSSC explicitly

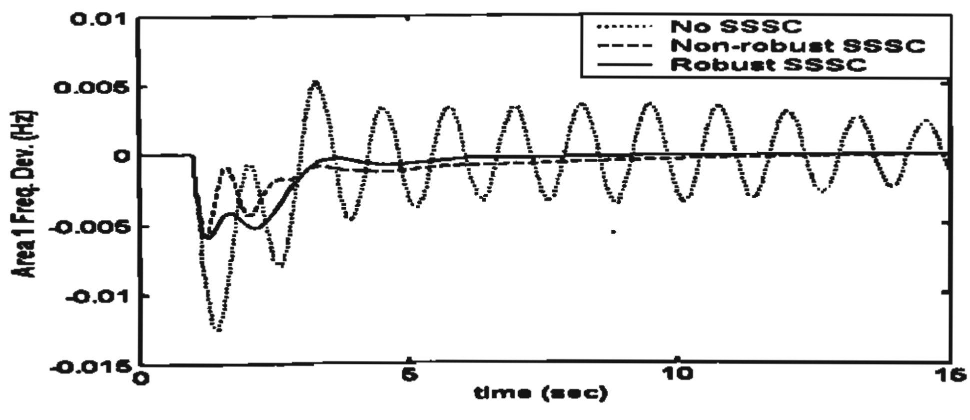

Fig. 9. Frequency deviation of area 1.

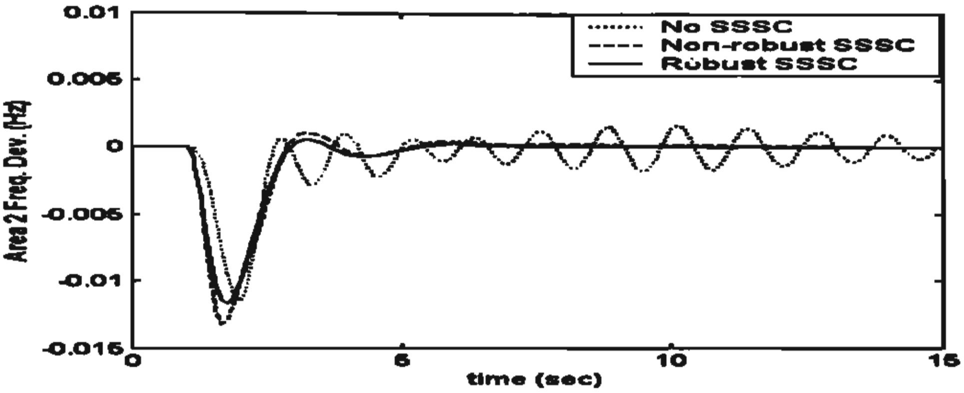

Fig. 10. Frequency deviation of area 2.

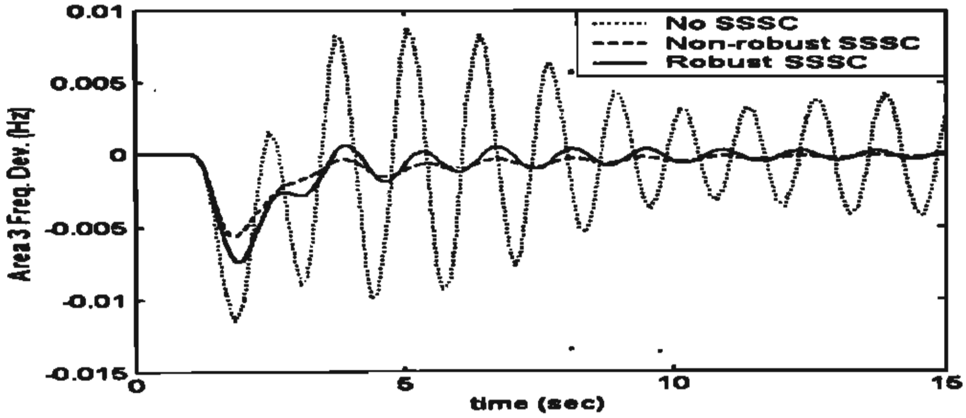

Fig. 11. Frequency deviation of area 3.

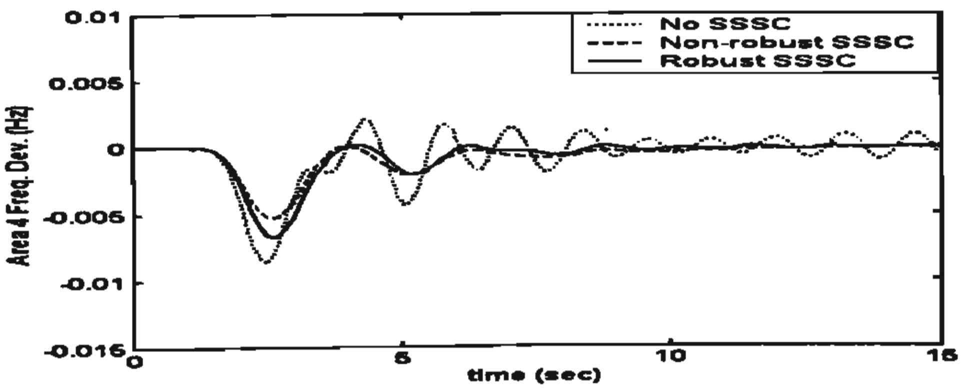

Fig. 12. Frequency deviation of area 4.

maintains its performance against large uncertainties and severe perturbations. Frequency oscillations in area 1 and other areas are perfectly stabilized. The efficiency of the Robust SSSC is also evident in Figs. 16 and 17, where the power deviation in the tie line 1–2 and the injected power deviation of SSSC are shown.

Finally, the performances of both SSSC controllers are evaluated when the load change occurs in area 2. Fig. 18 shows an additional load change in area 2. It is assumed that a sudden step load of 0.01 (p.u. MW) occurs in area 2 at $t = 1.0$ (s). As depicted in Fig. 19, both Non-robust SSSC and Robust SSSC are capable of

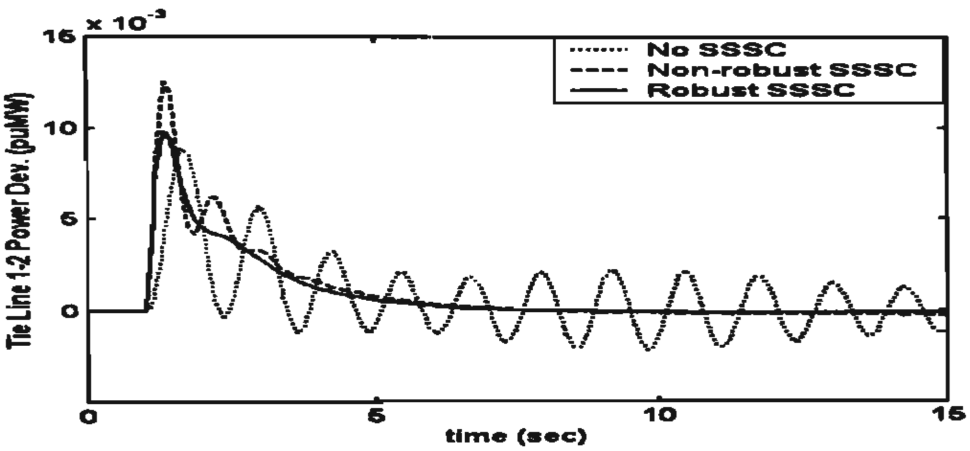

Fig. 13. Tie line 1–2 power deviation.

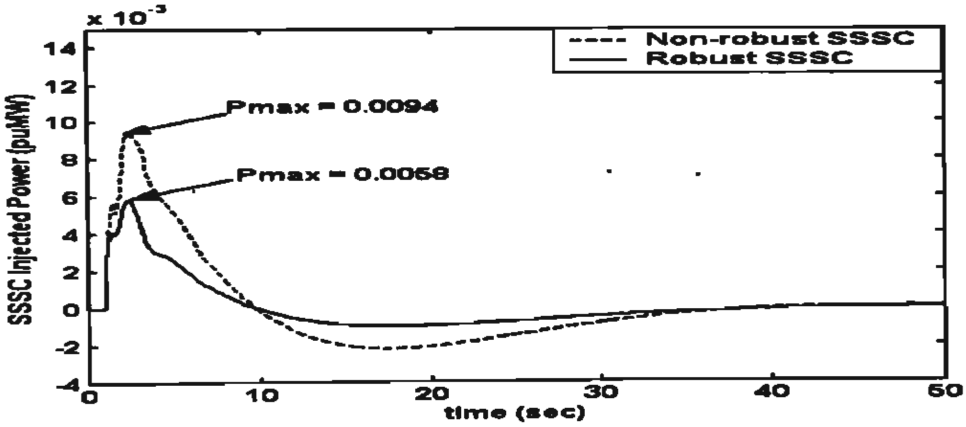

Fig. 14. Injected power deviation of SSSC.

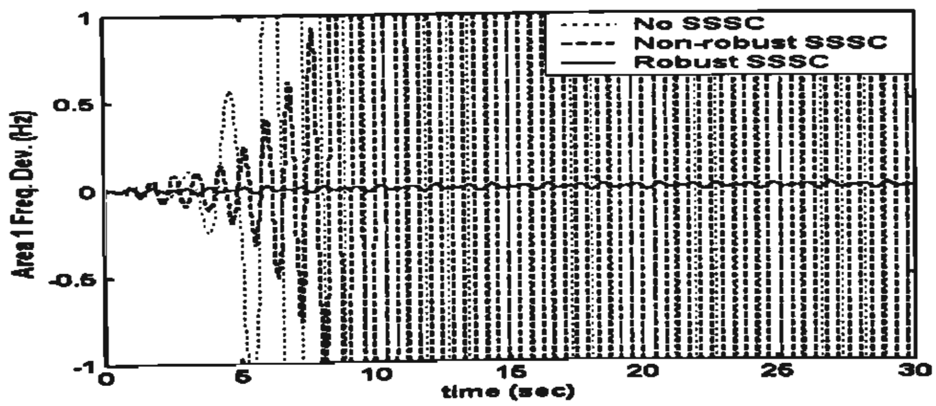

Fig. 15. Frequency deviation of area 1.

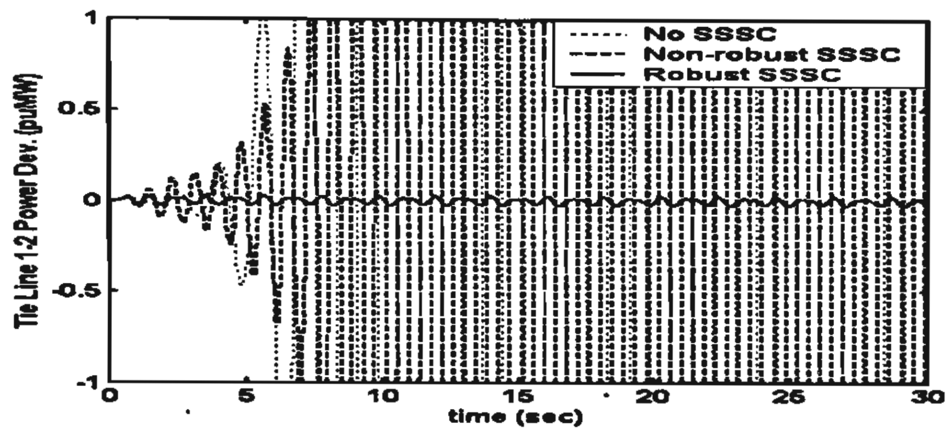

Fig. 16. Tie line 1-2 power deviation.

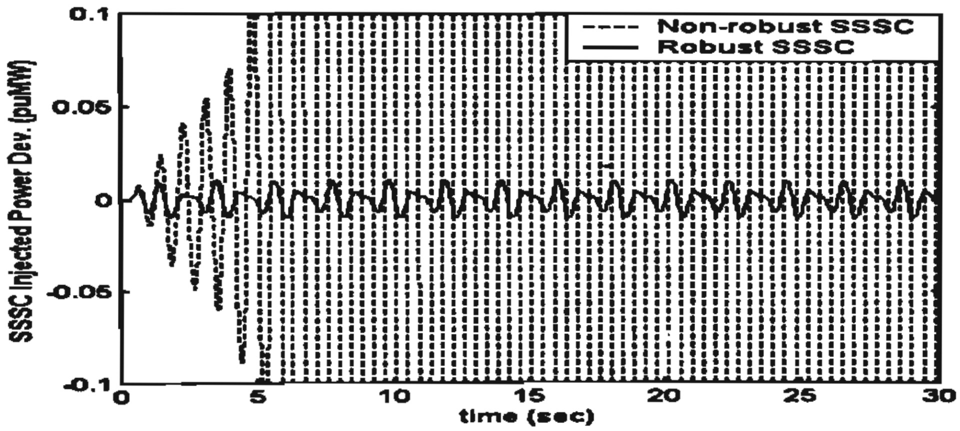

Fig. 17. Injected power deviation of SSSC.

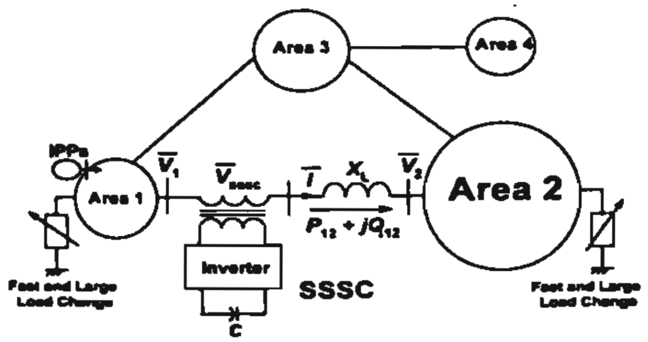

Fig. 18. An additional load change in area 2.

stabilizing frequency oscillations of area 1, even though a load disturbance occurs in area 2. For frequency deviations in other areas (Figs. 20–22) and tie line 1–2 power deviation (Fig. 23), the performance of Robust SSSC is comparatively better than that of Non-robust SSSC. As illustrated in Fig. 24, the peak values of injected power deviations of Robust SSSC and Non-robust SSSC are 0.01 and 0.027 (p.u. MW), respectively. This implies that the required MW capacity of Robust SSSC is lower than that of Non-robust SSSC.

5. Conclusions

In this paper, a robust design of the lead/lag controller equipped with the SSSC for stabilization of frequency oscillations is proposed. The TSA was employed to achieve the optimal parameters. By virtue of the objective function that limits the peak frequency deviation and maximizes the robust stability margin, the proposed design guarantees both performance and robustness of the resulted controller. More specifically, the designed controller uses only the frequency deviation of the controlled area as the feedback-input signal. This allows practical realization and implementation in a power system. Simulation results clearly demonstrate

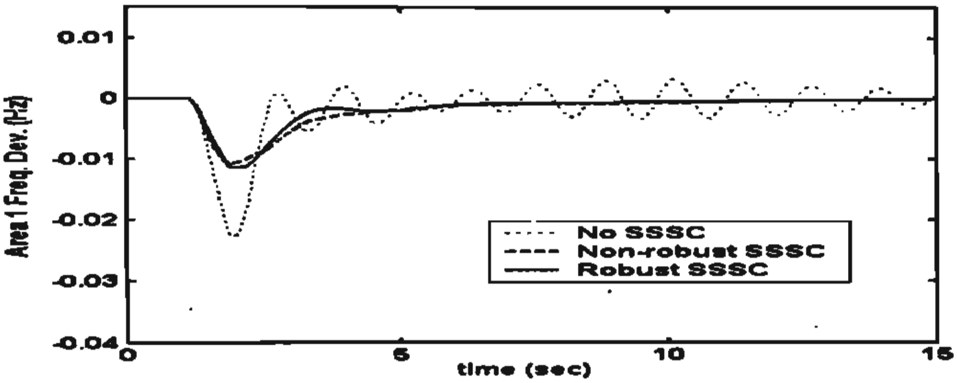

Fig. 19. Frequency deviation of area 1.

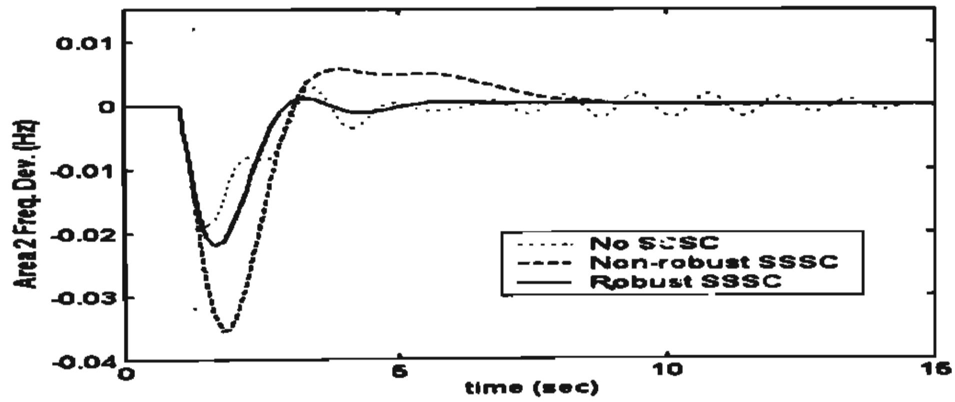

Fig. 20. Frequency deviation of area 2.

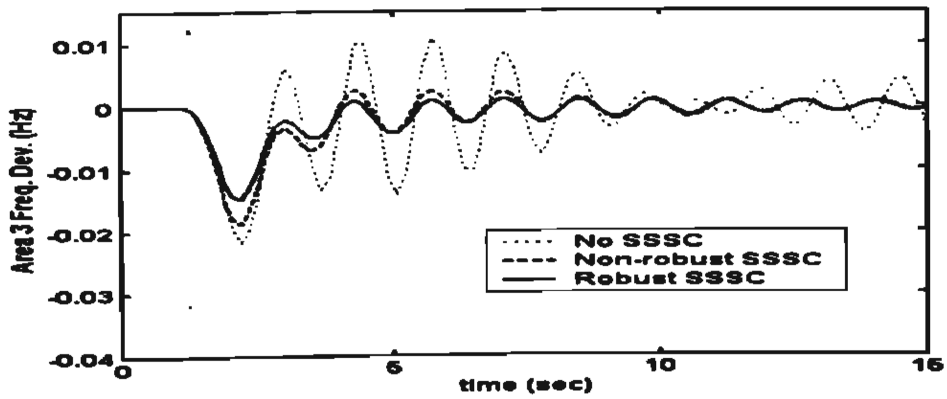

Fig. 21. Frequency deviation of area 3.

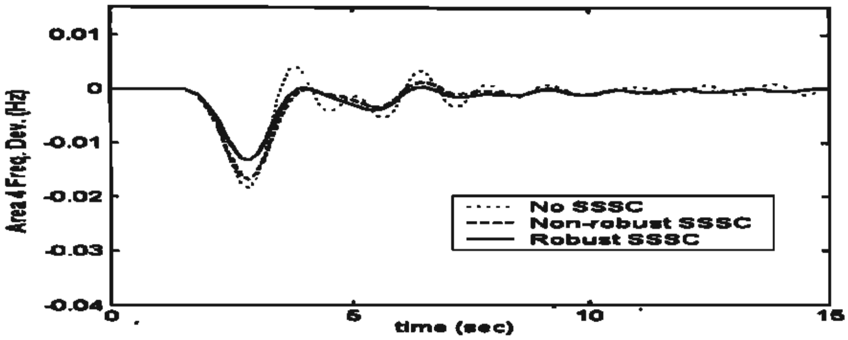

Fig. 22. Frequency deviation of area 4.

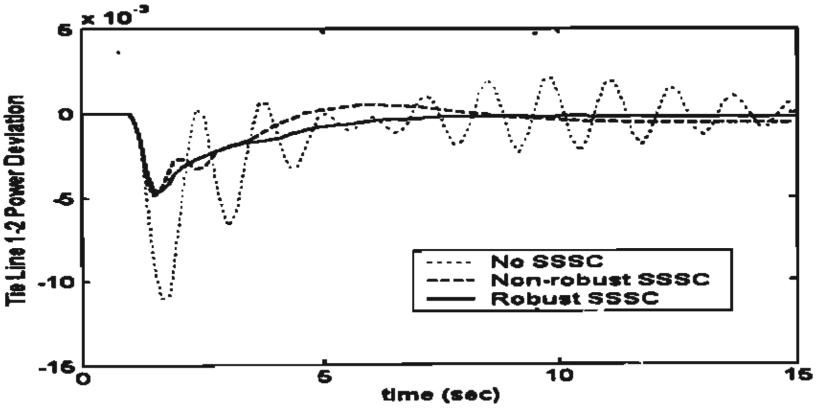

Fig. 23. Tie line 1–2 power deviation.

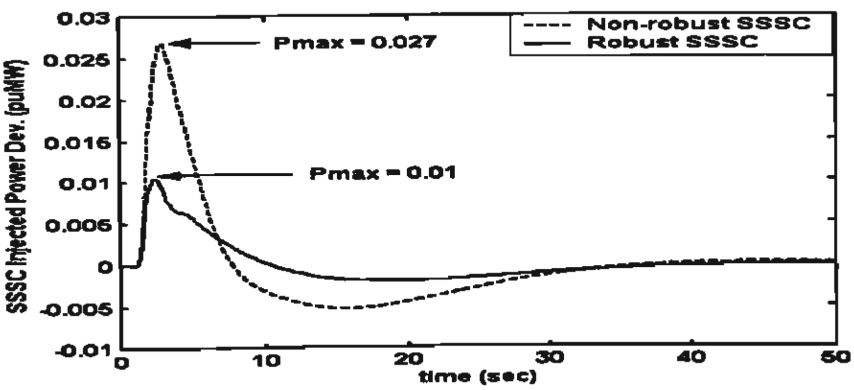

Fig. 24. Injected power deviation of SSSC.

the superior robustness and performance of the controller designed by the proposed method.

Acknowledgements

The authors deeply appreciate the support from the Thailand Research Fund through the postdoctoral fund program.

Appendix A

The system parameters of the four-area interconnected system with an area capacity ratio 5:10.2:0.8 are given below

$M_1 = 0.2$	$M_2 = 0.167$	$M_3 = 0.15$	$M_4 = 0.2$
$D_1 = 0.006$	$D_2 = 0.0083$	$D_3 = 0.005$	$D_4 = 0.006$
$T_{t1} = 0.25$	$T_{t2} = 0.3$	$T_{t3} = 0.3$	$T_{t4} = 0.25$
$T_{g1} = 0.1$	$T_{g2} = 0.08$	$T_{g3} = 0.1$	$T_{g4} = 0.1$
$R_1 = 2.4$	$R_2 = 2.4$	$R_3 = 2.4$	$R_4 = 2.4$
$B_1 = 0.5$	$B_2 = 0.5$	$B_3 = 0.5$	$B_4 = 0.5$
$K_{I1} = 0.5$	$K_{I2} = 0.5$	$K_{I3} = 0.5$	$K_{I4} = 0.5$
$T_{12} = 0.159$	$T_{23} = 0.064$	$T_{34} = 0.111$	$T_{41} = 0.079$
$a_{12} = 2.0$	$a_{23} = 0.2$	$a_{34} = 2.5$	$a_{41} = 0.4$
$T_{SSSC} = 0.05$			

Appendix B: Nomenclature

M_i:	inertia constant (p.u. MW s/Hz) of area i
D_i	damping coefficient (p.u. MW/Hz) of area i
T_{ti}	turbine time constant (s) of area i
T_{gi}:	governor time constant (s) of area i
R_i	regulation ratio (Hz/p.u. MW)
B_i	bias coefficient (p.u. MW/Hz)
K_{Ii}:	integral gain (1/s)
T_{ij}:	synchronizing coefficient (p.u. MW/rad) between areas i and j
a_{ij}:	area capacity ratio between areas i and j
T_{SSSC}:	time constant of SSSC (s)

References

[1] K.N. Zadeh, R.C. Meyer, G. Cauley, Practices and new concepts in power system control, IEEE Trans. Power Syst. 11 (1) (1996) 3–9.

[2] L.H. Fink, P.J.M. Van Son, On system control within a restructured industry, IEEE Trans. Power Syst. 13 (2) (1998) 611–616.

[3] N. Jaleeli, L.S. VanSlyck, D.N. Ewart, L.H. Fink, A.G. Hoffmann, Understanding automatic generation control, IEEE Trans. Power Syst. 7 (3) (1992) 1106–1122.

[4] I. Ngamroo, Application of static synchronous series compensation to stabilization of frequency oscillations in an interconnected power system, Proceedings of 2001 IEEE International Symposium on Circuits and Systems (ISCAS 2001), Sydney, Australia, 2001, vol. 2, pp. 113–116.

[5] L. Gyugyi, C.D. Schauder, K.K. Sen, Static synchronous series compensator: a solidstate approach to the series compensation of transmission line, IEEE Trans. Power Deliv. 12 (1) (1997) 406–417.

[6] F. Glover, M. Laguna, Tabu Search, Kluwer Academic Publishers, 2001.

[7] W. Ongsakul, P. Bhasaputra, Optimal power flow with FACTS devices by hybrid TS/SA approach, Intl. J. Elec. Power Energy Syst. 24 (10) (2002) 851–857.

[8] M.A. Abido, Y.L. Abdel-Magid, A tabu search based approach to power system stability enhancement via excitation and static phase shifter control, Elec. Power Syst. Res. 52 (2) (1999) 133–143.

[9] H. Mori, T. Hiyashima, New parallel tabu search for voltage and reactive power control in power systems, Proceedings of 1998 IEEE International Symposium on Circuits and Systems (ISCAS '98) vol. 3, pp. 431–434.

[10] W.G. Kim, G.H. Hwang, H.T. Kang, S.O. Lee, J.H. Park, Design of fuzzy logic controller for firing control of TCSC using real-type tabu search, Proceedings IEEE International Symposium on Industrial Electronics 2001 (ISIE 2001), vol. 1, pp. 575–580.

[11] Y.L. Abdel-Magid, M.A. Abido, A.H. Mantaway, Robust tuning of power system stabilizers in multimachine power systems, IEEE Trans. Power Syst. 15 (2) (2000) 735–740.

[12] O.L. Elgerd, Electric Energy Systems Theory: An Introduction, McGraw Hill, New York, USA, 1985.

[13] M. Ikeda, D.D. Siljak, D.E. White, Decentralized control with overlapping information sets, J. Optimization Theor. Appl. 34 (2) (1981) 279–310.

[14] P.B. Kundur, Power System Stability and Control, McGraw-Hill, 1994.

[15] B. Shahian, M. Hassul, Control System Design using MATLAB, Prentice Hall, 1993.

Biographies

Issarachai Ngamroo received the B.Eng. degree in Electrical Engineering from King Mongkut's Institute of Technology Ladkrabang (KMITL), Bangkok, Thailand in 1992. He was the recipient of a Monbusho scholarship from the Japanese Government to continue his graduate study in Japan during 1993–2000. He received his M.Eng. and the Ph.D. degrees in Electrical Engineering in 1997 and 2000, respectively, from Osaka University, Osaka, Japan. He is currently an Assistant Professor at Electrical Power Engineering Program, Sirindhorn International Institute of Technology (SIIT), Thammasat University. His research interests are in the areas of power system control and stabilization, Flexible AC Transmission System Devices (FACTS) applications, Robust control design of power system damping controllers.

Waree Kongprawechnon received the B.Eng. degree (1st Honors) in Electrical Engineering from Chulalongkorn University, Bangkok, Thailand. She received the

M.Eng. in control engineering from Osaka University and the Ph.D. degrees in Mathematical Engineering and Information Physics from The University of Tokyo, Japan. She is currently an Assistant Professor of the Instrumentation and Control Systems Program, Sirindhorn International Institute of Technology (SIIT), Thammasat University. Her research interests are in the areas of the theory in robust control, H^{∞} Control.

Paper submitted to *ASEAN Journal on Science & Technology for Development*

Robust Frequency Stabilizer Design of Static Synchronous Series Compensator Taking into Consideration System Uncertainties

Issarachai Ngamroo and Waree Kongprawechnon

Electrical Power Engineering Program
Sirindhorn International Institute of Technology
Thammasat University, Pathumthani, 12121 Thailand
E-mail: ngamroo@siit.tu.ac.th

ABSTRACT

As large loads with changing frequency in the vicinity of inter-area oscillation (0.2 – 0.8 Hz) mode occur in an interconnected power system, system frequency may be severely disturbed and oscillate. To compensate for such load changes and stabilize both frequency oscillations, the dynamic power flow control via a Static Synchronous Series Compensator (SSSC) installed in series with a tie-line between interconnected systems can be exploited. However, the frequency stabilizer of SSSC that is designed without regarding system uncertainties, e.g., various load changes, system parameters variations etc., may deteriorate the robust stability of power system and fail to damp out low frequency oscillations. To overcome this problem, a new robust design of frequency stabilizer of SSSC taking into consideration system uncertainties is proposed. The multiplicative uncertainty model is applied to represent all possible unstructured uncertainties in interconnected power systems. As a result, the robust stability margin against uncertainties can be easily guaranteed in terms of the multiplicative stability margin (MSM). Additionally, to implement the frequency stabilizer in real system, the configuration of frequency stabilizer presented here is practically based on a second-order lead/lag compensator. Without trial and error, the control parameters of the frequency stabilizer are automatically optimized by a tabu search algorithm, so that the desired damping ratio of the target inter-area mode and the best MSM are achieved. Simulation study exhibits the high robustness of the SSSC frequency stabilizer against load disturbances with changing frequency in the vicinity of the inter-area and negative damping in the study three-area loop interconnected power system.

Keywords: System uncertainties, Robust stability, Multiplicative uncertainty model, Static synchronous series compensator, Inter-area oscillations, Frequency stabilization, Overlapping decompositions, Tabu search algorithm

1. INTRODUCTION

At present, an electric power system is in transition to a fully competitive deregulated scenario. Under this circumstance, any power system controls such as frequency and voltage controls will be served as ancillary services [1-3]. Especially, in the case that the proliferation of non-utility generations, i.e. Independent Power Producers (IPPs) that do not possess sufficient frequency control capabilities, tends to increase considerably. Furthermore, various kinds of apparatus with large capacity and fast power consumption such as a magnetic levitation transportation, a testing plant for nuclear fusion, or even an ordinary scale factory like a steel manufacturer etc. increase significantly. When these loads are concentrated in a power system, they may cause a serious problem of frequency oscillation. The deviations of frequency oscillations that exceed the normal limit, directly interrupt the operation of power system. Especially, if the frequency of changing load is in the vicinity of the inter-area oscillation mode (0.2-0.8 Hz), system frequency oscillation may experience a serious stability problem due to an inadequate damping. Under this situation, the conventional frequency control, i.e. a governor, may no longer be able to absorb the large frequency oscillations due to its slow response [4, 5]. A new service of stabilization of frequency oscillations becomes challenging and is highly expected in the future competitive environment.

To solve this problem, the author has proposed a new stabilization of frequency oscillations by the Static Synchronous Series Compensator (SSSC) [6]. The SSSC is a FACTS (Flexible AC Transmission Systems) device, that has been highly expected as an effective apparatus with an ability of dynamic power flow control [7, 8]. In [6], the SSSC is located in series with the tie-line between a two-area interconnected power system. By regarding the system interconnection as the channel of power flow control by SSSC, the system frequency oscillations under a sudden load disturbance can be stabilized effectively. However, the proposed frequency stabilizer of SSSC in [6] is designed based on a state feedback scheme of variables. Therefore, it is not easy to realize in a multi-area interconnected power system. Besides, there are several uncertainties such as various load changes, system parameter variations etc. in interconnected power systems. The frequency stabilizer of SSSC that is designed without considering such uncertainties may deteriorate the robust stability of power system and fail to damp out low frequency oscillations.

By taking system uncertainties into consideration, a new robust frequency stabilizer of SSSC is proposed in this paper. The multiplicative uncertainty model [9-11] is applied to represent all possible unstructured uncertainties in interconnected power systems. As a result, the robust stability margin of the closed-loop control system can be easily guaranteed in terms of the multiplicative stability margin (MSM). First, the design method utilizes the merit of overlapping decompositions technique [12] to extract the subsystem embedded with the inter-area mode of interest. Next, by including the multiplicative uncertainty model in the extracted subsystem, the robust stability margin of system with designed frequency stabilizer can be enhanced. Here, the configuration of the robust frequency stabilizer is practically based on a second-order lead/lag compensator with single feedback input signal. Without trial and error, the control parameters of the robust frequency stabilizer are automatically optimized via a Tabu Search (TS) algorithm [13, 14]. In the formulation of the objective function, not only the desired damping ratio of the target inter-area mode, but also the MSM of system are included. In addition, the proposed method is applied to a design problem in case of many frequency stabilizers of SSSCs are installed in an interconnected power system. Simulation study in a three-area loop system shows the significant robustness of the designed frequency stabilizers against load changes and negative damping.

The organization of this paper is as follows. First, the motivation of stabilization of frequency oscillation by SSSC is provided. Next part deals with the design methodology including the coordinated control of SSSC and governors, the mathematical model of SSSC, the system reduction by overlapping decompositions, the objective function formulation, and the tabu search algorithm. Subsequently, the evaluation effects of the designed frequency stabilizers in a three-area interconnected power system are outlined by simulation study. Lastly, a conclusion is given.

2. PROBLEM STATEMENT

A three-area loop interconnected power system depicted in Fig.1 is used to explain the motivation of the proposed frequency stabilizer design. SSSC12 and SSSC23 are connected in series with tie-lines between areas 1 and 2, and areas 2 and 3, respectively. It is assumed that large loads with changing frequency in the vicinity of the inter-area oscillation mode (0.2-0.8 Hz) have been installed in areas 1 and 3. These load disturbances severely cause frequency oscillations in areas 1 and 3. In addition, Independent Power Producers (IPPs) that do not possess frequency control capabilities are also included in areas 1 and 3. Thus, it becomes beyond the abilities of governors in areas 1 and 3 to

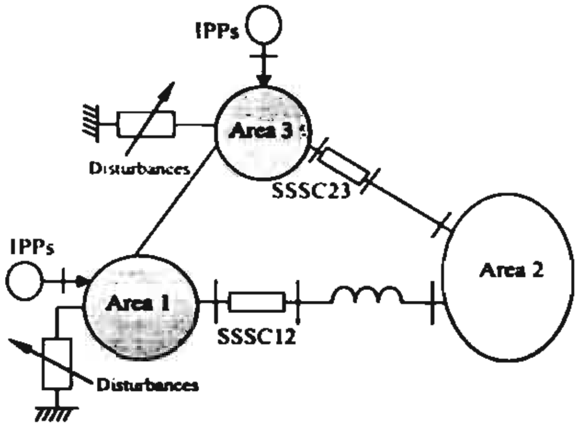

Figure 1: A three-area loop interconnected power system with SSSC

provide adequate frequency controls. Therefore, both SSSCs are applied to utilize the control capabilities of area 2 to compensate for fast load changes in areas 1 and 3.Moreover, by utilizing the area interconnections as the control channels of dynamic power flow control of SSSCs, the frequency oscillations in areas 1 and 3, due to inter-area modes can be effectively stabilized. Additionally, in the interconnected system, variations of system parameters, various load changes etc. cause several system uncertainties. To achieve the high robust stability of system, the effect of uncertainties should be taken into account in the design process. In this study, the aim of the proposed frequency stabilizer design is not only to enhance the damping of interested inter-area oscillation modes, but also to improve the robust stability of system against uncertainties.

3. Design Methodology

3.1 Coordinated Control of SSSC and Governor

The response of SSSC is extremely rapid when compared to the conventional frequency control system, i.e. a governor. The difference in responses signifies that the SSSC and governor can be coordinated. When a power system is subjected to a sudden load disturbance, the SSSC quickly acts to damp frequency oscillation in the transient period. Subsequently, the governor continues to eliminate the steady-state error in frequency oscillation. As the periods of operation for the SSSC and governor do not overlap, the dynamic of governor can then be neglected in the design of frequency stabilizer for the sake of simplicity.

3.2 Linearized Power System Model

The power system shown in Fig. 1 can be represented by a linearized power system model, as shown in Fig. 3. Note that the governors are eliminated in this system. The SSSC model is represented by the active power flow controller [6]. The dynamic characteristic of SSSC is modeled as the first order controller with a time constant $T_{SSSC} = 0.05$ sec. Note that the injected power deviation of each SSSC (ΔP_{SSSC12} and ΔP_{SSSC23}) acting positively on an area reacts negatively on another area [6]. Thus, each injected power flows into both areas with different signs (+,-), simultaneously. By neglecting T_{SSSC}, the linearized state equation of Fig. 3 can be expressed as

$$\Delta \dot{x} = A\Delta x + B\Delta u \qquad (1)$$

where

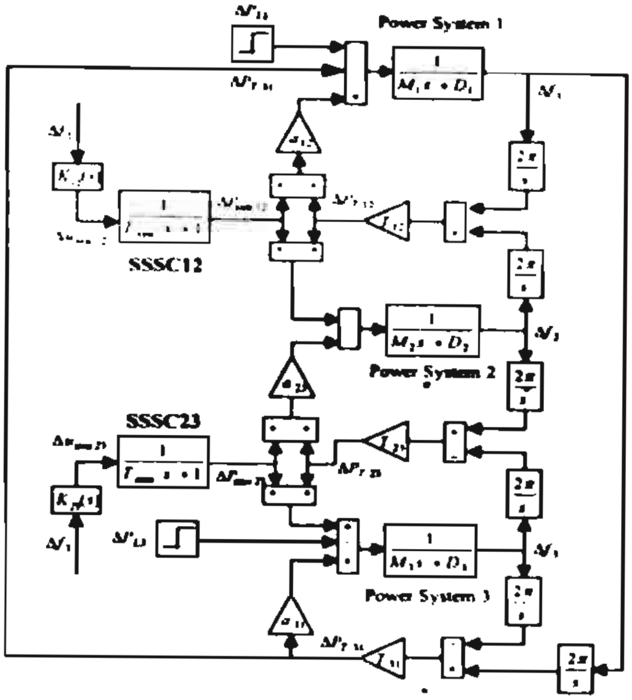

Figure 3. Frequency stabilizers of SSSCs in a linearized power system model without governors

$$A = \begin{bmatrix} -D_1/M_1 & a_{S12} & 0 & a_{S14} & 0 \\ -2\pi T_{12} & 0 & 2\pi T_{12} & 0 & 0 \\ 0 & -1/M_2 & -D_2/M_2 & -a_{23}/M_2 & 0 \\ 0 & 0 & 2\pi T_{23} & 0 & -2\pi T_{23} \\ 0 & a_{S52} & 0 & a_{S54} & -D_3/M_3 \end{bmatrix},$$

$$B = \begin{bmatrix} a_{12}/M_1 & 0 \\ 0 & 0 \\ -1/M_2 & -a_{23}/M_2 \\ 0 & 1/M_3 \\ 0 & 0 \end{bmatrix},$$

$$\Delta x = \begin{bmatrix} \Delta f_1 & \Delta P_{T12} & \Delta f_2 & \Delta P_{T23} & \Delta f_3 \end{bmatrix}^T,$$

$$\Delta u = \begin{bmatrix} \Delta P_{SSSC12} & \Delta P_{SSSC23} \end{bmatrix}^T.$$

Δf_i is the frequency deviation of area i, ΔP_{Tij} is the power deviation between areas i and j, M_i is the inertia constant of area i. D_i is the damping coefficient of area i. a_{ij} is the area capacity ratio between areas i and j, T_{ij} is the synchronizing power coefficient of the tie-line between areas i and j, where $i, j = 1,...,3$. Here $a_{S12} = (a_{12} + T_{31}/T_{12})/M_1$, $a_{S14} = -T_{31}/(M_1T_{23})$, $a_{S52} = -a_{31}T_{31}/(M_3T_{12})$, $a_{S54} = (1 + a_{31}T_{31}/T_{23})/M_3$. The variable ΔP_{T31} is represented in terms of ΔP_{T12} and ΔP_{T23} by

$$\Delta P_{T31} = -\frac{T_{31}}{T_{12}}\Delta P_{T12} + \frac{T_{31}}{T_{23}}\Delta P_{T23} \tag{2}$$

Thus, ΔP_{T31} has disappeared in (1). This system has two conjugate pairs of complex eigenvalues and a negative real eigenvalue. The former corresponds to two inter-area oscillation modes, and the latter the inertia center mode. Based on the mode controllability matrix [15], the inter-area modes between areas 1 and 2, and areas 2 and 3 are controllable for the control inputs Δu_{SSSC12} and Δu_{SSSC23}, respectively. Accordingly, the design purpose of frequency stabilizer is to enhance the damping of the mentioned inter-area modes.

3.3 Model Reduction by Overlapping Decompositions

The technique of overlapping decompositions [12] is applied to reduce the system (1) to a subsystem embedded with only the inter-area mode of interest. The original system (1) is referred to as the system S.

$$S : \begin{bmatrix} \dot{x}_1 \\ \dot{x}_2 \\ \dot{x}_3 \end{bmatrix} = \begin{bmatrix} A_{11} & A_{12} & A_{13} \\ A_{21} & A_{22} & A_{23} \\ A_{31} & A_{32} & A_{33} \end{bmatrix} \begin{bmatrix} x_1 \\ x_2 \\ x_3 \end{bmatrix} + \begin{bmatrix} B_{11} & B_{12} \\ B_{21} & B_{22} \\ B_{31} & B_{32} \end{bmatrix} \begin{bmatrix} u_1 \\ u_2 \end{bmatrix} \tag{3}$$

The sub-matrices A_{ij} and B_{ij}, $(i,j=1,2,3)$ have appropriate dimensions identical to the corresponding states and input vectors. According to the process of overlapping decompositions, the system S can be expressed as

$$\tilde{S} : \begin{bmatrix} \dot{z}_1 \\ \dot{z}_2 \end{bmatrix} = \begin{bmatrix} A_{11} & A_{12} & 0 & A_{13} \\ A_{21} & A_{22} & 0 & A_{23} \\ A_{21} & 0 & A_{22} & A_{23} \\ A_{31} & 0 & A_{32} & A_{33} \end{bmatrix} \begin{bmatrix} z_1 \\ z_2 \end{bmatrix} + \begin{bmatrix} B_{11} \\ B_{21} \\ B_{21} \\ B_{31} \end{bmatrix} \begin{bmatrix} u_1 \\ u_2 \end{bmatrix} \tag{4}$$

where $z_1 = \left[x_1^T, x_2^T\right]^T$ and $z_2 = \left[x_2^T, x_3^T\right]^T$. Subsequently, the system $\tilde{S}$ can be decomposed into two interconnected overlapping subsystems, i.e.

$$\tilde{S}_1 : \dot{z}_1 = \left(\begin{bmatrix} A_{11} & A_{12} \\ A_{21} & A_{22} \end{bmatrix} z_1 + \begin{bmatrix} B_{11} \\ B_{21} \end{bmatrix} u_1 \right) + \begin{bmatrix} 0 & A_{13} \\ 0 & A_{23} \end{bmatrix} z_2 + \begin{bmatrix} B_{12} \\ B_{22} \end{bmatrix} u_2 \tag{5}$$

and

$$\tilde{S}_2 : \dot{z}_2 = \left(\begin{bmatrix} A_{22} & A_{23} \\ A_{32} & A_{33} \end{bmatrix} z_2 + \begin{bmatrix} B_{21} \\ B_{31} \end{bmatrix} u_2 \right) + \begin{bmatrix} A_{21} & 0 \\ A_{31} & 0 \end{bmatrix} z_1 + \begin{bmatrix} B_{21} \\ B_{31} \end{bmatrix} u_1 \tag{6}$$

The state variable x_2 is repeatedly included in both subsystems, which implies "Overlapping Decompositions".

For system stabilization, two interconnected subsystems $\tilde{S}_1$ and $\tilde{S}_2$ are considered. The terms in the right hand sides of (5) and (6) can be separated into the decoupled subsystems (as indicated in the parenthesis in (5) and (6)) and the interconnected subsystems. As mentioned in [12], if each decoupled subsystem can be stabilized by its own input, the asymptotic stability of the interconnected overlapping subsystem $\tilde{S}_1$ and $\tilde{S}_2$ are maintained. Moreover, the asymptotic stability of the original system S is also guaranteed. Consequently, the interactions of the decoupled subsystems with the interconnection subsystems in (5) and (6) are regarded as perturbations. They can be neglected during control design. As a result, the decoupled subsystems of (5) and (6) can be expressed as

$$\tilde{S}_{D1} \; : \; \dot{z}_1 \; = \; \begin{bmatrix} A_{11} & A_{12} \\ A_{21} & A_{22} \end{bmatrix} z_1 \; + \; \begin{bmatrix} B_{11} \\ B_{21} \end{bmatrix} u_1 \tag{7}$$

and

$$\tilde{S}_{D2} \; : \; \dot{z}_2 \; = \; \begin{bmatrix} A_{22} & A_{23} \\ A_{32} & A_{33} \end{bmatrix} z_2 \; + \; \begin{bmatrix} B_{22} \\ B_{32} \end{bmatrix} u_2 \tag{8}$$

By regarding the power deviation between areas 1 and 2 (ΔP_{T12}) as the overlapped variable for design of frequency stabilizer of SSSC12, the subsystem embedded with the inter-area mode between areas 1 and 2 can be expressed as

$$\tilde{G}_{s1} \; : \; \begin{bmatrix} \Delta \dot{f}_1 \\ \Delta \dot{P}_{T12} \end{bmatrix} = \begin{bmatrix} -D_1/M_1 & a_{S12} \\ -2\pi T_{12} & 0 \end{bmatrix} \begin{bmatrix} \Delta f_1 \\ \Delta P_{T12} \end{bmatrix} + \begin{bmatrix} a_{12}/M_1 \\ 0 \end{bmatrix} \Delta P_{SSSC12} \tag{9}$$

Next, by considering the power deviation between areas 2 and 3 (ΔP_{T23}) as the overlapped variable for design of frequency stabilizer of SSSC23, the subsystem embedded with the inter-area mode between areas 2 and 3 can be expressed as

$$\tilde{G}_{s2} \; : \; \begin{bmatrix} \Delta \dot{P}_{T23} \\ \Delta \dot{f}_3 \end{bmatrix} = \begin{bmatrix} 0 & -2\pi T_{23} \\ a_{s34} & -D_3/M_3 \end{bmatrix} \begin{bmatrix} \Delta P_{T23} \\ \Delta f_3 \end{bmatrix} + \begin{bmatrix} 0 \\ 1/M_3 \end{bmatrix} \Delta P_{SSSC23} \tag{10}$$

By incorporating the dynamic characteristic of each SSSC as shown in Fig. 2, (9) and (10) become

$$G_{S1} \; : \; \begin{bmatrix} \Delta \dot{f}_1 \\ \Delta \dot{P}_{T12} \\ \Delta \dot{P}_{SSSC12} \end{bmatrix} = \begin{bmatrix} -D_1/M_1 & a_{S12} & a_{12}/M_1 \\ -2\pi T_{12} & 0 & 0 \\ 0 & 0 & -1/T_{SSSC12} \end{bmatrix} \begin{bmatrix} \Delta f_1 \\ \Delta P_{T12} \\ \Delta P_{SSSC12} \end{bmatrix} + \begin{bmatrix} 0 \\ 0 \\ 1/T_{SSSC12} \end{bmatrix} \Delta u_{SSSC12} \tag{11}$$

and

$$G_{S2} \; : \; \begin{bmatrix} \Delta \dot{P}_{T23} \\ \Delta \dot{f}_3 \\ \Delta \dot{P}_{SSSC23} \end{bmatrix} = \begin{bmatrix} -D_1/M_1 & a_{S12} & a_{12}/M_1 \\ -2\pi T_{12} & 0 & 0 \\ 0 & 0 & -1/T_{SSSC23} \end{bmatrix} \begin{bmatrix} \Delta P_{T23} \\ \Delta f_3 \\ \Delta P_{SSSC23} \end{bmatrix} + \begin{bmatrix} 0 \\ 0 \\ 1/T_{SSSC23} \end{bmatrix} \Delta u_{SSSC23} \tag{12}$$

where Δu_{SSSC12} and Δu_{SSSC23} are output signals of frequency stabilizers for SSSC12 and SSSC23, respectively. Equations (11) and (12) are used to design SSSC12 and SSSC23, respectively.

3.4 Structure of Frequency Stabilizer

In this study, the structure of the frequency stabilizer is based on a second-order lead/lag compensator as shown in Fig. 4.3. There are five parameters for each designed frequency stabilizer consisting of a stabilization gain K, time constants T_1, T_2, T_3, and T_4.

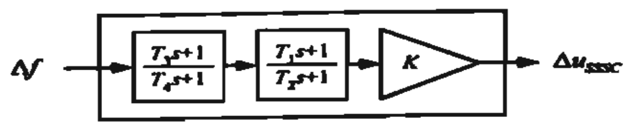

Figure 4. Configuration of 2nd order frequency stabilizer

Since the control purpose of the frequency stabilizer is to enhance the damping of the inter-area mode. The frequency deviation of each target area (Δf_i, $i=1$ and 3) which provides information of each mode of interest, is used as the input signal for each frequency stabilizer. The control parameters of each frequency stabilizer are optimized based on the following objective function.

3.5 Formulation of Objective Function

In deriving the objective function, not only the enhancement of system damping, but also the robust stability against system uncertainties are taken into consideration. Since the main purpose of the designed frequency stabilizer is to improve the system damping following any load disturbances, therefore, the damping ratio (ζ) of the inter-area mode is used as a design specification. Assuming that the eigenvalues corresponding to the mode of oscillation can be determined as $-\sigma \pm j\omega_d$, the damping ratio is given by

$$\zeta_{actual} = \frac{-\sigma}{\sqrt{\sigma^2 + \omega_d^2}} \tag{13}$$

The desired damping ratio of the eigenvalues corresponding to the mode of oscillation is specified as $\zeta_{desired}$. Accordingly, the difference between the desired and the actual damping ratios can be defined as

$$\alpha = \left|\zeta_{desired} - \zeta_{actual}\right| \tag{14}$$

For robust stability, the system uncertainties are modeled as a multiplicative form [9-11] demonstrated in Fig. 5. $\tilde{G}$ is a system and $\tilde{K}$ is a designed controller. Δ_m is a stable multiplicative uncertainty.

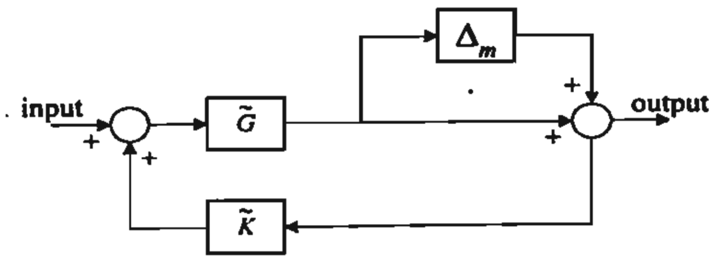

Figure 5. Control system with multiplicative uncertainty model

Based on the small-gain theorem [9-11], the closed loop system will be robustly stable if

$$\left|\Delta_m\right| < \frac{1}{\left|\tilde{G}\tilde{K}\left(1-\tilde{G}\tilde{K}\right)^{-1}\right|} \tag{15}$$

where $\tilde{G}\tilde{K}\left(1-\tilde{G}\tilde{K}\right)^{-1}$ is the complementary sensitivity function (T). Note that $|\bullet|$ is the magnitude of the transfer function "$\bullet$". Based on the multiplicative uncertainty model, the robust stability margin can be guaranteed in terms of multiplicative stability margin (MSM) as

$$MSM = 1/\|T\|_\infty \tag{16}$$

where $\|T\|_\infty$ is the ∞-norm of T. From (15) and (16), it is clear that by minimizing $\|T\|_\infty$, the MSM increases and the robust stability is ensured [9-11]. Thus, the normalized robustness index of the objective function is defined as

$$\gamma = \|T\|_\infty / \|T\|_{\infty(initial)} \tag{17}$$

where $\|T\|_{\infty(initial)}$ is the ∞-norm of T at the initial of a search process. Combining (14) and (17), the control problem can be formulated as the following optimization problem:

$$\begin{aligned} &\text{Minimize} && F(K,\ T_i) = c \cdot \alpha + \gamma \\ &\text{Subject to} && K_{min} \le K \le K_{max} \\ &&& T_{i,\ min} \le T_i \le T_{i,\ max}, \qquad i = 1,\dots,4 \end{aligned} \tag{18}$$

where $F(K,\ T_i)$ is the objective function. The minimum and maximum values of the gain K are set to 0.1 and 5, respectively. The minimum and maximum values of the time constants T_i are set to 0.01 and 2, respectively. The constant coefficient "c" is used to weight α-term, so that $c \cdot \alpha$ dominates γ during the parameters optimization. Note that, since γ is normalized to 1 at the initial solution, it is easy to find the value of c so that $c \cdot \alpha$ is greater than 1. Eventually, the search process minimizes both terms until $c \cdot \alpha$ meets the design specification and γ decreases to the possible minimum value. All searched parameters are optimized by a tabu search algorithm.

3.6 Tabu Search Algorithm

Tabu Search (TS) is an iterative improvement procedure that can start from any initial feasible solution (searched parameters) and attempted to determine a better solution. As a meta-heuristic, TS is based on a local search technique with the ability to escape from being trapped in local optima [13, 14]. Hereafter, components of TS and TS procedure are discussed.

Encoding and Decoding: The concatenated encoding method is used to encode each parameter into a binary string normalized over its range and also stack each normalized string in series with each other to construct the string individual. The same number of *nb* bits is used for each searched parameter. Figure 6 illustrates the example of concatenated encoding scheme.

Parameter 1	Parameter 2	Parameter 3
xx ... xxx	xx ... xxx	xx ... xxx

x x ... x x x

$2^{(nb-1)}$ $2^{(nb-2)}$ ... 2^2 2^1 2^0

Figure 6. Example of Concatenated Encoding Scheme

On the other hand, a decoding scheme is carried out by converting encoded parameters to their actual values by (19) prior to evaluation of objective function.

$$P_i = P_{i,min} + \frac{B_i \times \left[P_{i,max} - P_{i,min}\right]}{2^{n} - 1} \tag{19}$$

where P_i is the actual value of the i-th parameter, $P_{i,max}$ and $P_{i,min}$ are the maximum and minimum value of the i-th parameter. B_i is the decimal integer value of binary string of the i-th parameter. In this study, 16 bits are used to represent each parameter. The more the number of bits per searched parameter is, the higher the resolution will be.

Trial Solution Generation To generate a trial solution, one bit of a binary string of an initial solution is flipped at a time. Figure 7 conceptually illustrates the process. The maximum number of trial solutions in each iteration is referred to a neighborhood solution space (NS). In this paper, NS is set to 90 % of a total number of bits in a string individual ($\lfloor 0.9 \times nb \times NP \rfloor$ where NP is a number of searched parameters.

Initial solution :	1001011010	1100011010	1110010011
Trial solution 1:	0001011010	1100011010	1110010011
Trial solution 2:	1101011010	1100011010	1110010011
Trial solution 3:	1011011010	1100011010	1110010011

Figure 7 Example of Concatenated Encoding Scheme

Tabu List Restriction Tabu List (TL) is utilized to keep attributes (bit positions) that created the best solution in the past iterations for iterations so that they can not be used to create new solution candidates. As the iteration proceeds, TL stores a new attribute and releases the oldest one, as shown in Fig. 8. Particularly, the size of TL is the only control parameter of TS. The size of TL that provided good solutions usually grows with the size of the problem. In this paper, $\left\lfloor \sqrt{nb \times NP} \right\rfloor$ is used to determine the best size of TL.

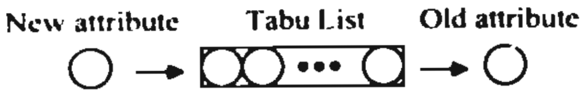

Figure 8. Mechanism of tabu list

Aspiration Level Criterion: The aspiration level (AL) criterion allows an attribute included in TL to override its tabu status if it leads to a more attractive solution. In particular, the AL is satisfied if the tabued attribute yields a solution that is better than the best solution reached at that iteration. After the AL is satisfied, updating TL is carried out by moving the tabued attribute back to the first position of the TL.

Termination Criteria: This criterion is set to allow the search process to stop and return the best solution found. The search process will terminate if the maximum allowable number of iterations is reached.

TS Procedure: firstly, the initial feasible solution is generated arbitrarily. A trial solution is searched if either it is not tabued or, in case of being tabued it passes the AL test. The best solution is always updated during the search process until the termination criterion is satisfied. The following notations are used for the TS procedure.

TL : the tabu list,
NS : the neighborhood solution space,
$F(X)$: the objective function of solution X,
X_o^k : the initial feasible solution at iteration k,
X_m^k : a trial solution m at iteration k,
X_{cb}^k : the current best trial solution at iteration k,
X_b^k : the best solution reached at iteration k,

k_{max} : the maximum allowable number of iterations.

The TS procedure can be described as follows.

1. Read constraints of searched parameters, the initial feasible solution X_0^k , and the design specification.
2. Specify the size of TL , k_{max}, and size of NS.
3. Initialize iteration counter k and termination criteria tc to zero, and empty TL.
4. Initialized AL by setting $X_b^k = X_0^k$.
5. Execute TS procedure:
   5.1 Initialize the trial counter m to zero.
   5.2 Generate a trial solution X_m^k from X_0^k.
   5.3 If X_m^k is not feasible, go to 5.9.
   5.4 If X_m^k is the first feasible solution, set $X_{cb}^k = X_m^k$.
   5.5 Perform Tabu test. If X_m^k is tabued, then go to 5.8.
   5.6 If $F(X_m^k) < F(X_{cb}^k)$, set $X_{cb}^k = X_m^k$. Otherwise, go to 5.9.
   5.7 If $F(X_m^k) < F(X_b^k)$, then update AL by setting $X_b^k = X_m^k$. Go to 5.9.
   5.8 Perform AL test. If $F(X_m^k) < F(X_b^k)$, set $X_{cb}^k = X_m^k$, and update AL by setting $X_b^k = X_m^k$.
   5.9 If m is less than NS, $m = m+1$ and go to 5.2.
   5.10 If there is no feasible solution, set $X_0^{k+1} = X_b^k$. Otherwise, set $X_0^{k+1} = X_{cb}^k$, and update TL.
6. If $k = 0$, go to 9.
7. Perform the convergence checking.
   If $X_b^k = X_b^{k-1}$, $tc = tc+1$. Otherwise, $tc = 0$.
8. If $tc =$ size of TL , set $tc = 0$ and go to 10.
9. If $k < k_{max}$, then $k = k+1$, and go to 5.
10. TS is terminated and X_b^k is the best solution found.

4. Experimental Results

In the design specification, the desired damping ratio $(\zeta_{desired})$ is set to 0.25. Also, the coefficient c is appropriately set to 5. For TS, the size of TL is set to 8 for the best solution. The area capacity ratio between areas 1, 2 and 3 is 5:10:2. System parameters are given in Table 1.

To exhibit the results of system reduction by overlapping decompositions, Table 2 shows eigenvalues of the original systems (1) in comparison to design subsystems (9) and (10). The damping ratio and oscillation frequency of the corresponding oscillation mode in the design subsystems are nearly equal to those of the original system. This reveals that the design subsystems (9) and (10) retain the physical characteristic of the original system (1).

As experimental results, the optimally tuned parameters of designed frequency stabilizers in (11) and (12) are obtained as given in Table 3. Note that the optimized frequency stabilizer based on (18) is referred to as "Robust frequency stabilizer".

For comparison purposes, the second-order lead/lag frequency stabilizer in (11) and (12) are also designed with the same design specification, which requires the same damping ratio $\zeta_{desired} = 0.25$. The control parameters $K, T_1, T_2, T_3,$ and T_4 are searched by TS via the optimization problem (20). Note that the robust stability index term (γ) is excluded.

$$
\begin{aligned}
\text{Minimize} \quad & F(K, T_i) = \alpha \\
\text{Subject to} \quad & K_{min} \le K \le K_{max} \\
& T_{i,\,min} \le T_i \le T_{i,\,max}, \qquad i = 1, \ldots, 4
\end{aligned}
\tag{20}
$$

Here, the optimized frequency stabilizer based on (20) is referred to as "Non-robust frequency stabilizer". Table 4 shows the control parameters of the non-robust frequency stabilizer.

Table 1. *Parameters of Three-area Loop Interconnected Power System (Area Capacity Ratio 5 : 10 : 2)*

System Parameters	Area 1	Area 2	Area 3
Inertia Constant (pu.MW.s/Hz)	$M_1 = 0.2$	$M_2 = 0.0167$	$M_3 = 0.15$
Damping Coefficient (pu.MW/Hz)	$D_1 = 0.006$	$D_2 = 0.00833$	$D_3 = 0.005$
Turbine Time Constant (s)	$T_{t1} = 0.25$	$T_{t2} = 0.3$	$T_{t3} = 0.25$
Governor Time Constant (s)	$T_{g1} = 0.1$	$T_{g2} = 0.08$	$T_{g3} = 0.1$
Regulation Ratio (Hz/pu.MW)	$R_1 = 2.4$	$R_2 = 2.4$	$R_3 = 2.4$
Bias Coefficient (pu.MW/Hz)	$B_1 = 0.5$	$B_2 = 0.5$	$B_3 = 0.5$
Integral Controller Gain (1/s)	$K_{i1} = 0.5$	$K_{i2} = 0.5$	$K_{i3} = 0.5$
Synchronizing Power Coefficient (pu.MW/rad)	$T_{12} = 0.159$, $T_{23} = 0.064$, $T_{31} = 0.079$		
Area Capacity Ratio	$a_{12} = 2.0$, $a_{23} = 0.2$, $a_{31} = 2.5$		

Table 2. ***Eigenvalues of Original System and Design Subsystems Before and After the Overlapping Decompositons***

Original System (1)	Subsystem (11)	Subsystem (12)
$\lambda_1 = -0.0415$	-	-
$\lambda_{2,3} = -0.0173 \pm j4.365$ ($\zeta = 0.0035$, $f = 0.695$ Hz)	$\lambda_{2,3} = -0.015 \pm j3.53$ ($\zeta = 0.0043$, $f = 0.562$ Hz)	-
$\lambda_{4,5} = -0.0185 \pm j3.291$ ($\zeta = 0.0056$, $f = 0.524$ Hz)	-	$\lambda_{4,5} = -0.0167 \pm j3.31$ ($\zeta = 0.005$, $f = 0.527$ Hz)

Table 3. Parameters of Robust Frequency Stabilizers

Robust Frequency Stabilizer	K	T_1	T_2	T_3	T_4
SSSC12	0.2188	0.2587	0.0158	0.0575	0.2316
SSSC23	0.2378	1.5025	0.5386	1.6268	0.5075

Table 4. Parameters of Non-Robust Frequency Stabilizers

Non-robust Frequency Stabilizer	K	T_1	T_2	T_3	T_4
SSSC12	4.2863	0.1344	1.0011	1.0978	1.3807
SSSC23	4.3683	0.1344	0.9933	1.3467	1.3802

Table 5. Comparison of Eigenvalues of Design Subsystems

Design Subsystem	SSSC with No Frequency Stabilizer	SSSC With Non-Robust Frequency Stabilizer	SSSC With Robust Frequency Stabilizer
G_{s1}	$-0.015 \pm j3.53$ $\zeta = 0.0043$	$-1.8369 \pm j7.1143$ $\zeta = 0.25$	$-0.6093 \pm j2.3595$ $\zeta = 0.25$
G_{s2}	$-0.0167 \pm j3.31$ $\zeta = 0.005$	$-1.667 \pm j6.4559$ $\zeta = 0.25$	$-0.3534 \pm j1.3685$ $\zeta = 0.25$

Table 5 shows eigenvalues of subsystems (11) and (12) in case of SSSCs with robust frequency stabilizers installed in comparison with a case of SSSCs with no frequency stabilizer and a case of SSSCs with non-robust frequency stabilizers installed. The results describe that the damping ratios of the eigenvalues corresponding to the desired inter-area modes are improved to 0.25, as design specification.

Next, the MSM is used to evaluate the robust stability margin of system (11) and (12) included with each frequency stabilizer. As shown in Table 6, the value of MSM in case of the system with robust frequency stabilizer is greater than that in case of the system with non-robust stabilizer. This clearly signifies that the better robust stability margin of the power system incorporated with robust frequency stabilizer can be achieved by the optimization problem (18).

Table 6. *Comparison of MSM*

System	With Non-Robust Frequency Stabilizer	With Robust Frequency Stabilizer
G_{S1}	0.5151	0.71430
G_{S2}	0.5332	0.61240

Table 7. *Comparison of Eigenvalues of Original System*

Inter-Area Oscillation Mode	No Frequency Stabilizer	With Non-Robust Frequency Stabilizer	With Robust Frequency Stabilizer
Between Areas 1 and 2	$-0.0173 \pm j4.365$ $\zeta = 0.0035$	$-1.7631 \pm j7.6011$ $\zeta = 0.226$	$-0.6619 \pm j2.898$ $\zeta = 0.223$
Between Areas 2 and 3	$-0.0185 \pm j3.291$ $\zeta = 0.0056$	$-1.6716 \pm j6.4702$ $\zeta = 0.25$	$-0.3596 \pm j1.376$ $\zeta = 0.253$

Table 7 shows the eigenvalues of the original system (1) before and after control. After each frequency stabilizer is included in the system, the damping ratios of the corresponding inter-area modes are enhanced as expected. This confirms the merit of overlapping decompositions that if the subsystems are stabilized by their own control inputs, the stability of the original system can be guaranteed.

Here, the performance and robustness of the designed frequency stabilizers are evaluated in a linearized model of the three-area interconnected system. Here, changing load disturbances which are simultaneously applied to areas 1 and 3, are composed of three different components in the frequency domain, one of which (underlined component) has a frequency corresponding to the inter-area mode of interest (see Table 6), as follows.

$$\text{Area } 1 : \Delta P_{L1} = \underline{0.003\sin(4.36t)} + 0.005\sin(5.3t) - 0.007\sin(6t) \tag{21}$$

$$\text{Area } 3 : \Delta P_{L3} = \underline{0.003\sin(3.29t)} + 0.007\sin(4t) - 0.005\sin(4.5t) \tag{22}$$

Note that the dynamic of governor as illustrated in Fig. 9, is also included into each area in this simulation study. Table 8 shows operating conditions and applied disturbances.

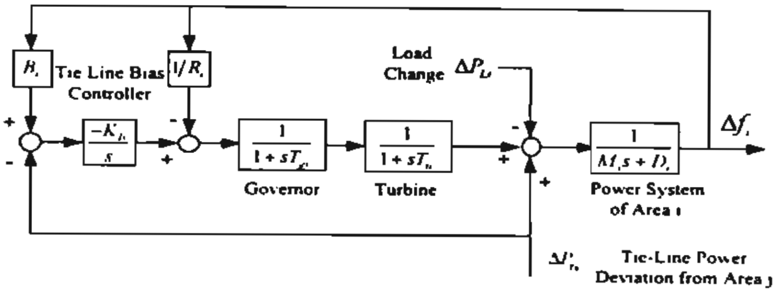

Figure 9. Linearized model of governor system

Table 8. *System Conditions and Applied Disturbances*

Case	Disturbances
1	At normal (design) condition, ΔP_{L1} is applied to area 1 and ΔP_{L3} is applied to area 3. (No parameter variations)
2	At unstable condition, ΔP_{L1} is applied to area 1 and ΔP_{L3} is applied at area 3 while damping coefficients D_1 and D_3 are set -0.45.

For case 1, the damping effect of each designed stabilizer is investigated. As demonstrated in Figs. 10 – 12, both robust and non-robust frequency stabilizers are able to damp the frequency oscillation in each area, effectively. Nevertheless, the damping effect of the robust frequency stabilizer is better than that of the non-robust case. As declared in Figs. 13 and 14, the power output deviation of the robust frequency stabilizer for each SSSC is almost equal to that of non-robust frequency stabilizer.

In case 2, not only damping effect but also robust stability of the system incorporated with each frequency stabilizer are evaluated. It is assumed that both power systems 1 and 3 are in unstable conditions, so that D_1 and D_3 are set to -0.45 (pu.MW/Hz). As the load disturbances applied to both areas, frequency deviations of areas 1, 2 and 3 in case of the non-robust frequency stabilizer severely fluctuate and finally diverge as depicted in Figs. 15– 17. Note that frequency deviation of each area in case of SSSCs without frequency stabilizers (not shown here) also heavily oscillates and finally diverges. On the other hand, frequency oscillations in all areas are completely stabilized by the robust frequency stabilizer. The interconnected power system can maintain the system stability. The power output deviations of robust frequency stabilizers are illustrated in Figs. 18 and 19. These simulation results confirm that under severe load disturbances and negative damping, the robustness of robust frequency stabilizer against such system uncertainties is considerably superior to that of non-robust frequency stabilizer.

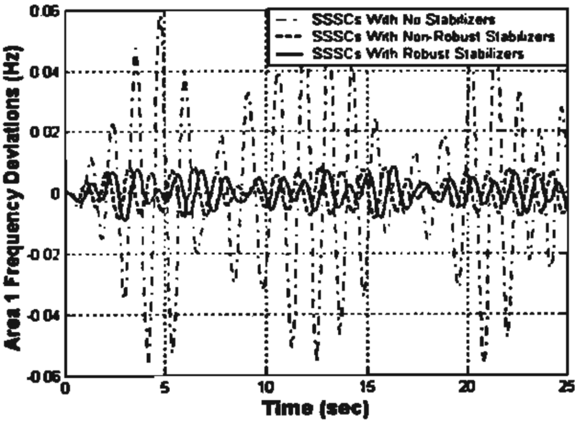

Figure 10. Case 1: Area 1 Frequency Deviation

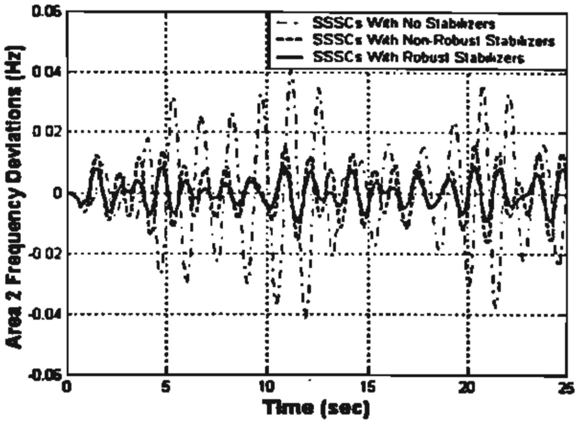

Figure 11. Case 1: Area 2 Frequency Deviation

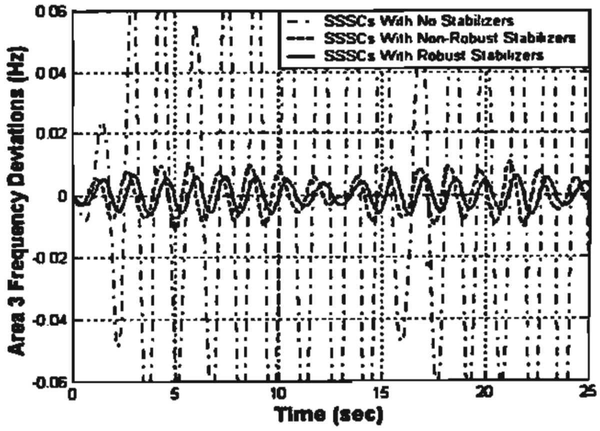

Figure 12. Case 1: Area 3 Frequency Deviation

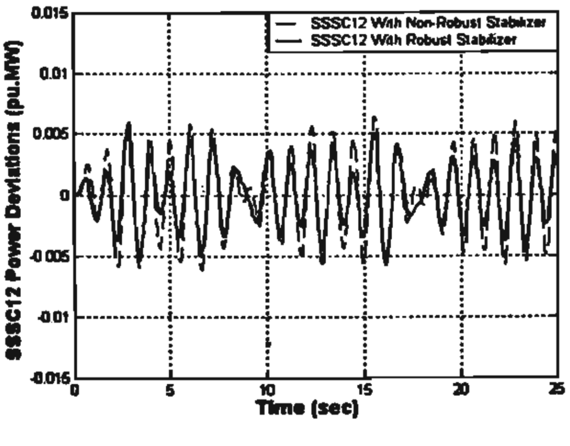

Figure 13. Case 1: SSSC12 Power Output

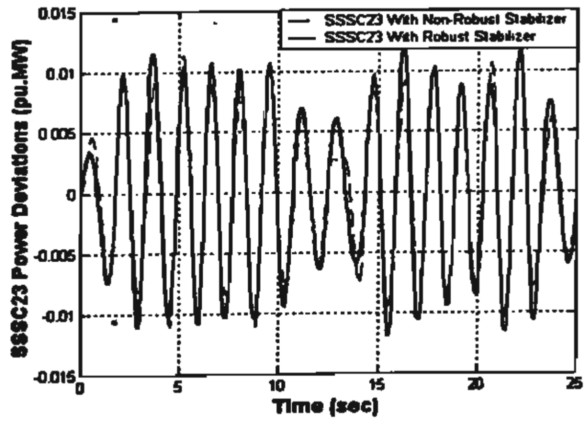

Figure 14. Case 1: SSSC23 Power Output

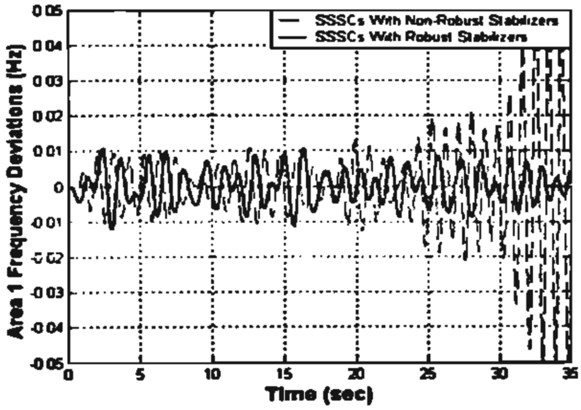

Figure 15. Case 2: Area 1 Frequency Deviation

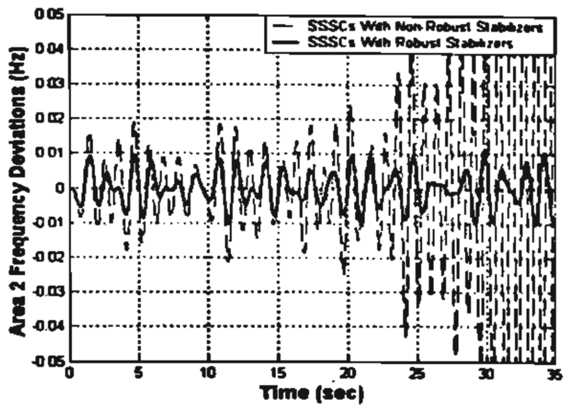

Figure 16. Case 2: Area 2 Frequency Deviation

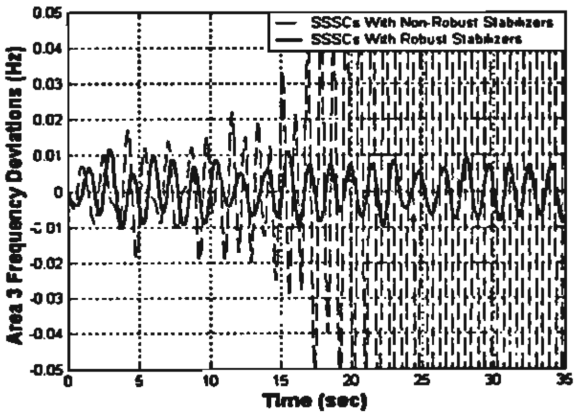

Figure 17. Case 2: Area 3 Frequency Deviation

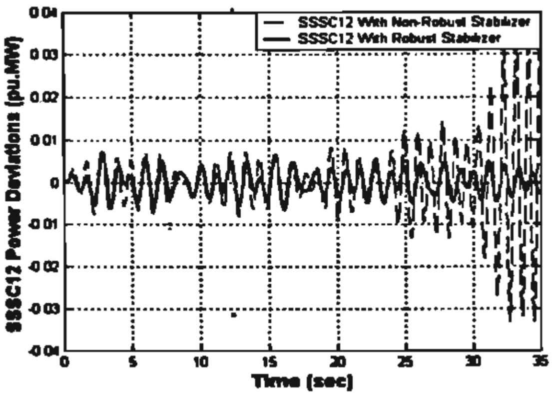

Figure 18. Case 2: SSSC12 Power Output

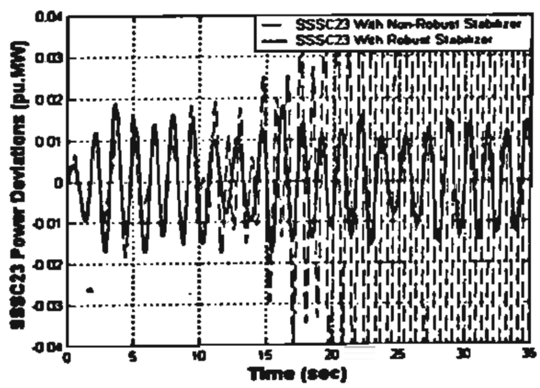

Figure 19. Case 2: SSSC23 Power Output

5. Conclusions

This paper focuses on the new robust design of frequency stabilizer of SSSC by taking system uncertainties into account. The design method utilizes the merit of overlapping decompositions technique to extract the subsystem embedded with the inter-area oscillation mode of interest. By including the multiplicative uncertainty model in the extracted subsystem, the robust stability index based on multiplicative stability margin can be applied in the formulation of objective function. As a result, the robust stability margin of system with designed frequency stabilizer can be enhanced by optimization technique. Without trial and error, the tabu search algorithm is automatically applied to search for the optimal control parameters of the second-order lead/lag based frequency stabilizer. The high robustness of the designed frequency stabilizer against various load disturbances with changing frequency in the vicinity of inter-area mode and negative damping, has been confirmed by simulation study.

6. Reference

1. F. D. Galliana and M. Illic, *Power System Restructuring*, Kluwer Academic Publishers, 1998.
2. K. N. Zadeh, R. C. Meyer and G. Cauley, Practices and new concepts in power system control, *IEEE Trans. on Power Systems* 11 (1) (1996) 3-9.
3. L. H. Fink and P. J. M. Van Son, On system control within a restructured Industry, *IEEE* Trans. on Power Systems, 13 (2) (1998) 611-616.
4. O.L. Elgerd, *Electric Energy System Theory, An Introduction 2nd*, McGraw-Hill, 1985.
5. N. Jaleeli, L.S. Vanslyck, D.N. Ewart, L.H. Fink and A.G. Hoffmann, Understanding automatic generation control, *IEEE Transactions on Power Systems*, Vol. 7, No. 3, pp. 1106-1122, 1999.
6. I. Ngamroo, Application of static synchronous series compensation to stabilization of frequency oscillations in an interconnected power system, *Proceedings of 2001 IEEE International Symposium on Circuits and Systems (ISCAS 2001), Sydney, Australia*, Vol. 2, pp. 113-116.
7. L. Gyugyi, Dynamic compensator of AC transmission lines by solid-state synchronous voltage source, *IEEE Trans. on Power Delivery*, Vol. 9, No. 2, pp. 904-911, 1994.
8. L. Gyugyi, C. D. Schauder and K.K. Sen, Static Synchronous Series Compensator: A Solid-State Approach to The Series Compensation of Transmission Lines, *IEEE Trans. on Power Delivery*, Vol. 12, No. 1, pp..406-417, 1997.
9. S. Skogestad and I. Postlethwaite, *Multivariable Feedback Control, Analysis and Design*, John Wiley & Sons, 1998.
10. G. C. Goodwin, S. F. Graebe and M. E. Salgado, *Control System Design*, Prentice Hall, 2001.
11. B. Shahian and M. Hassul, *Control System Design using MATLAB*, Prentice Hall,1993.
12. M. Ikeda, D.D. Siljak and D. E. White, Decentralized control with overlapping information sets. *Journal of Optimization Theory and Applications*, Vol. 34, No. 2, pp.279-310, 1981.
13. F. Glover and M. Laguna, *Tabu Search*, Kluwer Academic Publishers, 2000.
14. V. J. Rayward-Smith, I. H. Osman, C.R. Reeves, and G.D. Smith, *Modern Heuristic Search Methods*, John Wiley & Sons, UK, 1996.
15. P. Kundur, Power System Stability and Control, McGraw Hill, 1994.